

**Robust Hovering and Trajectory Tracking Control  
of a Quadrotor Helicopter Using Acceleration Feedback  
and a Novel Disturbance Observer**

by

Hammad Zaki

**Submitted to  
the Graduate School of Engineering and Natural Sciences  
in partial fulfillment of  
the requirements for the degree of  
Doctor of Philosophy**

**SABANCI UNIVERSITY**

July, 2019

Robust Hovering and Trajectory Tracking Control of a Quadrotor Helicopter  
Using Acceleration Feedback and a Novel Disturbance Observer

Hammad Zaki

APPROVED BY

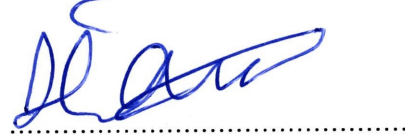
Prof. Dr. Mustafa Ünel  
(Thesis Advisor)



Asst. Prof. Dr. Meltem Elitaş



Asst. Prof. Dr. Hüseyin Özkan



Prof. Dr. Şeref Naci Engin



Asst. Prof. Dr. Ertuğrul Çetinsoy



DATE OF APPROVAL: .....17/07/2019.....

© Hammad Zaki 2019  
All Rights Reserved

Robust Hovering and Trajectory Tracking Control of a Quadrotor Helicopter  
Using Acceleration Feedback and a Novel Disturbance Observer

Hammad Zaki

ME, Ph.D Dissertation, 2019

Thesis Advisor: Prof. Dr. Mustafa Ünel

**Keywords:** Robust Control, Acceleration Feedback, Disturbance Observer, Quadrotor, Hierarchical Control, Sliding Mode Control, Nonlinear Optimization

## Abstract

Hovering and trajectory tracking control of rotary-wing aircrafts in the presence of uncertainties and external disturbances is a very challenging task. This thesis focuses on the development of the robust hovering and trajectory tracking control algorithms for a quadrotor helicopter subject to both periodic and aperiodic disturbances along with noise and parametric uncertainties. A hierarchical control structure is employed where high-level position controllers produce reference attitude angles for the low-level attitude controllers. Reference attitude angles are usually determined analytically from the position command signals that control the positional dynamics. However, such analytical formulas may produce large and non-smooth reference angles which must be saturated and low-pass filtered. In this thesis, desired attitude angles are determined numerically using constrained nonlinear optimization where certain magnitude and rate constraints are imposed. Furthermore, an acceleration based disturbance observer (AbDOB) is designed to estimate and suppress disturbances acting on the positional dynamics of the quadrotor. For the attitude control, a nested position, velocity, and inner acceleration feedback control structure consisting of PID and PI type controllers are developed to provide high stiffness against external disturbances. Reliable angular acceleration is estimated through an extended Kalman filter (EKF) cascaded with a classical Kalman filter (KF).

This thesis also proposes a novel disturbance observer which consists of a bank of band-pass filters connected parallel to the low-pass filter of a classical disturbance observer. Band-pass filters are centered at integer multiples of the fundamental frequency of the periodic disturbance. Number and bandwidth of the band-pass

filters are two crucial parameters to be tuned in the implementation of the new structure. Proposed disturbance observer is integrated with a sliding mode controller to tackle the robust hovering and trajectory tracking control problem. The sensitivity of the proposed disturbance observer based control system to the number and bandwidth of the band-pass filters are thoroughly investigated via several simulations. Simulations are carried out on a high fidelity model where sensor biases and measurement noise are also considered. Results show that the proposed controllers are very effective in providing robust hovering and trajectory tracking performance when the quadrotor helicopter is subject to the wind gusts generated by the Dryden wind model along with plant uncertainties and measurement noise. A comparison with the classical disturbance observer-based control is also provided where better tracking performance with improved robustness is achieved in the presence of noise and external disturbances.

İvme Geri Bildirimi ve Özgün Bir Bozucu Gözlemcisi Kullanarak  
Bir Quadrotor Helikopterin Gürbüz Havada Kalma  
ve Yörünge İzleme Kontrolü

Hammad Zaki

ME, Doktora Tezi, 2019

Tez Danışmanı: Prof. Dr. Mustafa Ünel

**Anahtar kelimeler:** Gürbüz Kontrol, İvme Geri Bildirimi, Bozucu Gözlemcisi, Quadrotor, Hiyerarşik Kontrol, Kayan Kipli Kontrol, Doğrusal Olmayan Optimizasyon

## Özet

Belirsizlikler ve dış bozucuların olduğu durumlarda döner kanatlı uçakların havada kalma ve yörünge izleme kontrolü çok zor bir iştir. Bu tez, gürültü ve parametrik belirsizliklerin yanı sıra periyodik ve aperiodyik bozuculara maruz kalan bir quadrotor helikopter için gürbüz havada kalma ve yörünge izleme kontrol algoritmalarının geliştirilmesine odaklanmaktadır. Yüksek seviye pozisyon kontrolcülerinin düşük seviye duruş kontrolcülerini için referans duruş açıları ürettiği hiyerarşik bir kontrol yapısı kullanılmaktadır. Referans duruş açıları çoğunlukla konumsal dinamikleri kontrol eden pozisyon komut sinyallerinden analitik olarak belirlenmektedir. Bununla birlikte, bu tür analitik formüller, sınırlandırılmayı ve alçak iletimli filtrelenmeyi gerektiren büyük ve pürüzsüz olmayan referans açıları üretebilir. Bu tezde, istenen duruş açıları, belirli büyüklük ve oran kısıtlamalarının uygulandığı kısıtlı doğrusal olmayan optimizasyon kullanılarak sayısal olarak belirlenmektedir. Ayrıca, bir ivmelenmeye dayalı bozucu gözlemcisi (AbDOB), quadrotorun konumsal dinamikleri üzerine etki eden bozucuları tahmin etmek ve bastırmak için tasarlanmıştır. Duruş kontrolü için, dış bozuculara karşı yüksek sertlik sağlamak üzere PID ve PI tipi kontrolcülerden oluşan iç içe konum, hız ve iç ivme geri besleme kontrol yapısı geliştirilmiştir. Güvenilir açısal ivmelenme, ardarda bağlanmış genişletilmiş bir Kalman filtresi (EKF) ile klasik bir Kalman filtresi (KF) üzerinden tahmin edilmektedir.

Bu tez ayrıca, klasik bir bozucu gözlemcisinin alçak iletimli filtresine paralel bağlanmış bir bant iletimli filtre bankasından oluşan yeni bir bozucu gözlemcisi önermektedir. Bant iletimli filtreler, periyodik bozucunun temel frekansının tam sayı katlarında ortalanmıştır. Bant iletimli filtrelerin sayısı ve bant genişliği, yeni yapının uygulanmasında ayarlanması gereken iki önemli parametredir. Önerilen bozucu gözlemcisi, gürbüz havada kalma ve yörünge izleme kontrol problemini ele almak için bir kayan kipli kontrolcüye entegre edilmiştir. Önerilen bozucu gözlemci temelli kontrol sisteminin, bant iletimli filtrelerin sayısına ve bant genişliğine duyarlılığı, birçok simülasyon yoluyla ayrıntılı bir şekilde incelenmiştir. Simülasyonlar, sensör sapmalarının ve ölçüm gürültüsünün de göz önünde bulundurulduğu yüksek kalitede bir model üzerinde gerçekleştirilmiştir. Sonuçlar, önerilen kontrolcülerin, quadrotor helikopterin sistem belirsizlikleri ve ölçüm gürültüsünün yanında Dryden rüzgar modelinin ürettiği rüzgarlara maruz kalması durumunda bile gürbüz havada kalma ve yörünge izleme performansını sağlamada çok etkili olduğunu göstermektedir. Ayrıca klasik bozucu gözlemcisi temelli kontrol ile bir karşılaştırma da yapılmış, gürültü ve dış bozucular varken düzeltilmiş gürbüzlük ile daha iyi izleme performansının elde edildiği görülmüştür.

# *Acknowledgements*

First and foremost, I would like to extend my sincere gratitude to my Ph.D thesis advisor Prof. Dr. Mustafa Ünel, for his unwavering guidance and continuous support throughout my Ph.D studies. He always shows great interest in the research activities of his students. He has the ability to catch the audience through his scientific understanding. I wish I could reach at that par someday. During interactions, I learned extensively from him, especially how to look at specific problems through different perspectives and constructive criticism. I am deeply indebted to him for his patience and cooperation. I greatly appreciate his invaluable advice on both my research and career. Besides being an academic expert, he is so welcoming and energetic that no one forgets when someone meets him.

I would like to express my deepest appreciation to Prof. Dr. Şeref Naci Engin and Asst. Prof. Dr. Meltem Elitaş for their precious comments and suggestions as my thesis progress committee members. I would also like to praise Asst. Prof. Dr. Hüseyin Özkan and Asst. Prof. Dr. Ertuğrul Çetinsoy for spending their valuable time to serve as my jurors.

I am also grateful to the Control, Vision, and Robotics (CVR) research group, Gökhan Alcan, Diyar Khalis Bilal , Naida Fetic, Emre Yılmaz and Mehmet Emin Mumcuoğlu for providing a pleasant environment in the Laboratory.

I owe my deepest gratitude to my better half Ammarah Zaki for her patience and support during my Ph.D studies. Her impeccable love playes an indispensable role to achieve my aspirations. I feel obliged to mention her sacrifices for all those times when I was not available. Without her, my Ph.D. course of studies would be much more difficult. She always remained supportive during my stressed periods and did not show any sign of discomfort and dejection. I would also like to thank my children, Muhammad Zuhair Zaki and Muhammad Ruvaid Zaki, for giving me happiness and enjoyable life.

Finally, I wish to express heartfelt gratitude to my parents, Muhammad Nazir and Sughra Shaheen for their moral and spiritual support throughout my life. Their immense love and encouragement always give me strength during the ups and downs of my life. I also like to thank my brothers, Faisal Imran and Bassam Sabri for their love and moral support.

# Contents

|  |             |
|--|-------------|
| <b>Abstract</b>                                  | <b>iii</b>  |
| <b>Özet</b>                                      | <b>v</b>    |
| <b>Acknowledgements</b>                          | <b>vii</b>  |
| <b>Contents</b>                                  | <b>viii</b> |
| <b>List of Figures</b>                           | <b>xi</b>   |
| <b>List of Tables</b>                            | <b>xv</b>   |
| <br>   |             |
| <b>1 Introduction</b>                            | <b>1</b>    |
| 1.1 Motivation . . . . .                         | 4           |
| 1.2 Contributions of the thesis . . . . .        | 7           |
| 1.3 Outline of the thesis . . . . .              | 8           |
| 1.4 Publications . . . . .                       | 8           |
| <br>   |             |
| <b>2 Literature Survey and Background</b>        | <b>12</b>   |
| 2.1 Disturbance Observer Based Control . . . . . | 13          |

---

|          |   |           |
|----------|---|-----------|
| 2.2      | Acceleration Feedback . . . . .   | 18        |
| 2.3      | Hierarchical Control . . . . .  | 20        |
| <b>3</b> | <b>Modeling of a Quadrotor System</b>   | <b>22</b> |
| 3.1      | Newton-Euler Model for Quadrotor . . . . .  | 23        |
| <b>4</b> | <b>A Novel Observer for Estimating Periodic Disturbances</b>  | <b>31</b> |
| 4.1      | A Novel Disturbance Observer . . . . .  | 33        |
| <b>5</b> | <b>Estimation of Attitude Angles Using Nonlinear Optimization</b>   | <b>38</b> |
| 5.1      | Nonlinear Optimization . . . . .  | 40        |
| 5.2      | SQP Implementation . . . . .  | 43        |
| <b>6</b> | <b>Robust Trajectory Tracking Control of the Quadrotor Helicopter Using Acceleration Feedback</b>                     | <b>47</b> |
| 6.1      | Position Control Using Acceleration Feedback . . . . .  | 48        |
| 6.2      | Attitude Control Using Nested Feedback Loops . . . . .  | 50        |
| 6.2.1    | Cascaded Kalman Filter . . . . .  | 51        |
| 6.2.2    | Nested Feedback Loops . . . . .   | 53        |
| <b>7</b> | <b>Robust Hovering and Trajectory Tracking Control of the Quadrotor Helicopter Using a Novel Disturbance Observer</b> | <b>55</b> |
| 7.1      | Position Control Utilizing Acceleration Based Disturbance Observer  | 56        |
| 7.2      | Attitude Control Utilizing Velocity Based Disturbance Observer . .  | 58        |
| <b>8</b> | <b>Simulation Results and Discussions</b>   | <b>63</b> |
| 8.1      | Results for Trajectory Tracking Control Using Acceleration Feedback   | 64        |
| 8.2      | Results for Hovering and Trajectory Tracking Control Using a Novel Disturbance Observer . . . . .                     | 78        |

---

|          |   |            |
|----------|---|------------|
| 8.2.1    | Hovering Case . . . . .                     | 78         |
| 8.2.1.1  | Number of the Bandpass filters . . . . .    | 80         |
| 8.2.1.2  | Bandwidth of the Bandpass filters . . . . . | 84         |
| 8.2.2    | Trajectory Tracking Case . . . . .          | 87         |
| 8.2.2.1  | Number of the Bandpass filters . . . . .    | 89         |
| 8.2.2.2  | Bandwidth of the Bandpass Filters . . . . . | 94         |
| <b>9</b> | <b>Conclusions</b>                          | <b>98</b>  |
|          | <b>Bibliography</b>                         | <b>101</b> |

# List of Figures

|     |   |    |
|-----|---|----|
| 1.1 | UAVs classifications . . . . .  | 3  |
| 1.2 | Various UAVs . . . . .  | 3  |
| 2.1 | Disturbance observer based control . . . . .  | 14 |
| 3.1 | Quadrotor dynamics . . . . .  | 23 |
| 4.1 | Disturbance observer based control . . . . .  | 33 |
| 4.2 | Frequency distribution . . . . .  | 35 |
| 4.3 | Band-pass filter construction . . . . .   | 36 |
| 4.4 | Novel disturbance observer block diagram . . . . .  | 37 |
| 6.1 | Overall control system architecture . . . . .   | 48 |
| 6.2 | Cascaded Kalman filters structure . . . . .   | 51 |
| 7.1 | Closed loop control system . . . . .  | 57 |
| 8.1 | Disturbances acting on the positional dynamics . . . . .  | 65 |
| 8.2 | Disturbances acting on the attitude dynamics . . . . .  | 65 |
| 8.3 | X Cartesian position of the quadrotor vs Time (desired in black,<br>proposed in red, analytical in green) . . . . . | 66 |
| 8.4 | Y Cartesian position of the quadrotor vs Time (desired in black,<br>proposed in red, analytical in green) . . . . . | 67 |

---

|      |  |    |
|------|--|----|
| 8.5  | Z Cartesian position of the quadrotor vs Time (desired in black, proposed in red, analytical in green) . . . . . | 67 |
| 8.6  | Position errors (proposed in red, analytical in green) . . . . .   | 68 |
| 8.7  | 3-D Trajectory (desired in black, proposed in red, analytical in green)  | 68 |
| 8.8  | Roll angle (proposed in red, analytical in green) . . . . .  | 69 |
| 8.9  | Pitch angle (proposed in red, analytical in green) . . . . .   | 70 |
| 8.10 | Yaw angle (proposed in red, analytical in green) . . . . .   | 70 |
| 8.11 | X axis disturbance estimation (desired in black, proposed in red, analytical in green) . . . . .                 | 71 |
| 8.12 | Y axis disturbance estimation (desired in black, proposed in red, analytical in green) . . . . .                 | 72 |
| 8.13 | Z axis disturbance estimation (desired in black, proposed in red, analytical in green) . . . . .                 | 72 |
| 8.14 | Control efforts . . . . .  | 73 |
| 8.15 | X Cartesian position of the quadrotor vs Time (desired in black, with AF in red, without AF in green) . . . . .  | 74 |
| 8.16 | Y Cartesian position of the quadrotor vs Time (desired in black, with AF in red, without AF in green) . . . . .  | 74 |
| 8.17 | Z Cartesian position of the quadrotor vs Time (desired in black, with AF in red, without AF in green) . . . . .  | 75 |
| 8.18 | Position errors (with AF in red, without AF in green) . . . . .  | 75 |
| 8.19 | Roll angle (with AF in red, without AF in green) . . . . .   | 76 |
| 8.20 | Pitch angle (with AF in red, without AF in green) . . . . .  | 76 |
| 8.21 | Yaw angle (with AF in red, without AF in green) . . . . .  | 77 |
| 8.22 | Disturbances acting on the positional dynamics . . . . .   | 79 |
| 8.23 | Disturbances acting on the attitude dynamics . . . . .   | 79 |

---

|      |   |    |
|------|---|----|
| 8.24 | X Cartesian position (proposed DOB (5 BPFs in red, 3 BPFs in blue), DOB in green) . . . . .                   | 80 |
| 8.25 | Y Cartesian position (proposed DOB (5 BPFs in red, 3 BPFs in blue), DOB in green) . . . . .                   | 81 |
| 8.26 | Z Cartesian position (proposed DOB (5 BPFs in red, 3 BPFs in blue), DOB in green) . . . . .                   | 81 |
| 8.27 | Position errors (proposed DOB (5 BPFs in red, 3 BPFs in blue), DOB in green) . . . . .                        | 82 |
| 8.28 | Roll angle (proposed DOB (5 BPFs in red, 3 BPFs in blue), DOB in green) . . . . .                             | 82 |
| 8.29 | Pitch angle (proposed DOB (5 BPFs in red, 3 BPFs in blue), DOB in green) . . . . .                            | 83 |
| 8.30 | Yaw angle (proposed DOB (5 BPFs in red, 3 BPFs in blue), DOB in green) . . . . .                              | 83 |
| 8.31 | X Cartesian position (proposed DOB (30 rad/sec in red, 20 rad/sec in blue), DOB in green) . . . . .           | 84 |
| 8.32 | Y Cartesian position (proposed DOB (30 rad/sec in red, 20 rad/sec in blue), DOB in green) . . . . .           | 85 |
| 8.33 | Z Cartesian position (proposed DOB (30 rad/sec in red, 20 rad/sec in blue), DOB in green) . . . . .           | 85 |
| 8.34 | Position errors (proposed DOB with bandwidth (30 rad/sec in red, 20 rad/sec in blue), DOB in green) . . . . . | 86 |
| 8.35 | Roll angle (proposed DOB with bandwidth (30 rad/sec in red, 20 rad/sec in blue), DOB in green) . . . . .      | 87 |
| 8.36 | Pitch angle (proposed DOB with bandwidth (30 rad/sec in red, 20 rad/sec in blue), DOB in green) . . . . .     | 87 |
| 8.37 | Yaw angle (proposed DOB with bandwidth (30 rad/sec in red, 20 rad/sec in blue), DOB in green) . . . . .       | 88 |
| 8.38 | Disturbances acting on positional dynamics . . . . .  | 89 |

|  |    |
|--|----|
| 8.39 Disturbances acting on attitude dynamics . . . . .  | 89 |
| 8.40 X Cartesian position (proposed DOB (5 BPFs in red, 3 BPFs in blue), DOB in green) . . . . .                   | 90 |
| 8.41 Y Cartesian position (proposed DOB (5 BPFs in red, 3 BPFs in blue), DOB in green) . . . . .                   | 90 |
| 8.42 Z Cartesian position (proposed DOB (5 BPFs in red, 3 BPFs in blue), DOB in green) . . . . .                   | 91 |
| 8.43 Position errors (proposed DOB (5 BPFs in red, 3 BPFs in blue), DOB in green) . . . . .                        | 91 |
| 8.44 Roll angle (proposed DOB (5 BPFs in red, 3 BPFs in blue), DOB in green) . . . . .                             | 92 |
| 8.45 Pitch angle (proposed DOB (5 BPFs in red, 3 BPFs in blue), DOB in green) . . . . .                            | 92 |
| 8.46 Yaw angle (proposed DOB (5 BPFs in red, 3 BPFs in blue), DOB in green) . . . . .                              | 93 |
| 8.47 X Cartesian position (proposed DOB (30 rad/sec in red, 20 rad/sec in blue), DOB in green) . . . . .           | 94 |
| 8.48 Y Cartesian position (proposed DOB (30 rad/sec in red, 20 rad/sec in blue), DOB in green) . . . . .           | 94 |
| 8.49 Z Cartesian position (proposed DOB (30 rad/sec in red, 20 rad/sec in blue), DOB in green) . . . . .           | 95 |
| 8.50 Position errors (proposed DOB with bandwidth (30 rad/sec in red, 20 rad/sec in blue), DOB in green) . . . . . | 95 |
| 8.51 Roll angle (proposed DOB with bandwidth (30 rad/sec in red, 20 rad/sec in blue), DOB in green) . . . . .      | 96 |
| 8.52 Pitch angle (proposed DOB with bandwidth (30 rad/sec in red, 20 rad/sec in blue), DOB in green) . . . . .     | 96 |
| 8.53 Yaw angle (proposed DOB with bandwidth (30 rad/sec in red, 20 rad/sec in blue), DOB in green) . . . . .       | 97 |

# List of Tables

|     |  |    |
|-----|--|----|
| 8.1 | Model Parameters . . . . .   | 65 |
| 8.2 | Trajectory Tracking Performance . . . . .  | 71 |
| 8.3 | Trajectory Tracking Performance . . . . .  | 77 |
| 8.4 | Hovering Performance with Different Number of the BPFs . . . . .                   | 84 |
| 8.5 | Hovering Performance with Different Bandwidths of the BPFs . . . . .               | 88 |
| 8.6 | Trajectory Tracking Performance with Different Number of the BPFs . . . . .        | 93 |
| 8.7 | Trajectory Tracking Performance with Different Bandwidths of the<br>BPFs . . . . . | 97 |

# Chapter 1

## Introduction

According to the recent research made by Grand View Research, a market research and consulting company [1], the applications of unmanned aerial vehicles (UAVs) has gained considerable attention in the global market and it is expected to reach USD 2.07 billion by 2022. Recently, we have seen an increase in the application of drones in the existing industries. The reasons for this much interest in UAVs is due to their ability to perform those tasks which are difficult or dangerous for humans. Sometimes cost of the operation increases if the similar task is performed by human beings as compared to UAVs which require less investment of resources, i.e., it would require fewer resources to use a drone to check up the condition of machinery, structures or infrastructures located in remote areas or considerably high altitude with respect to the ground, patrol certain areas, transportation, deliveries and even data collection [2].

In many military and civilian applications, aerial inspection is needed for the successful reconnaissance and rescue applications; therefore, UAVs are the essential elements in those operations nowadays. Also, UAVs are used for image recognition and capturing to scan certain areas to build a virtual model which can benefit the area of civil engineering.

Flexible assembly is based on the dynamic and continuous re-sequencing of the assembly objects different from the conventional assembly. Therefore smart logistics is used to cope with a flexible assembly that needs a smart control unit and new principles of material supply. UAVs can be used in smart logistics where 3D logistics can be applied due to the availability of the extra dimension for internal logistics processes [3]. Further applications of the UAV are listed below.

- Reconnaissance and Close Air Support Missions [4]
- Search and Rescue missions [5]
- Traffic Monitoring [6]
- Law enforcement [7]
- Power lines inspection and fault detection [8]
- Wildlife monitoring [9]
- Remote sensing-based monitoring system for gas pipelines [10]
- Automatic forest fire monitoring [11]
- Bridge inspection [12]
- 3D mapping of the archaeological sites [13].
- Aerial manipulation and delivery [14]

Due to extensive usage of the UAV, various types of UAVs are produced depending on their applications. UAVs are classified based on the mechanical structure and operations, as shown in the Fig 1.1.

Fixed-wing UAVs require a certain velocity to take off and landing; therefore, a runway is necessary for such designs. However, they can fly with high speed and long endurance. Rotary-wing UAVs have the capability of vertical take-off and landing (VTOL); therefore, rotor aircrafts can hover at a certain altitude and can show high maneuverability. In order to maintain the capabilities of both fixed-wing

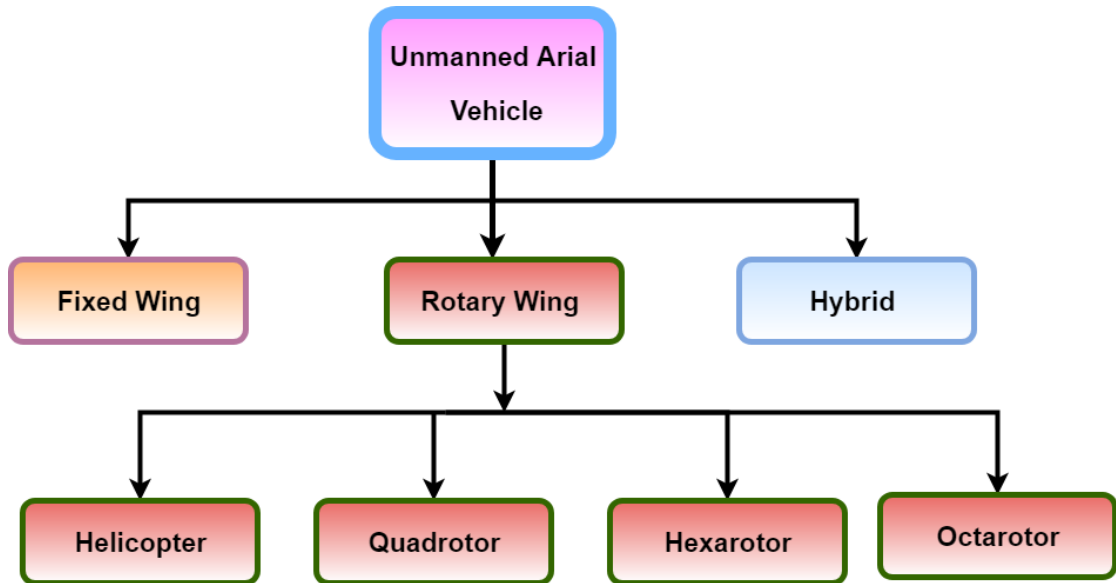


FIGURE 1.1: UAVs classifications

and rotary-wing aircrafts, hybrid design has been recently introduced to develop aircraft with both VTOL and high speed capabilities. Different structures for UAVs have been shown in Fig 1.2.



FIGURE 1.2: Various UAVs

Among UAVs, quadrotor is one of the most used kinds in many civilian and military applications such as precision farming [15], city monitoring [16] and surveillance [17] due to its vertical take-off and landing (VTOL) capability. Therefore

extensive efforts have been made to the quadrotor related research topics due to its simple structure and better maneuverability with low speed flight. However, these advantages come with the challenging task of tracking control of the quadrotor due to inherently unstable, nonlinear, coupled and underactuated dynamics.

## 1.1 Motivation

Robust control algorithms are needed to achieve the efficient trajectory tracking control of UAVs with less errors in the presence of external disturbances, parametric uncertainties and noisy measurements. External disturbances are one of the main problems in efficient trajectory tracking control, so it must be tackled and counteract in order to get better tracking performance. Acceleration feedback control focuses on designing closed-loop control using acceleration signals to enhance robustness against external disturbances. The acceleration feedback signal contains the effects of unknown disturbances. Therefore, acceleration control responds faster and rejects the disturbances successfully. Schmidt and Lorenz [18] demonstrated the principles, design methodologies and implementation of acceleration feedback to substantially improve the performance of dc servo drives. They showed that acceleration feedback acts as electronic inertia to provide higher stiffness to the system. The success of acceleration control techniques in literature depends on the accurate and continuous acceleration feedback. Robust angular accelerations which are estimated by the sensor fusion algorithms are incorporated as feedback signals.

In this thesis, acceleration feedback control is utilized in a hierarchical control structure for robust trajectory control of a quadrotor subject to external disturbances where reference attitude angles are determined through an optimization algorithm. An acceleration based disturbance observer (AbDOB) is designed to reject disturbances acting on the positional dynamics of the quadrotor by utilizing the linear accelerometer readings. For the attitude control, a nested position, velocity, and inner acceleration feedback control structure consisting of PID and

PI type controllers is developed to provide high stiffness against external disturbances. Inertial measurement unit (IMU) is used to measure the angular position of the system. A 9 degree of freedom (DOF) IMU consists of 3-axis accelerometer, 3-axis gyroscope and 3-axis magnetometer. Typically the accelerometer is used to measure specific forces along 3 axes, the angular velocity of the system is measured through the 3-axis gyroscope and the earth's magnetic field is measured through the 3-axis magnetometer. Euler angles are estimated through sensor fusion algorithm such as Kalman filter by utilizing the raw sensor data of the IMU [19]. Unlike the numerical differentiation to generate angular acceleration which induces noise amplification, a cascaded structure which consists of an extended Kalman filter (EKF) and a classical Kalman filter (KF) is used to estimate reliable angular accelerations. By fusing the data from the accelerometer, gyroscope and magnetometer models, an extended Kalman filter is used to estimate the Euler angles and gyro biases. In order to avoid noise amplification due to numerical differentiation, the classical Kalman filter is used to estimate the angular velocities and accelerations from the compensated gyro data. Simulations are carried out on a high fidelity model where sensor noise and bias are also considered. Simulation results show that the proposed controllers provide robust trajectory tracking performance when the quadrotor is subject to wind gusts generated by the Dryden wind model along with the uncertainties and measurement noise.

External disturbances can be constant, periodic or nonperiodic. Disturbance observer is used to estimate the disturbances acting on the system. Especially the acceleration controller realized by the DOB is an effective control concept in motion control of UAV. The acceleration controller realizes an ideal acceleration response suppressing disturbances. In addition, the acceleration controller can design performances of trajectory tracking and disturbance suppression independently. In DOB design, the performance of the disturbance suppression is determined by the Q filter [20]-[21]. As conventional DOB is sensitive to the cutoff frequency of the low-pass filter, higher order and infinite order disturbance observers are used to remove the high-frequency periodic disturbances, but they are not capable to suppress the low-frequency disturbance. The objective of this thesis is to come

up with a new structure of the disturbance observer along with robust nonlinear control to deal with nonlinearities of the system. However, the success of the disturbance observer depends upon the estimation of both low and high-frequency disturbances by the Q filter. Therefore, a new structure for the disturbance observer will be developed to get more robust performance against both periodic and nonperiodic disturbances in the low and high-frequency regions.

Trajectory tracking control of a UAV is usually tackled in a hierarchical framework where reference attitude angles are analytically determined from the desired command signals, i.e., virtual controls (VC), that control the positional dynamics of the UAV and the desired yaw angle is set to some constant value. Although this method is relatively straightforward, it may produce large and nonsmooth reference angles which must be saturated and low-pass filtered. So, a numerical method will be developed to produce reference angles. Determination of desired attitude angles from virtual controls can be viewed as a control allocation problem and it can be solved numerically using nonlinear optimization where the certain magnitude and rate constraints can be imposed on the desired attitude angles and the yaw angle need not be constant. In control allocation, nonlinear constraint optimization is used to obtain required actuator inputs according to command signals by solving an underdetermined system. High-level controller will be designed to obtain the desired command signals from the positional dynamics. Nonlinear constrained optimization will be used to get desired attitude angles from the command signals. Low-level controllers are implemented to ensure that the attitude angles are adjusted according to the desired trajectory. The fully autonomous execution of inspection and aerial manipulation tasks requires UAVs to operate in a wide variety of unknown environmental conditions, including wind gusts, vortices and under uncertain or changing system parameters. Unknown environment forces can arise when a UAV is in contact with a static environment. If large external forces are present, large attitude angles are required for their compensation. To compensate for general uncertainties, disturbance observation (DO) can be utilized. Acceleration-based disturbance observation is well-suited for small

UAVs because acceleration measurements are provided by the Inertial Measurement Unit (IMU). A benefit of a disturbance observer over robust control is that it can directly estimate external disturbances from the system model. This estimate can also be used for environment interaction if no applicable sensors are available. More robustness can be achieved through acceleration based disturbance observer in the attitude dynamics by using angular acceleration feedback obtained through some estimation algorithm.

## 1.2 Contributions of the thesis

Contributions of the thesis are highlighted below.

- A hierarchical control structure is employed where high-level position controllers integrated with acceleration based disturbance observers produce reference angles for the low-level attitude controllers.
- Nonlinear optimization with different magnitude and rate constraints is used to generate smooth and desired bounded attitude angles by considering the positional dynamics of the quadrotor as an underdetermined system. Sequential quadratic programming (SQP) is utilized in nonlinear constraint optimization.
- In order to provide high stiffness against disturbances acting on the attitude dynamics, a nested position, velocity and inner acceleration feedback control structure that utilizes PID and PI type controllers are developed. In order to get reliable angular acceleration signals, a cascaded estimation technique which consists of an extended Kalman filter (EKF) and a classical Kalman filter (KF) is utilized.
- A new disturbance observer is proposed which consists of a bank of band-pass filters connected parallel to the low-pass filter of a classical disturbance observer. Band-pass filters are centered at integer multiples of the fundamental frequency of the periodic disturbance. Sensitivity of the proposed

disturbance observer structure is investigated with increased number and bandwidth of the of band-pass filters.

- The proposed disturbance observer is used in both position and attitude control where it is integrated with PID controllers for the position control and with sliding mode controllers for the attitude control. To ensure fast convergence of the system trajectories toward the sliding surface, a nonlinear sliding surface with an integral term is designed.
- Closed-loop stability of the attitude subsystem is provided through a Lyapunov analysis to show that all system signals remain bounded.

### 1.3 Outline of the thesis

Chapter 2 presents the literature survey and theoretical background for the linear and nonlinear control techniques for the hovering and trajectory tracking control of the UAV, disturbance observers structures, disturbance observer based control, hierarchical control and acceleration feedback. Chapter 3 details the modeling of a quadrotor system. Chapter 4 presents a novel disturbance observer. Chapter 5 explains the estimation of the desired attitude angles through nonlinear optimization. Chapter 6 details the development of the acceleration feedback based trajectory tracking control of a UAV. Chapter 7 presents the robust hovering and trajectory control of the quadrotor subject to both periodic and aperiodic disturbances using the novel disturbance observer. Chapter 8 provides simulation results along with discussions. Finally, Chapter 9 concludes the thesis with several remarks and indicate possible future directions.

### 1.4 Publications

- Hammad Zaki, Gokhan Alcan, Mustafa Unel (2019) Robust Trajectory Control of an Unmanned Aerial Vehicle Using Acceleration Feedback. International Journal of Mechatronics and Manufacturing Systems. (In press)

- 
- Emre Yilmaz, Hammad Zaki, Mustafa Unel (2019) Nonlinear Adaptive Control of an Aerial Manipulation System. In: European Control Conference (ECC 2019), Napoli, Italy, June 25-28.
  - Hammad Zaki, Mustafa Unel (2018) Control of a hovering quadrotor UAV subject to periodic disturbances. In: 6th International Conference on Control Engineering and Information Technology, Istanbul, Turkey 25-26 October.
  - Hammad Zaki, Mustafa Unel, Yildiray Yildiz (2017) Trajectory control of a quadrotor using a control allocation approach. In: International Conference on Unmanned Aircraft Systems (ICUAS 2017), Miami, Florida, USA.
  - Hammad Zaki, Mustafa Unel, Seref Naci Engin (2019) Robust Hovering and Trajectory Tracking Control of a Quadrotor Helicopter Using a Novel Disturbance Observer. (To be submitted)

---

| <i>Abbreviation</i> | <i>Description</i>                                    |
|---------------------|---|
| AADC                | Active Anti Disturbance Control                       |
| AbDOB               | Acceleration based Disturbance Observer               |
| ADRC                | Active Disturbance Rejection Control                  |
| ALS                 | Autocovariance Least Square                           |
| BFGS                | Broyden–Fletcher–Goldfarb–Shanno                      |
| BPF                 | Band-pass Filter                                      |
| COM                 | Center of Mass  |
| DAC                 | Disturbance Accommodation Control                     |
| DOB                 | Disturbance Observer                                  |
| DOBC                | Disturbance Observer Based Control                    |
| DOF                 | Degree of Freedom                                     |
| DUEA                | Disturbance/Uncertainty Estimation and Attenuation    |
| EIFDOB              | Enhanced Infinite Order Disturbance Observer          |
| EKF                 | Extended Kalman Filter                                |
| ESO                 | Extended State Observer                               |
| FC                  | Feedforward Control                                   |
| FTDO                | Finite Time Disturbance Observer                      |
| IFDOB               | Infinite Order Disturbance Observer                   |
| IMU                 | Inertial Measurement Unit                             |
| KF                  | Kalman Filter   |
| KKT                 | Karush Kuhn Tucker                                    |
| LC                  | Learning Control                                      |
| LDUE                | Linear Disturbance and Uncertainty Estimation         |
| LPF                 | Low-pass Filter                                       |
| NDOB                | Nonlinear Disturbance Observer                        |
| NDUE                | Nonlinear Disturbance and Uncertainty Estimation      |
| PAIDO               | Position Acceleration Integrated Disturbance Observer |
| PADC                | Passive Anti Disturbance Control                      |
| PDA                 | Position Derivative Acceleration                      |
| PD                  | Proportional Derivative                               |

---

---

| <i>Abbreviation</i> | <i>Description</i>                  |
|---------------------|-------------------------------------|
| PI                  | Proportional Integral               |
| PID                 | Proportional Derivative Integral    |
| QP                  | Quadratic Programming               |
| SMC                 | Sliding Mode Control                |
| SQP                 | Sequential Quadratic Programming    |
| UAVs                | Unmanned Aerial Vehicles            |
| UIDO                | Unknown Input Disturbance Observer  |
| VbDOB               | Velocity based Disturbance Observer |
| VTOL                | Vertical Take Off and Landing       |
| VC                  | Virtual Control                     |

---

## Chapter 2

# Literature Survey and Background

In recent years, numerous papers dealt with the various problems related to the motion control of the quadrotor. Dynamic modeling issues were addressed in [22] where a linear model was used and the results of a linear quadratic controller were compared with those of a PID controller. Both controllers showed stability issues in the presence of external disturbances. In order to improve the robust performance, feedback linearization technique is employed in [23] where full and partial knowledge of the system is required and also the control accuracy degraded in the presence of uncertainties and noise. Classical and nonlinear control techniques are merged together in [24] to get robust trajectory tracking where integral backstepping and PID controller are combined to stabilize the dynamics. Backstepping based adaptive control technique is proposed by Madani in [25] where the quadrotor type UAV is divided into many linearly connected subsystems and full-state backstepping and adaptive control technique based on the Lyapunov stability theory is proposed for trajectory tracking. Drouot et al. utilizes the backstepping control technique, but the robustness of the controller is limited by the uncertainties.

Sliding mode control and backstepping control are utilized in [26], but this approach provided average results to stabilize the attitude while the structural changes affected the control quality because of the high-frequency disturbances. Zheng et al. in [27] utilized SMC where second order sliding surface is employed to avoid the chattering; however, the prior knowledge of the upper bound of the disturbances is necessary for the satisfactory performance.

Fuzzy controllers based on backstepping technique were developed in [28] and [29] which utilized an adaptive type fuzzy system to generate the control law. However, desired robustness is difficult to achieve due to min-max rules. Type-2 fuzzy neural networks for trajectory tracking were developed by Kayacan et al. with a conventional PD controller and integral of the square of the sliding surface was used for optimal parameter update rules [30].

Alexis et al. in [31] and [32] presented switching model predictive control (MPC) where piecewise affine (PWA) model is developed. However, the robustness of the MPC depends on the development of accurate prediction models, which requires a tedious effort for the control design.

Global trajectory tracking control was proposed without linear velocity measurements in [33]. Nonlinear  $H_\infty$  trajectory tracking controller with input coupling was designed in [34] for the quadrotor with four tilted propellers and the proposed controllers considered the remaining degrees of freedom, apart from the degree of freedom being controlled.

## 2.1 Disturbance Observer Based Control

Almost every physical system is sensitive to external disturbances and parametric uncertainties. Several control techniques have been presented in the literature for robust tracking control. Sometimes disturbances are feed-forwarded if it is measurable, but often it is difficult and expensive to measure the disturbances. Therefore, disturbance observer (DOB) is used to estimate the disturbances, which

is the most popular technique due to its simple structure and disturbance rejection capabilities. DOB employs dynamics and measurable states of the system to estimate the disturbances [35]. As disturbances are not only restricted to the external ones but also plant uncertainties and unmodeled dynamics are taken into consideration, so this kind of technique for disturbance rejection is referred as *disturbance/uncertainty estimation and attenuation* (DUEA) [36].

Different structures for the disturbance observer has been presented based on the applications. These methods are divided into linear disturbance and uncertainty estimation (LDUE) and nonlinear disturbance and uncertainty estimation (NDUE).

Ohnishi presented the frequency domain LDUE, as shown in Fig 2.1 [37] and [38]. It should be noted that the sum of external disturbances acting on the system, nonlinearities and parametric uncertainties in the plant is considered as a total disturbance ( $D$ ) acting from the input side.

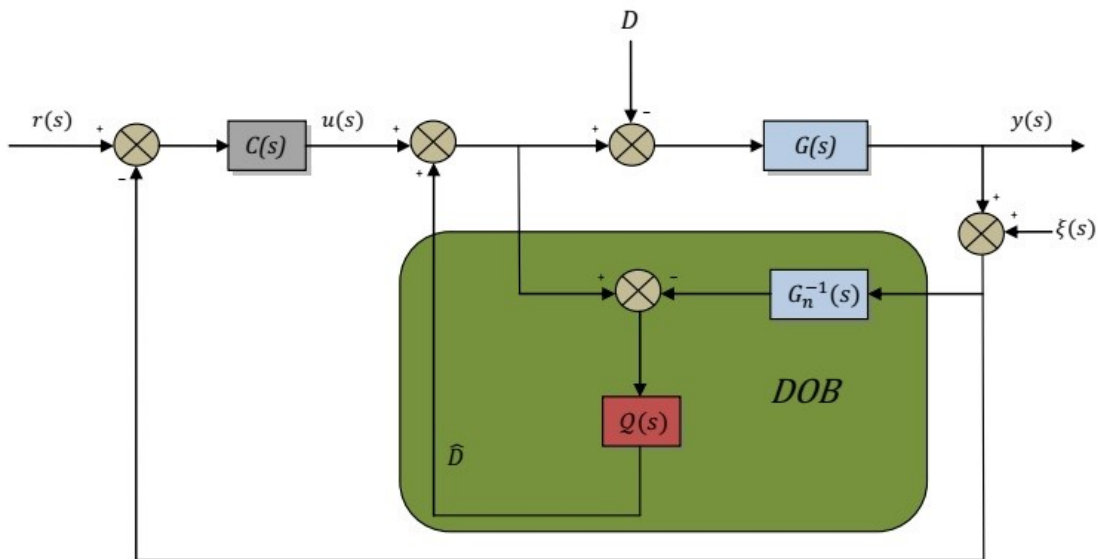


FIGURE 2.1: Disturbance observer based control

Periodic disturbances are one of the main serious issues because of high-frequency harmonics in motion control. Disturbance observer is used to cancel the disturbances [39]. In industrial applications, conventional disturbance observer based control is popular because of its simplicity. It is used to estimate the disturbances,

which includes uncertainties and external disturbances. The estimated signal is then fed back as a compensation signal to cancel the disturbance. Therefore, the disturbance observer aims to counteract the disturbances directly rather than attenuating their effect through (or via) feedback regulation. Disturbances can be estimated if they stay within the bandwidth of the low-pass filter of disturbance observer. In a conventional disturbance observer, the performance depends on the low-pass filter (Q filter) cutoff frequency, which is very critical, and the bandwidth of the disturbance observer is desired to be set as high as possible to estimate/suppress disturbances in a wide frequency range; however, it is limited by noise and robustness constraints. Hence periodic disturbance suppression is difficult to achieve with the conventional disturbance observer structure [40].

Yamada et al. in [41] presented high order disturbance observer to improve the performance against periodic disturbances. Disturbance compensation loop of the disturbance observer had been utilized to transform the plant into two degrees of freedom control system with a cascaded compensator such as P and PI depending on the order of the disturbance observer. Disturbance rejection performance in the low-frequency region had been analyzed and the relationship between the stability and the order of the Q filter of the disturbance observer had been studied. As such observer was studied for the low-frequency region only, high-frequency harmonics cannot be removed. In order to compensate for high-frequency periodic disturbances, infinite order disturbance observer (IFDOB) had been studied by considering all frequencies of the periodic disturbances [40]. However, with IFDOB it is difficult to suppress the low-frequency disturbances if the fundamental frequency lies in the low-frequency region. Enhanced infinite order disturbance observer (EIFDOB) had been presented recently to remove the disturbances in the low as well as high-frequency regions [42].

Han proposed the extended state observer (ESO) which is categorized as the time domain disturbance observer [43],[44] and [45]. Single input single output system

with disturbances can be written as

$$\begin{aligned}\dot{x}_i &= x_{i+1}, \quad i = 1, \dots, n-1 \\ \dot{x}_n &= f(x_1, x_2, \dots, x_n, d, t) + bu\end{aligned}\tag{2.1}$$

where  $u$  and  $d$  are input and disturbance respectively. By selecting a new state as

$$\begin{aligned}x_{n+1} &= f(x_1, x_2, \dots, x_n, d, t) \\ \dot{x}_{n+1} &= h(t)\end{aligned}\tag{2.2}$$

with  $h(t) = \dot{f}(x_1, x_2, \dots, x_n, d, t)$ . All the lumped disturbances and states are estimated through ESO as

$$\begin{aligned}\dot{\hat{x}}_i &= \hat{x}_{i+1} + \beta_i(y - \hat{x}_1), \quad i = 1, \dots, n-1 \\ \dot{\hat{x}}_{n+1} &= \beta_{n+1}(y - \hat{x}_1)\end{aligned}\tag{2.3}$$

From eq (2.3), it can be observed that the uncertainties and external disturbances can be estimated by ESO. Various versions of ESO can be found in [46].

Unknown input disturbance observer (UIDO) was proposed by Johanson [47] by utilizing the state observer technique for joint state and disturbances estimation. State feedback controller can be combined with such observer to produce disturbance accommodation control (DAC). Dynamical system in the state space form can be written as

$$\begin{aligned}\dot{x} &= Ax + B_u u + B_d d \\ y &= Cx\end{aligned}\tag{2.4}$$

Disturbance can be considered to be generated by the following exogenous system

$$\begin{aligned}\dot{\xi} &= W\xi \\ d &= V\xi\end{aligned}\tag{2.5}$$

The observer was designed to estimate the state and disturbance simultaneously as

$$\begin{aligned}\dot{\hat{x}} &= A\hat{x} + L_x(y - \hat{y}) + B_u u + B_d \hat{d} \\ \hat{y} &= C\hat{x}\end{aligned}\tag{2.6}$$

$$\begin{aligned}\dot{\hat{\xi}} &= W\hat{\xi} + L_d(y - \hat{y}) \\ \hat{d} &= V\hat{\xi}\end{aligned}\tag{2.7}$$

where  $\hat{x}$ ,  $\hat{d}$  and  $\hat{\xi}$  are the estimates of the state vector  $x$ , disturbances  $d$  and exogenous system state vector  $\xi$ , respectively.  $L_x$  and  $L_d$  are the observer gains to be designed in such a way that states in eq (2.6) and disturbances in eq (2.7) asymptotically estimate the states and disturbances by forcing the observer error dynamics to zero. Further different modified structures of the UIDO can be found in [48] and [49].

In LDUE nonlinear terms are considered as a lumped disturbance along with the parametric uncertainties and external disturbances, however appropriate control action is required to compensate the effect of nonlinearities [50] and [51]. This is the idea behind the active disturbance rejection control (ADRC) [43] where dynamics of the system is considered as integrator chain system by ignoring both the linear and nonlinear dynamics of the system and disturbance observer takes care of all the ignored terms. However, if the nonlinear dynamics of the system is fully or partially known, disturbance rejection performance can be improved by exploiting the dynamics. This motivation led researchers to the development of nonlinear disturbance observer for nonlinear systems.

Chen et al. developed the nonlinear disturbance observer (NDOB) for the robotic manipulator system [52]. Consider the affine nonlinear system as

$$\begin{aligned}\dot{x} &= f(x) + g_1(x)x + g_2(x)d \\ y &= h(x)\end{aligned}\tag{2.8}$$

The following NDOB was proposed to cancel the unknown disturbances

$$\begin{aligned}\dot{z} &= -l(x)g_2(x)z - l(x)[g_2(x)p(x) + f(x) + g_1(x)u] \\ \hat{d} &= z + p(x)\end{aligned}\tag{2.9}$$

where  $z$  is the internal state of the observer and  $p(x)$  is the nonlinear function to be designed whereas  $l(x)$  is given as

$$l(x) = \frac{\partial p(x)}{\partial x}\tag{2.10}$$

Disturbance observer error dynamics is given

$$\dot{e}_d = -l(x)g_2(x)e_d\tag{2.11}$$

where  $e_d = \hat{d} - d$ . From eq (2.11) it can be concluded that if  $l(x)$  is carefully designed, then the estimation error asymptotically goes to zero. Further studies about NDOB can be found in [53–58].

## 2.2 Acceleration Feedback

Acceleration feedback based control employs acceleration signal in designing the closed-loop control to increase the dynamic stiffness against the disturbances. Acceleration feedback acts like electronic inertia against the disturbance; therefore, acceleration control responds more quickly and counteracts the disturbances by moving the system opposite to the disturbance response.

Schmidt and Lorenz utilized the acceleration feedback to improve the performance of the DC drives [59] and [18]. Acceleration feedback was utilized to improve the stiffness of the drive in motion control application where load variation significantly affects the performance.

The success of acceleration control techniques in literature depend on the accurate and continuous acceleration feedback. Han et al. utilized acceleration feedback

for multiple degrees of freedom mechatronics systems where angular acceleration signals are estimated through Newton predictor enhanced Kalman filter [60]. In-sperger et al. showed the improvement induced by acceleration feedback utilizing proportional-derivative-acceleration (PDA) feedback in a model for human postural balance where the problem of the feedback delay was encountered [61].

Disturbance observer based on acceleration feedback has been presented in [62],[63] and [64] to show the improved robustness introduced due to acceleration feedback. Jeong et al. proposed an acceleration based disturbance observer (AbDOB) to introduce robustness for the attitude control of the quadrotor against external disturbances, where angular acceleration is generated through the numerical differentiation [65]. Angular velocity measurements from the gyro sensor are exploited to get the angular acceleration through differentiation. Further disturbance observer based on the estimated acceleration signal is used to estimate the control input and disturbance are estimated through the difference of the nominal and estimated control input. Estimated disturbances are feedforwarded to cancel the disturbance which perform better than the classical controllers like PD. Conventional disturbance observer employed the second derivative to get acceleration signal; therefore, the bandwidth of the disturbance observer is constrained by the noise. Tomic et al. in [66] utilized acceleration based disturbance observation with a boundary-layer integral sliding mode control in attitude control of small UAVs to reject modeling uncertainties and external disturbances. Position acceleration integrated disturbance observer (PAIDO) was proposed to increase the bandwidth of a disturbance observer in the presence of noise [67]. Mizochi et al. [68] presented the relationship between the bandwidth of the disturbance observer and the sampling frequency of the acceleration signal. Disturbance observer based on multirate sampling frequency is employed to enhance the disturbance rejection performance. Shang and Cong [69] proposed dynamic acceleration feedback for the disturbance rejection in trajectory tracking control where acceleration signals are estimated through closed-loop constrained equations. The authors provided experimental results to show the considerable improvement in the tracking performance, achieved through sudden increase and decrease in acceleration.

Hybrid  $H_\infty$  adaptive fuzzy controller was proposed in [70] by combining the  $H_\infty$  with acceleration feedback and adaptive fuzzy logic controller for the motion control system like brushless servo drive system. Both controllers are integrated together to provide increased stiffness against the parametric uncertainties and external disturbances where adaptive law for fuzzy controller is developed through Lyapunov analysis.

## 2.3 Hierarchical Control

Hierarchical control for rotary wing UAVs is one of the most interesting techniques which rely on the time scale separation of the translational dynamics (slow time scale) and rotational dynamics (fast time scale). It consists of two parts, namely a high-level control for translational dynamics (outer loop) which produces desired commands, which in turn used to produce desired attitude angles for accurate trajectory tracking. Later on, based on the desired attitude angles, a low-level control is implemented for efficient orientation tracking.

Control of a rotary-wing UAV using a hierarchical structure was considered in [71], [72] where disturbance observer and PID controllers were used for high and low-level controllers. Yildiz et al. in [73] and [74] applied hierarchical control structure on the tilt-wing quadrotor by exploiting the dynamics of the quadrotor where model reference adaptive control is used for the outer loop and nonlinear adaptive control is used for the inner loop control. Drouot et al. utilizes the backstepping control technique in the hierarchical control framework, but the robustness of the controller is limited by the uncertainties [75]. Tracking controllers were proposed in Formentin and Lovera in [76] where a flatness based technique was utilized for the position and global stability was shown for attitude control. Predictive control and nonlinear  $H_\infty$  control were developed by Raffo et al. in [34] for trajectory tracking where model predictive control was used for positional dynamics and nonlinear  $H_\infty$  controller was formulated through the game theory.

---

Aboudonia et al. recently proposed the composite hierarchical anti-disturbance control of quadrotor in the presence of matched and mismatched disturbance where sliding mode control is positional control and nonlinear disturbance observer is integrated with sliding mode for the attitude control [77]. Disturbance observer is used to estimate the slowly varying matched and mismatched disturbances and sliding mode is used to counteract the fast varying disturbances. Mokhtari et al. presented finite time disturbance observer (FTDO) blended with integral backstepping control in a hierarchical control framework for positional and attitude control of the rotary-wing UAV. FTDO is used for fast convergence for timely compensation of disturbance observer [78].

## Chapter 3

# Modeling of a Quadrotor System

A quadrotor is a kind of unmanned aerial vehicle (UAV) which consists of a cross structure with four rotors connected at each edge. The crossed configuration presents robustness although the mechanically linked motors are heavier than the frame [79]. Propellers are connected to the motors with the help of reduction gears. The motion of the quadrotor depends upon the direction of the rotation of the propellers. Front and rear propellers rotate counterclockwise, while the left and the right ones turn clockwise. Unlike the standard helicopter structure, the tail rotor is not required because of the opposite rotation directions of the propeller pairs. Fig. 3.1 shows the model in a hovering state, where all the propellers have the same speed. Two frames of references are used to describe the motion of a quadrotor, one of which is fixed and called inertial frame and the other one, which is moving, called body frame. By increasing (decreasing) the speed of the propellers equally, quadrotor is raised (or lowered) with the help of thrust command ( $U_1$ ), which is the vertical force w.r.t body frame. Similarly, increasing (or decreasing) the speed of the left propeller and decreasing (or increasing) the right one results into roll command ( $U_2$ ), which makes the quadrotor to turn due to the torque around the x-axis. The pitch command ( $U_3$ ) is very similar to the roll, but in this case, increase (or decrease) in the rear propeller speed and decrease (or increase) in the front one leads to torque around the y-axis, which makes the quadrotor to turn. In order to enable the quadrotor to turn around the z-axis,

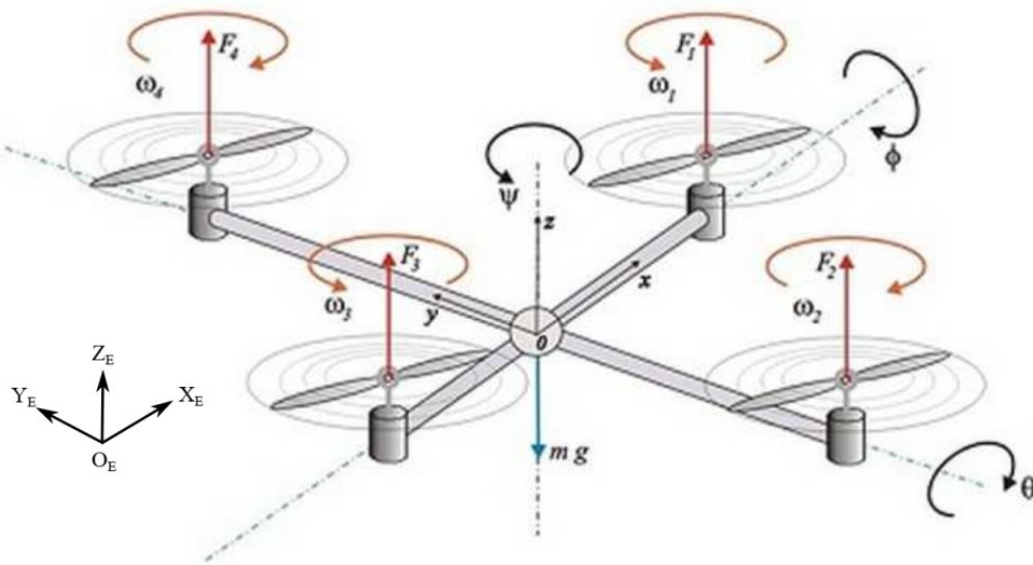


FIGURE 3.1: Quadrotor dynamics

torque is provided by the yaw command ( $U_4$ ), which is generated by increasing (or decreasing) the front-rear propellers speed and by decreasing (or increasing) the speed of the left-right couple propellers. A detailed description of the quadrotor dynamics can be found in [79]. The quadrotor positional dynamics is expressed in the inertial frame ( $X_E, Y_E, Z_E$ ) and the attitude dynamics is expressed in the body frame.

### 3.1 Newton-Euler Model for Quadrotor

In this section, by considering the aerial vehicle as 6 degree of freedom (DOF) rigid body, a complete dynamical model is derived using Newton-Euler formulation. Linear positions and velocities of the vehicle are expressed in the world fixed earth frame, and angular position and velocities are expressed in the body frame of the vehicle.  $O_E$  is the origin of the world frame, and  $O$  is the origin of the body frame. Origin of the body frame  $O$  is considered coincident with the center of mass (COM) of the body which makes the derivation of the equations considerably easy. The inertia matrix  $I_B$  is taken as a diagonal matrix, considering the fact that axes of the body frame are consistent with the body axes of inertia [80] and [71].

The generalized matrix form of 6 DOF rigid-body of the quadrotor is given as

$$\dot{\xi} = H_{\Theta}\rho \quad (3.1)$$

where  $\dot{\xi}$  is the velocity vector is expressed in the world frame,  $\rho$  is the velocity vector in the body frame and  $H_{\Theta}$  is the generalized matrix.

Position coordinates and linear velocity expressed in the earth fixed frame are defined by the vector.

$$\varrho = [X, Y, Z], \quad V_W = \dot{\varrho} = [\dot{X}, \dot{Y}, \dot{Z}], \quad (3.2)$$

Euler angles and Euler rates in the earth fixed frame are defined by the vectors as

$$\Theta = [\phi, \theta, \psi]^T, \quad \dot{\Theta} = [\dot{\phi}, \dot{\theta}, \dot{\psi}]^T \quad (3.3)$$

where  $\phi, \theta$  and  $\psi$  are roll, pitch and yaw angles respectively. Angular velocity and acceleration of the quadrotor expressed in the body frame are defined as

$$\omega = [p, q, r]^T, \quad \alpha = [\dot{p}, \dot{q}, \dot{r}]^T \quad (3.4)$$

$H_{\Theta}$  in eq (3.1) is the combination of the matrices which is given as

$$H_{\Theta} = \begin{bmatrix} R_{\Theta} & 0_{3 \times 3} \\ 0_{3 \times 3} & T_{\Theta} \end{bmatrix} \quad (3.5)$$

where  $R_{\Theta}$  is the rotational matrix to express the orientation of the body frame with respect to earth frame which is given as

$$R_{\Theta} = \begin{bmatrix} c_{\psi}c_{\theta} & -s_{\psi}c_{\theta} + c_{\psi}s_{\theta}s_{\phi} & c_{\phi}s_{\theta}c_{\psi} + s_{\phi}s_{\psi} \\ s_{\psi}c_{\theta} & c_{\psi}c_{\theta} + s_{\psi}s_{\theta}s_{\phi} & c_{\phi}s_{\theta}s_{\psi} - s_{\phi}c_{\psi} \\ -s_{\theta} & c_{\theta}s_{\phi} & c_{\theta}s_{\phi} \end{bmatrix} \quad (3.6)$$

Therefore linear velocities in the world frame and body frame are related as

$$V_B = R_{\Theta}^T V_W \quad (3.7)$$

$T_{\Theta}$  is the transformation matrix to relate the angular velocity ( $\Omega$ ) in the body to the Euler rates ( $\dot{\Theta}$ ) in the world frame of the vehicle

$$T_{\Theta} = \begin{bmatrix} 1 & s_{\phi} t_{\theta} & c_{\phi} t_{\theta} \\ 0 & c_{\phi} & -s_{\phi} \\ 0 & \frac{s_{\phi}}{c_{\theta}} & \frac{c_{\phi}}{c_{\theta}} \end{bmatrix} \quad (3.8)$$

In this equation  $c(\cdot)$  and  $s(\cdot)$  denotes  $\cos(\cdot)$  and  $\sin(\cdot)$  respectively.

By considering the mass of the body  $m$  [kg] and its inertia matrix  $I_B$  [Nm.s<sup>2</sup>] of the quadrotor, its dynamics can be written as

$$\begin{bmatrix} mI_{3 \times 3} & 0_{3 \times 3} \\ 0_{3 \times 3} & I \end{bmatrix} \begin{bmatrix} \dot{V}_B \\ \dot{\omega}_B \end{bmatrix} + \begin{bmatrix} \omega_B \times (mV_B) \\ \omega_B \times (I \omega_B) \end{bmatrix} = \begin{bmatrix} F_B \\ \tau_B \end{bmatrix} = F_T \quad (3.9)$$

$\dot{V}_B$  linear acceleration vector and  $\dot{\omega}_B$  angular acceleration vector of the quadrotor with respect to body frame respectively. In addition,  $F_B$  is the quadrotor total forces vector and  $\tau_B$  is the quadrotor moments vector expressed in the body frame.

By considering the external disturbances, the dynamics of a quadrotor can be rewritten in vector-matrix notation as

$$M_B \dot{v} + C_B(v)v = F_T \quad (3.10)$$

Where  $\dot{v}$  and  $v$  are the acceleration velocity vector with respect to body frame, respectively.  $M_B$  is the system mass-inertia matrix and  $C_B(v)$  is the Coriolis-centripetal matrix in the body frame.

$$M_B = \begin{bmatrix} m I_{3 \times 3} & 0_{3 \times 3} \\ 0_{3 \times 3} & I_B \end{bmatrix} \quad (3.11)$$

Coriolis-centripetal matrix is given by

$$C_B(v) = \begin{bmatrix} 0_{3 \times 3} & -m S(V_B) \\ 0_{3 \times 3} & -S(I \omega) \end{bmatrix} = \begin{bmatrix} 0 & 0 & 0 & 0 & m w & -m u \\ 0 & 0 & 0 & -m w & 0 & m u \\ 0 & 0 & 0 & m v & -m u & 0 \\ 0 & 0 & 0 & 0 & I_{zz} r & I_{yy} q \\ 0 & 0 & 0 & -I_{zz} r & 0 & I_{xx} p \\ 0 & 0 & 0 & I_{yy} q & -I_{xx} p & 0 \end{bmatrix} \quad (3.12)$$

where  $S$  is the skew matrix. Right hand side of the eq (3.10) can be expressed as a combination of four components.

$$F_T = G_B + O_B(\rho)\omega_p + E_B(\varrho)\omega_p^2 + D \quad (3.13)$$

The first term in the eq (3.13) is the gravitational vector  $G$  from the acceleration due to gravity. From Fig. 3.1, it can be concluded easily that this term is just a force; therefore, it only contributes to the linear dynamics of the quadrotor.  $G_B(\xi)$  is given as

$$G_B(\xi) = \begin{bmatrix} R_{\Theta}^T \\ 0_{3 \times 1} \end{bmatrix} \begin{bmatrix} 0_{2 \times 1} \\ -mg \end{bmatrix} = \begin{bmatrix} m g s_{\theta} \\ -m g c_{\theta} s_{\phi} \\ -m g c_{\theta} s_{\phi} \\ 0_{3 \times 1} \end{bmatrix} \quad (3.14)$$

The second term in the compact dynamic equation of the quadrotor takes into account the gyroscopic effects, which is due to the unbalanced rotational speed of the four rotors. Since the front and rear propellers rotate counter-clockwise and left and right propeller rotated clockwise, each rotor produces reactive torque. The magnitude of the reactive torque is proportional to the rotor speed. If the rotor speed are well synchronized in the hover condition, the reactive torques will be well balanced and quadrotor will not rotate during vertical take-off and landing.

The gyroscopic term in the body frame is given as

$$O_B(\rho)\omega_p = \begin{bmatrix} 0_{3 \times 1} \\ J_{TP} \begin{bmatrix} -q \\ p \\ 0 \end{bmatrix} \end{bmatrix} \omega_p = J_{TP} \begin{bmatrix} 0 & 0 & 0 & 0 \\ 0 & 0 & 0 & 0 \\ 0 & 0 & 0 & 0 \\ q & -q & q & -q \\ -p & p & p & p \\ 0 & 0 & 0 & 0 \end{bmatrix} \omega_p \quad (3.15)$$

$O_B$  is the gyroscopic propeller matrix and  $J_{TP}$  is the total rotational moment of inertia around the propeller axis. It is easy to see that the gyroscopic effects produced by the propeller rotation are just related to the angular and not the linear equations. Combined propeller speed is given by

$$\omega_p = -\omega_1 + \omega_2 - \omega_3 + \omega_4 \quad (3.16)$$

The third vector in the eq (3.13) shows the forces and torque generated by the rotors. According to the well known phenomenon in aerodynamics, forces and moment are proportional to the square of each propeller speeds [81]. Moment vector is given by

$$E_B\omega_p^2 = \begin{bmatrix} 0 \\ 0 \\ U_1 \\ U_2 \\ U_3 \\ U_4 \end{bmatrix} = \begin{bmatrix} 0 \\ 0 \\ b(\omega_1^2 + \omega_2^2 + \omega_3^2 + \omega_4^2) \\ lb(-\omega_2^2 + \omega_4^2) \\ lb(-\omega_1^2 + \omega_3^2) \\ d(-\omega_1^2 + \omega_2^2 - \omega_3^2 + \omega_4^2) \end{bmatrix} \quad (3.17)$$

where  $E_B$  is expressed as

$$E_B = \begin{bmatrix} 0 & 0 & 0 & 0 \\ 0 & 0 & 0 & 0 \\ b & b & b & b \\ 0 & -bl & 0 & bl \\ -bl & 0 & bl & 0 \\ -d & d & -d & d \end{bmatrix} \quad (3.18)$$

where  $l, b$  and  $d$  are length of rotor arm, thrust factor and drag factor respectively.

$$M_B \dot{v} + C_B(v)v = G_B + O_B(v)\omega_p + E_B \omega_p^2 \quad (3.19)$$

By rearranging equation it is possible to isolate the derivative of the generalized

$$\dot{v} = M_B^{-1}(-C_B(v)v + G_B + O_B(v)\omega_p + E_B \omega_p^2) \quad (3.20)$$

All the dynamics stated so far is expressed in the body frame of the quadrotor; therefore, there is a need to define the hybrid frame where translational motion is expressed in earth fixed inertial frame and angular motion expressed in the body frame. Therefore eq (3.10) can be expressed in the hybrid frame as

$$M_{B,W} \dot{\xi} + C_{B,W}(\xi)\xi = G_{B,W} + O_{B,W}(\xi)\omega_p + E_{B,W}\omega_p^2 + D \quad (3.21)$$

where  $\dot{\xi}$  and  $\xi$  are acceleration and velocity vectors w.r.t hybrid frame respectively. Since  $M_B$  consists of mass and inertia expressed in world and body frame respectively,  $M_{B,W}$  will remain unchanged. However, the Coriolis matrix can be

redefined in the hybrid frame as

$$C_{B,W}(v) = \begin{bmatrix} 0_{3 \times 3} & 0_{3 \times 3} \\ 0_{3 \times 3} & -S(I \omega^B) \end{bmatrix} = \begin{bmatrix} 0 & 0 & 0 & 0 & 0 & 0 \\ 0 & 0 & 0 & 0 & 0 & 0 \\ 0 & 0 & 0 & 0 & 0 & 0 \\ 0 & 0 & 0 & 0 & I_{zz} r & I_{yy} q \\ 0 & 0 & 0 & -I_{zz} r & 0 & I_{xx} p \\ 0 & 0 & 0 & I_{yy} q & -I_{xx} p & 0 \end{bmatrix} \quad (3.22)$$

Gravitational vector is defined in hybrid frame as

$$G_{B,W}(\xi) = \begin{bmatrix} 0_{2 \times 1} \\ -m g \\ 0_{3 \times 1} \end{bmatrix} \quad (3.23)$$

As mentioned earlier, the gyroscopic effects  $O(\xi)$  only affect the rotational dynamics of the quadrotor in the body frame; therefore, it remains unvaried as in eq (3.15).

Moment matrix  $E_{B,W}$  in the hybrid frame will not be same as in the body frame because input  $U_1$  will be related to all three translational motion equations through the rotational matrix  $R_\Theta$ . Moment matrix can be redefined as

$$E_{B,W}(\varrho)\omega_p^2 = \begin{bmatrix} R_\Theta & 0_{3 \times 3} \\ 0_{3 \times 3} & I_{3 \times 3} \end{bmatrix} E_B(\varrho)\omega_p^2 = \begin{bmatrix} (c_\phi s_\theta c_\psi + s_\phi s_\psi)U_1 \\ (c_\phi s_\theta s_\psi - s_\phi c_\psi)U_1 \\ (c_\phi c_\theta)U_1 \\ U_2 \\ U_3 \\ U_4 \end{bmatrix} \quad (3.24)$$

where the control inputs  $U_{1,2,3,4}$  explicitly expressed as

$$\begin{aligned}
 U_1 &= b(\omega_1^2 + \omega_2^2 + \omega_3^2 + \omega_4^2) \\
 U_2 &= lb(-\omega_2^2 + \omega_4^2) \\
 U_3 &= lb(-\omega_1^2 + \omega_3^2) \\
 U_4 &= d(-\omega_1^2 + \omega_2^2 - \omega_3^2 + \omega_4^2)
 \end{aligned} \tag{3.25}$$

The fourth term in the hybrid dynamics equation represents the disturbance acting on the positional and attitude dynamics of the quadrotor and can be defined as

$$D = \begin{bmatrix} D_X & D_Z & D_Z & D_\phi & D_\theta & D_\psi \end{bmatrix}^T \tag{3.26}$$

After combining all the terms defined in eq (3.21), the positional and attitude dynamics of the quadrotor can be expressed as follows.

$$\begin{aligned}
 \ddot{X} &= (\sin \psi \sin \phi + \cos \psi \sin \theta \cos \phi) \frac{U_1}{m} + D_X \\
 \ddot{Y} &= (-\cos \psi \sin \phi + \sin \psi \sin \theta \cos \phi) \frac{U_1}{m} + D_Y \\
 \ddot{Z} &= -g + (\cos \theta \cos \phi) \frac{U_1}{m} + D_Z \\
 \dot{p} &= \frac{I_{yy} - I_{zz}}{I_{xx}} qr - \frac{J_{prop}}{I_{xx}} q \omega_p + \frac{U_2}{I_{xx}} + D_\phi \\
 \dot{q} &= \frac{I_{zz} - I_{xx}}{I_{yy}} pr + \frac{J_{prop}}{I_{yy}} p \omega_p + \frac{U_3}{I_{yy}} + D_\theta \\
 \dot{r} &= \frac{I_{xx} - I_{yy}}{I_{zz}} pq + \frac{U_4}{I_{zz}} + D_\psi
 \end{aligned} \tag{3.27}$$

Noticed that there are four inputs  $U_{1,2,3,4}$  to control the 6 DOF system, therefore quadrotor is an underactuated system.

## Chapter 4

# A Novel Observer for Estimating Periodic Disturbances

Disturbances and plant uncertainties widely exist in every physical system, which are inevitable and bring significant effect to the stability and performance of the control systems. Therefore disturbance rejection is the critical issue in designing the control system. For this purpose, different techniques are used in the literature such as adaptive, robust and sliding mode control where feedback control is used to suppress the disturbances. The controllers designed through feedback regulation depend upon the tracking error between the actual value and the desired value; therefore, the controllers react slowly to suppress the disturbances [82]. The techniques based on feedback control are classified as passive anti disturbance control (PADC) [43].

In order to get the fast response and surpass the performance of the PADC methods in rejecting the disturbances, an active anti disturbance control (AADC) approach was proposed [82]. The key concept behind the AADC method is to design a control system based on feedforward compensation by measuring or estimating the disturbances directly.

Traditionally, feedforward control (FC) is realized through sensors in the AADC method to measure the disturbances directly. FC is one of the direct methods

to attenuate the disturbances by utilizing the system model, disturbance channel model and measurements [39]. However, in most cases, especially the industrial processes, it is impossible or difficult to measure the disturbances directly due to unavailability or the cost of the sensors. In order to implement the FC approach and overcome the problem of direct measurement, disturbance estimation techniques greatly attracted the control community to meet both ends together. Disturbance observer is a popular AADC technique in motion control due to its simple control architecture. External disturbances and uncertainties are modeled as unknown input signals. Disturbance observer (DOB) gives the estimate of the disturbance; then control input can be designed based on the estimated disturbance to eliminate the effect of the disturbance. One of the major advantages of this approach lies in the utilization of the separation principle, that is, disturbance rejection and the tracking performance can be achieved by designing the feedback and feedforward controllers separately. Such promising characteristic results into the following advantages as compared to the passive disturbance rejection approach where feedback regulation is utilized [39].

- Disturbance observer based control method provides a faster response as compare to passive disturbance control technique as it depends on the feedforward compensation.
- Disturbance observer based control method estimates and compensates disturbances online; therefore it is less conservative than most of the robust control techniques where worst case design is utilized to achieve the better robustness performance on the cost of degraded nominal performance.
- Due to the separation principle, no change in the baseline control is required in disturbance observer based control method. Therefore instead of designing completely new control techniques which require verification, existing control strategies can be combined with disturbance observer to improve robustness of the control systems.

### 4.1 A Novel Disturbance Observer

The block diagram of the conventional/classical disturbance observer [39] is shown in Fig. 4.1, which consists of a simple low-pass filter (Q filter).  $D$  is the disturbance and  $\hat{D}$  is the estimated disturbance.  $G_n^{-1}(s)$  is the inverse of the nominal plant and  $\zeta(s)$  represents the sensor noise. The disturbance observer based controller exhibits better robustness as it is placed in the inner loop. An inner loop is used to compensate for the uncertainties and external disturbances. As all the external disturbances are dealt by the inner loop, the outer loop considers the rest of the plant as nominal. Therefore, there is plenty of freedom in designing the controller for the outer loop. It also has the advantage of simple structure; consequently, it is used in many applications. However, the performance decreases with the increase in the level of uncertainty and noise. From Fig. 4.1, the transfer function from

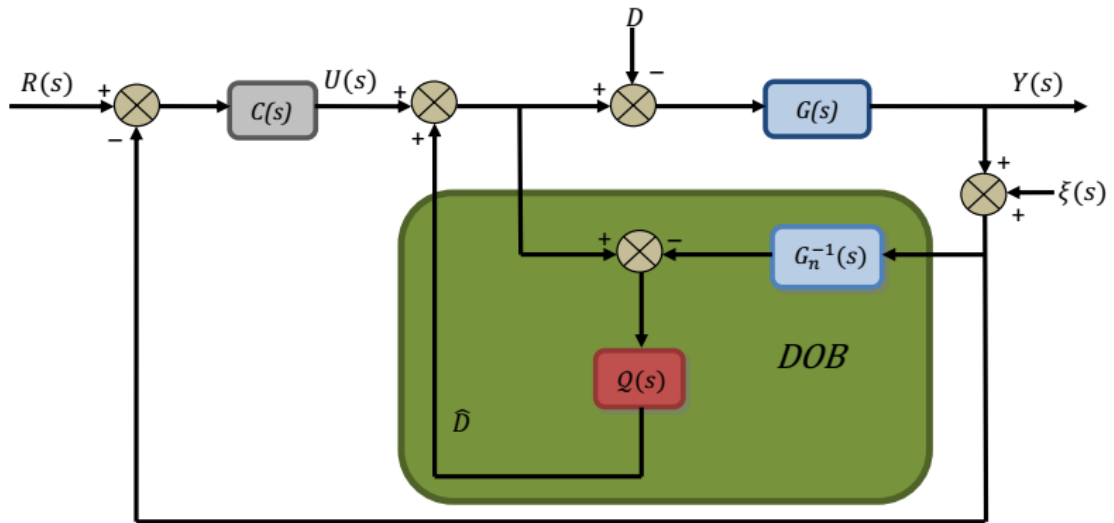


FIGURE 4.1: Disturbance observer based control

the inputs  $(u, D, \zeta)$  of the DOB loop to the output  $(y)$  can be written as

$$y(s) = G_{Dy}D + G_{uy}u(s) + G_{\zeta y}\zeta(s) \tag{4.1}$$

where  $G_{Dy}$ ,  $G_{uy}$  and  $G_{\zeta y}$  are given as

$$G_{Dy} = \frac{GG_n(1 - Q)}{Q(G - G_n) + G_n} \tag{4.2}$$

$$G_{wy} = \frac{GG_n}{Q(G - G_n) + G_n} \quad (4.3)$$

$$G_{\zeta y} = \frac{GQ}{Q(G - G_n) + G_n} \quad (4.4)$$

From the above transfer functions when  $Q \approx 1$ , it follows that  $G_{Dy} \approx 0$  and  $G_{wy} \approx G_n$ . Therefore, the total disturbance acting on the system is suppressed in the low-frequency region and the system is linearized with a nominal transfer function. However, at the same time,  $G_{\zeta y} = 1$  and noise will pass unattenuated. When  $Q = 0$ , the noise will be blocked, but disturbances will not be rejected and  $G_{wy}$  will not be equal to the nominal plant. In order to make the disturbance observer loop realizable,  $Q$  cannot be constant.

The disturbance rejection performance of the DOB is directly related to the low-pass filter  $Q(s)$ . The cutoff frequency of the low-pass filter is very critical due to characteristics of the disturbances  $D$ , uncertainties and  $\xi$  measurement noise. In order to compensate the high-frequency disturbances, the bandwidth of the low-pass filter should be large enough to estimate all frequency components of the disturbances.

In the case of aerial vehicles, external disturbances are always consist of winds, such as a constant wind, gusts and a buffeting wind. A buffeting periodic wind disturbance along with high-frequency sensor noise could be considered as the worst case scenario for such a vehicle making control very difficult. Periodic disturbances have generally higher frequency harmonics, and in order to estimate the high-frequency components with the help of classical disturbance observer structure, large bandwidth of the  $Q(s)$  filter can be selected to capture all frequency components. However, increasing the bandwidth can affect the robustness of the system and degrades the disturbance rejection performance of the classical disturbance observer [36]. This situation becomes worse with an increased noise level.

Since it is difficult to achieve the desired disturbance rejection performance in the presence of high-frequency periodic disturbances with classical disturbance observer, the following key factors are taken into account for designing the  $Q$  filter of the new disturbance observer.

- A low-pass filter is added to capture the low-frequency components with limited bandwidth in order to maintain the robustness of disturbance observer, which is constrained by the noise.
- In order to capture the high-frequency periodic disturbances, instead of using one band-pass filter with large bandwidth where high-frequency noise components can compromise the robustness of the observer, several band-pass filters are added in parallel with the low-pass filter as shown in Fig 4.2.
- The central frequency of the band-pass filters are the integral multiples of the fundamental frequency of the periodic disturbances which is assumed to be known and can be estimated through different algorithms in the literature.
- Bandwidth and number of the band-pass filters are two main factors which are studied in this work.
- Increased number of band-pass filters also improved the disturbance estimation performance but at the cost of more computation.
- The bandwidth of the band-pass filters is an important parameter to design. Increasing the bandwidth will accommodate more high-frequency components; therefore, disturbance estimation can be improved with increased bandwidth.

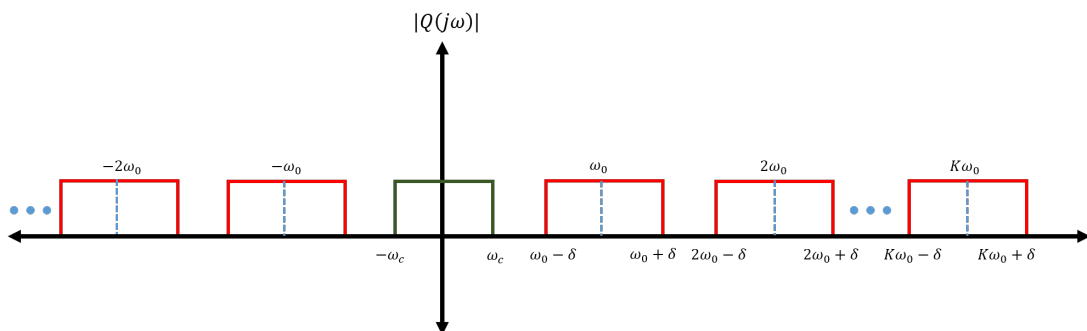


FIGURE 4.2: Frequency distribution

The difference of two low-pass filters or high-pass filters with different cutoff frequencies can be utilized to achieve the band-pass filter characteristics. In this study, we used low-pass filters, as shown in Fig 4.3. Q filter of the new distur-

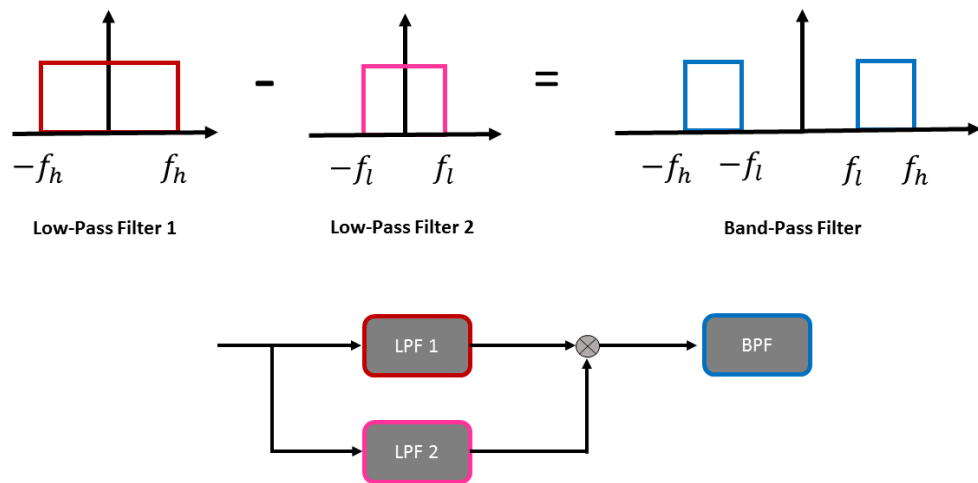


FIGURE 4.3: Band-pass filter construction

bance observer is defined as the sum of a low-pass filter and a bank of band-pass filters, i.e.

$$Q(s) = \frac{g}{s + g} + Q_1(s) \tag{4.5}$$

where  $Q_1(s)$  is given as

$$Q_1(s) = \sum_{i=1}^N \frac{g_{i+1}}{s + g_{i+1}} - \frac{g_i}{s + g_i} \tag{4.6}$$

where  $N$  is the number of band-pass filters utilized in the implementation. A new structure is shown in Fig 4.4.

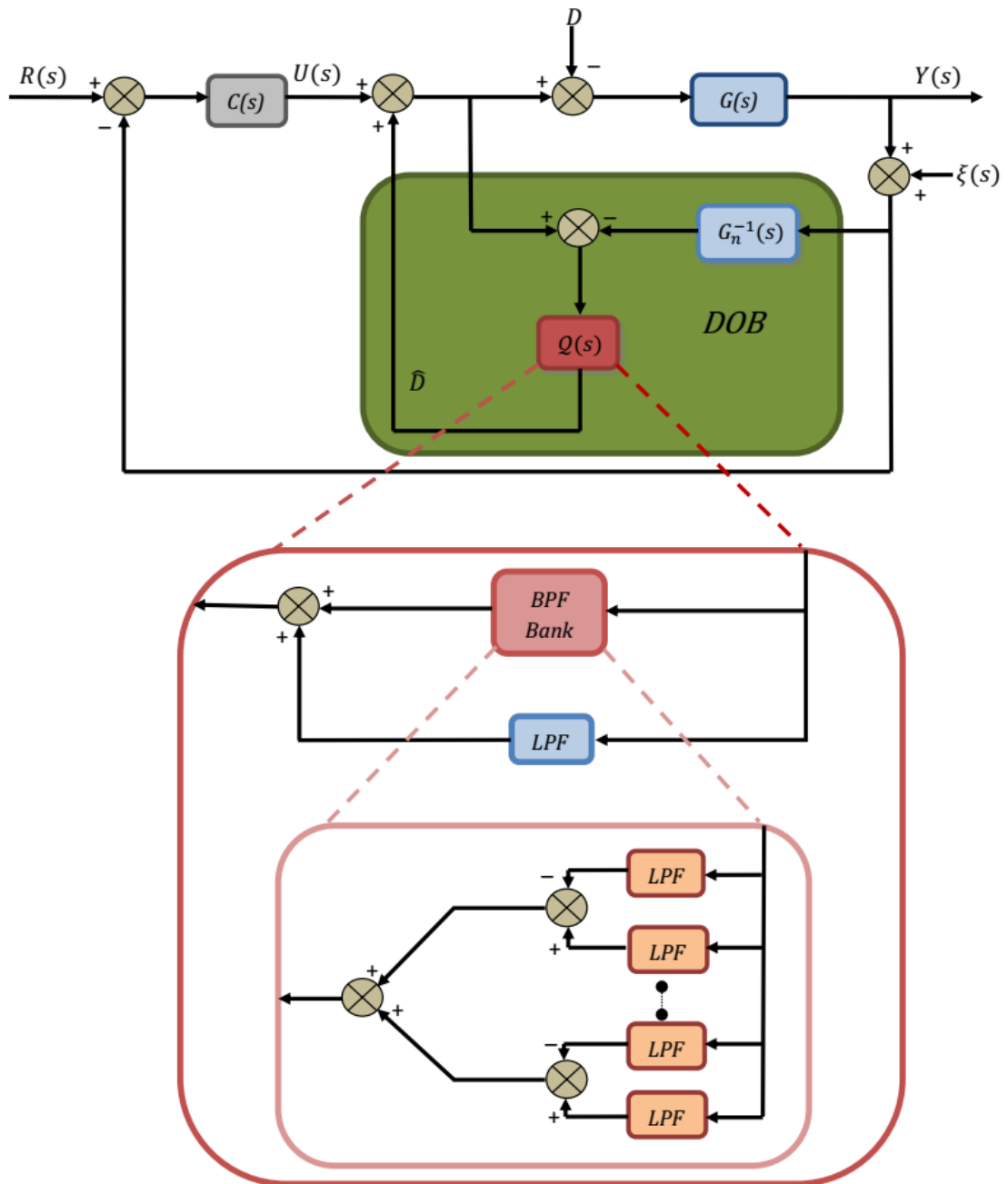


FIGURE 4.4: Novel disturbance observer block diagram

# Chapter 5

## Estimation of Attitude Angles Using Nonlinear Optimization

This chapter deals with the development of the optimization problem to estimate the desired attitude angles from command signals generated by the high-level controller of the hierarchical control structure. Typically the desired attitude angles are generated through analytical formulas which may return large and nonsmooth values. Therefore, a saturation function and low-pass filter are applied, which can degrade the performance of the controller. As the translational motion of the quadrotor is coupled with the angular motion of the quadrotor, it also affects the Cartesian position tracking of the vehicle.

In this work, estimation of the desired attitude angles of the quadrotor is considered as a control allocation problem. Control allocation is a hierarchical type algorithm which consists of the following three parts [83]

**High-level controller** is used to produce virtual command inputs.

**Optimization** is used to distribute the total virtual command among the actuators through linear and nonlinear optimization depending upon the cost function to be minimized and constraints.

**Low-level controller** is used to produce required force depending upon the optimized values.

Positional dynamics of the quadrotor is exploited in this approach which is considered as an underdetermined part of the vehicle. If we look at the positional dynamics in (3.27), it consists of three equations and four unknown variables  $(\phi, \theta, \psi, U_1)$ . In [84] control allocation approach had been used to solve the underdetermined system where nonlinear optimization problem had been formulated. As positional dynamics of the quadrotor consists of nonlinear equations, so nonlinear optimization is required to get the optimal solution. The purpose of the control allocation is to generate command input that must be produced jointly by all actuators, which in this thesis are  $\phi, \theta, \psi$  and  $U_1$ . Our goal here is to minimize the following objective function with respect to the nonlinear and linear constraints.

$$J(\zeta) = \min \frac{1}{2}(S^T S) \quad (5.1)$$

where  $J(\zeta)$  is the cost function to be minimized.  $S$  is a slack variable which is defines as

$$S = \varsigma - B(\zeta) \quad (5.2)$$

where  $\varsigma$  is the desired command inputs that is provided by the high-level controller of the hierarchical control.  $\varsigma$  and  $B(\zeta)$  are given as

$$\varsigma = [\ddot{X} \ \ddot{Y} \ \ddot{Z}]^T \quad (5.3)$$

$$B(\zeta) = \begin{bmatrix} (\sin \psi \sin \phi + \cos \psi \sin \theta \cos \phi) \frac{U_1}{m} \\ (-\cos \psi \sin \phi + \sin \psi \sin \theta \cos \phi) \frac{U_1}{m} \\ -g + (\cos \theta \cos \phi) \frac{U_1}{m} \end{bmatrix} \quad (5.4)$$

$\zeta$  consists of the desired attitude and total thrust which is defined as

$$\zeta = [\phi, \theta, \psi, U_1] \quad (5.5)$$

The cost function is minimized subject to the following nonlinear and linear constraints

$$\zeta_{min} \leq \zeta \leq \zeta_{max} \quad (5.6)$$

$$\Delta\zeta \leq C \quad (5.7)$$

where  $\zeta_{min}$  and the  $\zeta_{max}$  are the constrained range for  $\zeta$ . Rate constraint  $\Delta\zeta$  is included in the formulation by limiting the change in the control inputs  $\zeta$  from the last sampling instant to some constant  $C$ . The constraint in eq (5.6) is applied to limit the values to our desired bound, whereas eq (5.7) defines the rate constraints to get the smooth results.

## 5.1 Nonlinear Optimization

Optimization is an important tool to compute the quantitative measure of the system by defining a certain objective function. The objective relies on the essential parameters of the system that need to be considered called variables or unknowns. In the optimization problem, the aim is to find a certain set of values of the variables that can maximize or minimize the objective function. Often the variables are restricted, or constrained, by some values or the range of the values.

The classification of the optimization problems is based on the characteristics of the objective function and constraints (linear or nonlinear and differentiable or nondifferentiable). Typically two important types of optimization problems are unconstrained and constrained optimization [85].

Unconstrained optimization deals with the problems where the objective function is to be maximized/minimized when no condition is imposed on the variables. Sometimes, a sequence of unconstrained optimizations can be used to solve the

more stringent problems like constrained optimization [86]. In unconstrained optimization, feasible solutions converge to some finite values.

Constrained optimization is used to find the best possible solution when the objective function is subjected to certain conditions imposed on the variables called constraints. These restriction/conditions can be linear and nonlinear. Besides its nature, constraints can be imposed in the form of equality and inequality bounds.

Nonlinear programming is a mathematical tool used to minimize the cost function subject to linear and nonlinear constraints. Feasible regions show the set of optimized variables which lie in the range of constraints. In nonlinear constrained optimization, the problem is converted into easy subproblems and iterative process is used to solve utilizing different algorithms. Sequential quadratic programming (*SQP*) is a nonlinear optimization tool which is one of the most effective iterative methods. *SQP* programming is the method which is based on the calculation of the second order Karush-Kuhn-Tucker (*KKT*) equations with the help of quasi Newton method. Quasi Newton is the line search method to get the optimal direction to minimize the cost function, which depends on direction search ( $d_k$ ) and step length ( $\beta$ ) as [86]

$$\zeta_{k+1} = \zeta_k + \beta d_k \tag{5.8}$$

The selection of search direction  $d_k$  and step length  $\beta$  is vital for the success of the line search method. In the case of Newton method  $d_k$  is given by

$$d_k = -H_k^{-1} \nabla J_k \tag{5.9}$$

where above equation is derived from the gradient of second order Taylor expansion ( $d = 0$ ):

$$V_k(d) = J(\zeta_k) + \nabla J^T(\zeta_k) d_k + \frac{1}{2} d^T H_k d_k \tag{5.10}$$

where  $H_k$  is the Hessian matrix which is given by

$$H_k = \nabla^2 J(\zeta_k) \tag{5.11}$$

In case of quasi-Newton method,  $H_k$  is the approximation of the Hessian matrix at each iteration  $k$  instead of true Hessian which is based on the change in gradients. Step length  $\beta$  must be able to decrease the required cost function in a limited time. There are different conditions to terminate the search for optimal step length, such as the Wolfe and Goldstein conditions. Wolfe conditions, used for the quasi-Newton method to guarantee convergence are given by [85]

$$J(\zeta_k + \beta d_k) \leq J(\zeta_k) + c_1 \beta \nabla J_k^T d_k \quad (5.12)$$

where  $c_1$  is the constant between 0 and 1.  $c_1 \beta \nabla J_k^T d_k$  has a negative slope and it is considered that step length  $\beta$  is acceptable when

$$J(\zeta_k + \beta d_k) \leq c_1 \beta \nabla J_k^T d_k \quad (5.13)$$

As from above equation, so many values can be considered which are less than  $c_1 \beta \nabla J_k^T d_k$  so another condition is also required to specify the stopping criterion for step length to terminate at the suitable value, which is known as *curvature conditions*.

$$\nabla J(\zeta_k + \beta d_k)^T d_k \geq c_2 \nabla J_k^T d_k \quad (5.14)$$

where  $c_2$  is the constant between  $c_1$  and 1. As we can see that left hand side of the (5.14) is simply the derivative of the  $J(\zeta_k + \beta d_k)$  which is used to specify the step length ( $\beta$ ) because slope at  $\beta$  will be greater than initial slope times the  $c_2$ . The curvature condition is important when slope w.r.t step length is more negative, which shows that cost function can decrease more in the same direction and vice versa.

The solution to Karush-Kuhn-Tucker (*KKT*) equations forms the basis for many constrained nonlinear programming. *KKT* equations are defined as

$$\begin{aligned} \nabla J(\zeta) + \sum_{i=1}^m \lambda_i \cdot \nabla g_i(\zeta) &= 0 \\ \lambda_i \cdot g_i(\zeta) &= 0, \quad i = 1, 2, \dots, m_e \\ \lambda_i &\geq 0, \quad i = m_e + 1, \dots, m \end{aligned} \tag{5.15}$$

where  $\lambda$  is the Lagrange multiplier and  $\nabla g_i(\zeta)$  is the gradient of constraints, which is used to cancel the gradients between the cost functions and active constraints at the solution point. Lagrange multiplier for non-active constraints is taken to be zero which is shown by the last two equations in (5.15).

Quasi Newton method guarantees the convergence by acquiring second order information regarding the *KKT* equations using a quasi-Newton updating procedure. *SQP* is one of the tools in the quasi Newton method, which is used to find local minimizer for the cost function by dividing the nonlinear problem into subprogram for quadratic programming (*QP*). The cost function needs to be twice differentiable because the second derivative is required to show the direction of the objective function and the constraints. The solution to the quadratic programming at each iteration is used to find optimal direction for the next iteration [85].

## 5.2 SQP Implementation

Implementation of the *SQP* consists of the following three parts [86].

**The BFGS method and Hessian matrix:-** BFGS is the quasi Newton optimization method for Lagrange function which is named after the discoverers Broyden–Fletcher–Goldfarb–Shanno. This method can be expressed by defining the second order Taylor expansion equation at the current state of the  $\zeta$  in (5.10). The gradient of the second order equation is given by

$$\nabla V_k = \nabla J(\zeta_k) + H d_k \tag{5.16}$$

which is minimized to produce  $d_k$  as in (5.9).  $H_{k+1}$  is updated at every iteration, instead of finding new Hessian matrix. At next iteration  $k + 1$ , second order model becomes

$$V_{k+1}(d) = J(\zeta_{k+1}) + \nabla J(\zeta_{k+1})^T d + \frac{1}{2} d^T H_{k+1} d \quad (5.17)$$

In order to find the Hessian matrix, the following conditions are applied.

1.  $H_{k+1}$  should be symmetric.
2. In order to form a quadratic model using  $H_{k+1}$ , gradients of the model, must be equal to the gradient of the cost function at  $\zeta_k$  and  $\zeta_{k+1}$ .

In light of above conditions, it follows that

$$\nabla V_{k+1}(-\beta d_k) = \nabla J(\zeta_{k+1}) - \beta H_{k+1} d_k = \nabla J(\zeta_k) \quad (5.18)$$

$$\implies \beta H_{k+1} d_k = \nabla J(\zeta_{k+1}) - \nabla J(\zeta_k) \quad (5.19)$$

The displacement vector and the change in the gradient vector are defined as

$$l_k \triangleq \zeta_{k+1} - \zeta_k = \beta d_k \quad (5.20)$$

$$q_k \triangleq \nabla J(\zeta_{k+1}) - \nabla J(\zeta_k) \quad (5.21)$$

Then, (5.19) becomes

$$H_{k+1} l_k = q_k \quad (5.22)$$

$H_k$  and  $H_{k+1}$  should be close. Frobenius norm is used to find the difference between two Hessian matrices using weights. In order to find  $H_{k+1}$  uniquely, the following optimization is considered.

$$H_{k+1} = \arg \min(\|H - H_k\|_W) \quad (5.23)$$

subject to

$$H = H^T \quad (5.24)$$

$$H_{k+1} l_k = q_k$$

The unique solution to (5.23) is given by

$$H_{k+1} = (I - \rho_k l_k q_k^T) H_k (I - \rho_k q_k l_k^T) + \rho_k l_k l_k^T \quad (5.25)$$

Sherman-Morrison-Woodbury formula is applied to derive the formula for  $\hat{H}_{k+1}$  which is useful when it is used for calculating search direction by means of simple matrix-vector calculations and it is given as

$$\begin{aligned} \hat{H}_{k+1} &= H_{k+1}^{-1} \\ \hat{H}_{k+1} &= \hat{H}_k + \frac{q_k q_k^T}{q_k^T l_k} - \frac{\hat{H}_k l_k l_k^T \hat{H}_k}{l_k^T \hat{H}_k l_k} \end{aligned} \quad (5.26)$$

In SQP, an active set algorithm is applied where only active constraints take part in minimization, so Lagrange multipliers are also introduced to balance the change in the magnitude of cost function and constraints gradients. Therefore  $q_k$  is given as

$$q_k = \nabla J(\zeta_{k+1}) + \sum_{i=1}^m \lambda_i \nabla g_i(\zeta_{k+1}) - (\nabla J(\zeta_k) + \sum_{i=1}^m \lambda_i \nabla g_i(\zeta_k)) \quad (5.27)$$

At every iteration, positive definiteness of the Hessian matrix is ensured by positive  $q_k^T s_k$ . The BFGS algorithm for the approximation of Hessian matrix is summarized in Algorithm 5.1 [86].

---

**Algorithm 5.1** BFGS Method

---

Get the Starting point  $\zeta_0$   
 Set convergence tolerance  $(\epsilon) > 0$   
 Compute Hessian matrix approximation  $H_0$   
 $0 \rightarrow k$   
**while**  $\|\nabla J_k\| > \epsilon$  **do**  
     Compute search direction  
      $d_k = -\hat{H}_k \nabla J_k$   
     Set  $\zeta_{k+1} = \zeta_k + \beta d_k$   
     where  $\beta$  is computed to satisfy (5.13) and (5.14)  
     Define  $l_k = \zeta_{k+1} - \zeta_k$   
     Define  $q_k = \nabla J_{k+1} - \nabla J_k$   
     Compute  $\hat{H}_{k+1}$  from (5.26)  
      $k \rightarrow k + 1$   
**end while**

---

**Quadratic Programming Solution:-** This part consists of two steps:

1. First step gives the feasible point.
2. Second step produces the iterative process of feasible points to converge within the constraints.

During this part of nonlinear programming, the problem is converted to subproblems by linearizing the constraints and then quadratic programming (QP) is used to solve as

$$\begin{aligned} \min & \frac{1}{2}d^T H_k d + \nabla J(\zeta_k)^T d \\ & \nabla g_i(\zeta_k)^T d + g_i(\zeta_k) = 0, i = 1, 2, \dots, m_e \\ & \nabla g_i(\zeta_k)^T d + g_i(\zeta_k) \leq 0, i = m_e + 1, \dots, m \end{aligned} \quad (5.28)$$

The following QP form is used at every iteration.

$$\min q(d) = \frac{1}{2}d^T H d + c^T d \quad (5.29)$$

subject to the following equality and inequality constraints.

$$\begin{aligned} A_i d &= b_i, i = 1, 2, \dots, m_e \\ A_i d &\leq b_i, i = m_e + 1, \dots, m \end{aligned} \quad (5.30)$$

The solutions of quadratic programming give  $d_k$ , which is feasible region search direction. Active constraints are updated at every iteration to form a basis for new search direction  $d_k$ .

**Optimal Line Search:-** This part of the programming is used to produce new iteration using updated search direction ( $d_k$ ) obtained from the QP solution.

$$\zeta_{k+1} = \zeta_k + \beta d_k \quad (5.31)$$

# Chapter 6

## Robust Trajectory Tracking

## Control of the Quadrotor

## Helicopter Using Acceleration

## Feedback

This chapter develops the acceleration feedback based robust controllers for the positional and attitude dynamics of the quadrotor. As a control strategy, a hierarchical structure is utilized where the dynamics of the quadrotor is divided into two parts: positional and attitude dynamics. PID controllers with acceleration based disturbance observer are used as a high-level controller to provide virtual command inputs. Nonlinear optimization is used to obtain the bounded and smooth reference attitude angles  $[\phi_r, \theta_r, \psi_r]$  based on the desired virtual command signals.

For the low-level control, a nested position, velocity, and inner acceleration feedback control structure which consists of PID and PI type controllers are developed to provide high stiffness against disturbances. Angular acceleration and velocity signals are estimated through the cascaded structure of extended and classical Kalman filters. Fig 6.1 is presented to elaborate the complete closed-loop control structure.

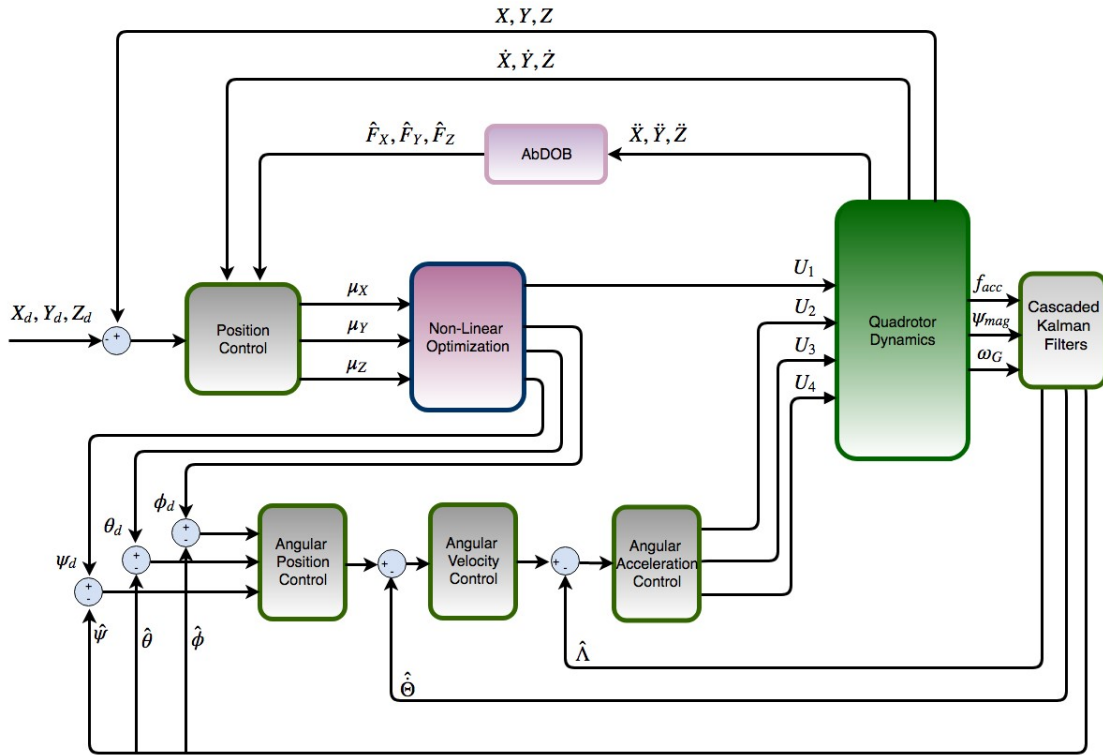


FIGURE 6.1: Overall control system architecture

## 6.1 Position Control Using Acceleration Feedback

For the positional dynamics of the quadrotor, acceleration based disturbance observer (AbDOB) is designed to estimate the total disturbance that includes external disturbances, nonlinear terms and parametric uncertainties through linear acceleration signals. Classical disturbance observer estimates the total disturbances acting on the system, which is then fed back to cancel these effects as shown in Fig 4.1. The nominal plant model for the AbDOB is selected as

$$G_n(s) = \begin{bmatrix} \frac{1}{m_n s^2} & 0 & 0 \\ 0 & \frac{1}{m_n s^2} & 0 \\ 0 & 0 & \frac{1}{m_n s^2} \end{bmatrix} \quad (6.1)$$

where  $m_n$  is the nominal mass of the quadrotor. From the positional dynamics of quadrotor in (3.27)

$$\begin{aligned}\ddot{X} &= (\sin \psi \sin \phi + \cos \psi \sin \theta \cos \phi) \frac{U_1}{m} + D_X \\ \ddot{Y} &= (-\cos \psi \sin \phi + \sin \psi \sin \theta \cos \phi) \frac{U_1}{m} + D_Y \\ \ddot{Z} &= -g + (\cos \theta \cos \phi) \frac{U_1}{m} + D_Z\end{aligned}\tag{6.2}$$

where  $U_1$  is the control input,  $D_X, D_Y$  and  $D_Z$  are the disturbances. Errors are defined as

$$e_X = X_d - X, \quad e_Y = Y_d - Y, \quad e_Z = Z_d - Z\tag{6.3}$$

Error dynamics can be derived as

$$\dot{e}_X = \dot{X}_d - \dot{X} \quad \Rightarrow \quad \ddot{e}_X = \ddot{X}_d - \ddot{X}\tag{6.4}$$

$$\dot{e}_Y = \dot{Y}_d - \dot{Y} \quad \Rightarrow \quad \ddot{e}_Y = \ddot{Y}_d - \ddot{Y}\tag{6.5}$$

$$\dot{e}_Z = \dot{Z}_d - \dot{Z} \quad \Rightarrow \quad \ddot{e}_Z = \ddot{Z}_d - \ddot{Z}\tag{6.6}$$

From the positional dynamics,  $\ddot{X}$  can be written as

$$\ddot{X} = \mu_X + D_X\tag{6.7}$$

Therefore, error dynamics in (6.4) becomes

$$\ddot{e}_X = \ddot{X}_d - \mu_X - D_X\tag{6.8}$$

where  $\mu_X$  can be designed using both feedforward and feedback terms as

$$\mu_X = \ddot{X}_d + K_{p,X}e_X + K_{d,X}\dot{e}_X + K_{i,X} \int e_X dt - \hat{D}_X\tag{6.9}$$

$\hat{F}_X$  is the estimated disturbance, which is used as the feedforward term along with the  $\ddot{X}_d$ . PID is used as the feedback controller. Closed-loop error dynamics in

(6.8) becomes

$$\ddot{e}_X + K_{p,X}e_X + K_{d,X}\dot{e}_X + K_{i,X} \int e_X dt = \tilde{D}_X \quad (6.10)$$

By selecting positive controller gains for PID, the second order error dynamics will imply a stable system with zero steady-state error for constant disturbances. Similarly, the following virtual controller can be designed for  $Y$  and  $Z$  positional axes.

$$\begin{aligned} \mu_Y &= \ddot{Y}_d + K_{p,Y}e_Y + K_{d,Y}\dot{e}_Y + K_{i,Y} \int e_Y dt - \hat{D}_Y \\ \mu_Z &= \ddot{Z}_d + K_{p,Z}e_Z + K_{d,Z}\dot{e}_Z + K_{i,Z} \int e_Z dt - \hat{D}_Z \end{aligned} \quad (6.11)$$

Once the virtual controllers are synthesized as above,  $U_1$  can be calculated from  $\mu_x, \mu_y$  and  $\mu_z$  as [73]

$$U_1 = m\sqrt{\mu_X^2 + \mu_Y^2 + (\mu_Z + g)^2} \quad (6.12)$$

In order to calculate the desired attitude angles of the aerial vehicle from desired the acceleration vector, the yaw angle ( $\psi$ ) is set to some fixed value ( $\psi_r = \psi^*$ ). Desired angles are calculated as [74]

$$\phi_r = \arcsin\left(\frac{s_{\psi_r}\mu_X - c_{\psi_r}\mu_Y}{\sqrt{\mu_X^2 + \mu_Y^2 + (\mu_Z + g)^2}}\right) \quad (6.13)$$

$$\theta_r = \arcsin\left(\frac{c_{\psi_r}\mu_X + s_{\psi_r}\mu_Y}{\sqrt{\mu_X^2 + \mu_Y^2 + (\mu_Z + g)^2}c_{\phi_r}}\right) \quad (6.14)$$

## 6.2 Attitude Control Using Nested Feedback Loops

During the trajectory tracking, translational motion relies on the desired attitude angle; therefore, robust attitude control plays an important role in trajectory tracking control of the quadrotor in the presence of disturbances acting on the attitude dynamics. To cancel the effects of the disturbances, nested angular position, velocity, and acceleration feedback control is utilized. In order to estimate the reliable angular position, velocity, and acceleration, Kalman filters are used in a cascaded mode.

### 6.2.1 Cascaded Kalman Filter

A cascaded structure of Kalman filters which was developed in [87] is utilized to estimate angular positions, velocities and accelerations. This structure is shown in Fig 6.2. The process of estimating the Euler angles, rates and acceleration consists

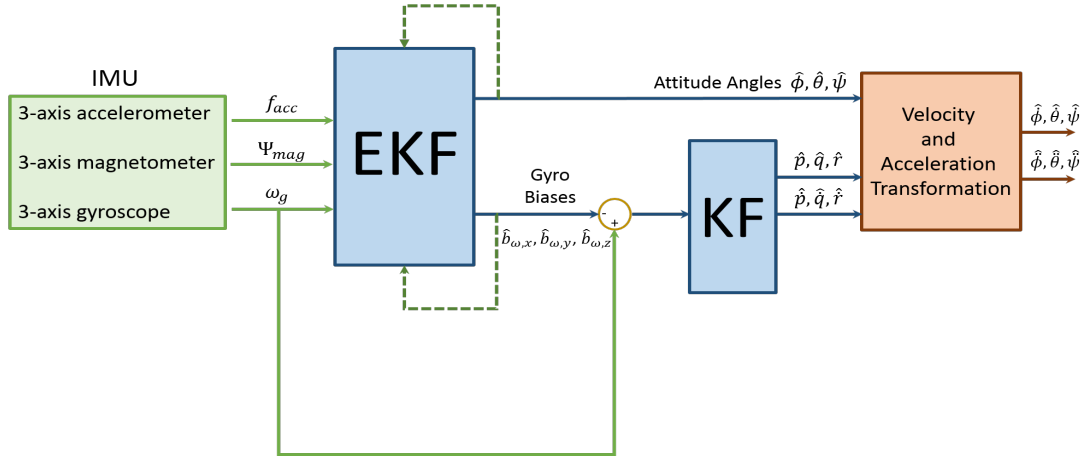


FIGURE 6.2: Cascaded Kalman filters structure

of two steps as described below.

#### **First Step**

During the estimation process, initially extended Kalman filter is used to estimate the attitude angles  $(\phi, \theta, \psi)$  and gyro biases  $(b_{\omega,x}, b_{\omega,y}, b_{\omega,z})$ . Angular velocity readings  $\omega_G = (\omega_{G,x}, \omega_{G,y}, \omega_{G,z})$  from 3-axis gyroscope are considered as the inputs for the process model whereas accelerometer and magnetometer values are taken as measurements. The process model can be written as

$$\begin{bmatrix} \dot{\phi} \\ \dot{\theta} \\ \dot{\psi} \\ \dot{b}_\omega \end{bmatrix} = \begin{bmatrix} E(\vartheta)\omega_{G,b} \\ 0_{3 \times 1} \end{bmatrix} + w(t) \quad (6.15)$$

where  $w(t)$  is the process noise.  $\omega_{G,b}$  and  $b_\omega$  are defined as

$$\omega_{G,b} \triangleq \begin{bmatrix} \omega_{G,x} - b_{\omega,x} \\ \omega_{G,y} - b_{\omega,y} \\ \omega_{G,z} - b_{\omega,z} \end{bmatrix} \quad (6.16)$$

$$b_\omega \triangleq \begin{bmatrix} b_{\omega,x} \\ b_{\omega,y} \\ b_{\omega,z} \end{bmatrix}$$

Measurement model can be written by considering the readings from 3-axis accelerometer ( $f_{acc} = [f_{acc,x}, f_{acc,y}, f_{acc,z}]^T$ ) and yaw angle  $\psi_{mag}$  reading from the 3-axis magnetometer

$$z = \begin{bmatrix} f_{acc} \\ \Psi_{mag} \end{bmatrix} \begin{bmatrix} \omega_{G,b} \times V_r - g\mathcal{K}(\vartheta) \\ \Psi \end{bmatrix} + \nu(t) \quad (6.17)$$

where  $V_B$  is the linear velocity and  $\nu(t)$  is the measurement noise.  $\mathcal{K}(\vartheta)$  is given as

$$\mathcal{K}(\vartheta) = \begin{bmatrix} \sin(\theta) \\ \sin(\phi)\cos(\theta) \\ \cos(\phi)\cos(\theta) \end{bmatrix} \quad (6.18)$$

### **Second Step**

Once attitude angles and gyro biases are estimated by the extended Kalman filter (EKF) which utilizes process and measurement models given in 6.15 and 6.17, the estimated gyro biases are subtracted from the gyro measurements, moreover, the resulting compensated angular velocity is used as a measurement in a classical Kalman filter (KF) to estimate the angular velocity  $\Omega = [p, q, r]^T$  and the angular acceleration  $\alpha = [\dot{p}, \dot{q}, \dot{r}]$ .

$$\begin{bmatrix} \dot{\Omega} \\ \dot{\alpha} \end{bmatrix} = \begin{bmatrix} I_{3 \times 3} & TI_{3 \times 3} \\ 0_{3 \times 3} & I_{3 \times 3} \end{bmatrix} \begin{bmatrix} \Omega \\ \alpha \end{bmatrix} + \begin{bmatrix} 0.5T^2 I_{3 \times 3} \\ TI_{3 \times 3} \end{bmatrix} \Gamma \quad (6.19)$$

where  $\Gamma = [\ddot{p}, \ddot{q}, \ddot{r}]$  is the angular jerk vector which is considered as the stochastic input to the system i.e., additive Gaussian noise. Compensated measurement model can be written as

$$z = \omega_g - \hat{b}_\omega = \begin{bmatrix} I_{3 \times 3} & 0_{3 \times 3} \end{bmatrix} \begin{bmatrix} \Omega \\ \alpha \end{bmatrix} + \nu_k \quad (6.20)$$

where  $\nu_k$  is the noise due to the overall cascaded structure. Estimated angular velocity can be transformed into Euler rates in world frame as

$$\hat{\Theta} = \begin{bmatrix} \hat{\phi} \\ \hat{\theta} \\ \hat{\psi} \end{bmatrix} = E(\vartheta) \hat{\Omega} \quad (6.21)$$

Similarly estimated angular acceleration can be transformed as

$$\begin{bmatrix} \hat{\dot{\phi}} \\ \hat{\dot{\theta}} \\ \hat{\dot{\psi}} \end{bmatrix} = \dot{E}(\hat{\phi}, \hat{\theta}, \hat{\phi}, \hat{\theta}) \begin{bmatrix} \hat{p} \\ \hat{q} \\ \hat{r} \end{bmatrix} + E(\hat{\phi}, \hat{\theta}) \begin{bmatrix} \hat{\dot{p}} \\ \hat{\dot{q}} \\ \hat{\dot{r}} \end{bmatrix} \quad (6.22)$$

where  $\dot{E}(\hat{\phi}, \hat{\theta}, \hat{\phi}, \hat{\theta})$  is obtained as

$$\dot{E}(\hat{\phi}, \hat{\theta}, \hat{\phi}, \hat{\theta}) = \begin{bmatrix} 0 & \hat{\phi} \cos(\phi) \tan(\theta) + \sin(\phi) \hat{\theta} \sec^2(\theta) & \hat{\phi} \sin(\phi) \tan(\theta) + \cos(\phi) \hat{\theta} \sec^2(\theta) \\ 0 & \hat{\phi} \sin(\phi) & \hat{\phi} \cos(\phi) \\ 0 & \frac{\hat{\phi} \cos(\phi) \tan(\theta) + \sin(\phi) \hat{\theta} \sin(\theta)}{\cos^2(\theta)} & \frac{\hat{\phi} \sin(\phi) \cos(\theta) + \cos(\phi) \hat{\theta} \sin(\theta)}{\cos^2(\theta)} \end{bmatrix} \quad (6.23)$$

## 6.2.2 Nested Feedback Loops

Estimated Euler angles, rates and acceleration are now utilized as feedback signals in a nested loop control structure to get high stiffness against the external disturbances in the attitude dynamics. In order to design the nested loop controllers,

errors in attitude angles can be defined as

$$e_\phi = \phi_r - \phi, \quad e_\theta = \theta_r - \theta, \quad e_\psi = \psi_r - \psi \quad (6.24)$$

where error dynamics are written as

$$\dot{e}_\phi = \dot{\phi}_r - \dot{\phi}, \quad \dot{e}_\theta = \dot{\theta}_r - \dot{\theta}, \quad \dot{e}_\psi = \dot{\psi}_r - \dot{\psi} \quad (6.25)$$

PID controllers are used as the angular position control to provide  $\dot{\Theta}_r = [\dot{\phi}_r, \dot{\theta}_r, \dot{\psi}_r]$  for angular velocity control loops which are designed as

$$\dot{\phi}_r = K_{p,\phi}e_\phi + K_{d,\phi}\dot{e}_\phi + K_{i,\phi} \int e_\phi dt \quad (6.26)$$

$$\dot{\theta}_r = K_{p,\theta}e_\theta + K_{d,\theta}\dot{e}_\theta + K_{i,\theta} \int e_\theta dt \quad (6.27)$$

$$\dot{\psi}_r = K_{p,\psi}e_\psi + K_{d,\psi}\dot{e}_\psi + K_{i,\psi} \int e_\psi dt \quad (6.28)$$

Estimated Euler rates  $\hat{\theta}$  in eq (6.21) are utilized to develop the velocity control as

$$e_\Omega = \dot{\Theta}_r - \hat{\Theta} \quad (6.29)$$

$$\Lambda_r = (1 + k_\Lambda)(K_{p,\Omega} e_\Omega + K_{i,\Omega} \int e_\Omega dt) \quad (6.30)$$

Finally, the control inputs for the attitude dynamics of the quadrotor are designed as PI controllers by utilizing the reference generated in eq (6.30) and estimated Euler acceleration in eq (6.22) as

$$U_{2,3,4} = K_{p,\Lambda} e_\Lambda + K_{i,\Lambda} \int e_\Lambda dt \quad (6.31)$$

where  $e_\Lambda = \Lambda_r - k_\Lambda \hat{\Lambda}$  and  $k_\Lambda$  is the acceleration gain to get high dynamic stiffness against the disturbance moments acting on the attitude dynamics of the quadrotor.

## Chapter 7

# Robust Hovering and Trajectory Tracking Control of the Quadrotor Helicopter Using a Novel Disturbance Observer

This chapter presents the development of the controller based on the novel disturbance observer designed in Chapter 4. Control structure is developed in the hierarchical framework, where high-level and low-level controllers are designed for the positional and attitude dynamics, respectively. High-level controller is used to get the desired command signals. Analytical formulas are used to get the desired reference angles  $(\phi_d, \theta_d, \psi_d)$  for low-level attitude control.

For the high-level control, linear acceleration signals are utilized to design acceleration based disturbance observer (AbDOB). Estimated disturbances are added as a feedforward term with PID controller to provide stiffness against the disturbances acting on the positional dynamics of the vehicle. For the disturbance acting on the attitude dynamics, velocity based disturbance observer (VbDOB) is utilized to estimate the disturbances. Furthermore, a nonlinear controller based on the nonsingular and nonlinear sliding surface is designed through Lyapunov

stability analysis [88]. The composite low-level controller is designed through Vb-DOB and nonlinear controller to increase the robustness of the system against the external disturbances in the attitude dynamics. Closed-loop stability analysis for the attitude dynamics is presented to show that all signals remain bounded. The closed-loop control architecture is presented in Fig. 7.1.

## 7.1 Position Control Utilizing Acceleration Based Disturbance Observer

Estimating the external disturbance is not an easy task in an underactuated nonlinear system due to noise and uncertainties. However, it can be estimated if the reliable acceleration signals are available from linear accelerometers. In order to reject disturbances acting on the positional dynamics of the quadrotor, acceleration based disturbance observer (AbDOB) is utilized. AbDOB is used to estimate the total disturbances, which include external disturbances, nonlinear terms, and parametric uncertainties. The following nominal plant is used in AbDOB.

$$G_n(s) = \begin{bmatrix} \frac{1}{m_n s^2} & 0 & 0 \\ 0 & \frac{1}{m_n s^2} & 0 \\ 0 & 0 & \frac{1}{m_n s^2} \end{bmatrix} \quad (7.1)$$

where  $m_n$  is the nominal mass of the quadrotor.

From the positional dynamics of quadrotor in (3.27)

$$\begin{aligned} \ddot{X} &= (\sin \psi \sin \phi + \cos \psi \sin \theta \cos \phi) \frac{U_1}{m} + D_X \\ \ddot{Y} &= (-\cos \psi \sin \phi + \sin \psi \sin \theta \cos \phi) \frac{U_1}{m} + D_Y \\ \ddot{Z} &= -g + (\cos \theta \cos \phi) \frac{U_1}{m} + D_Z \end{aligned} \quad (7.2)$$

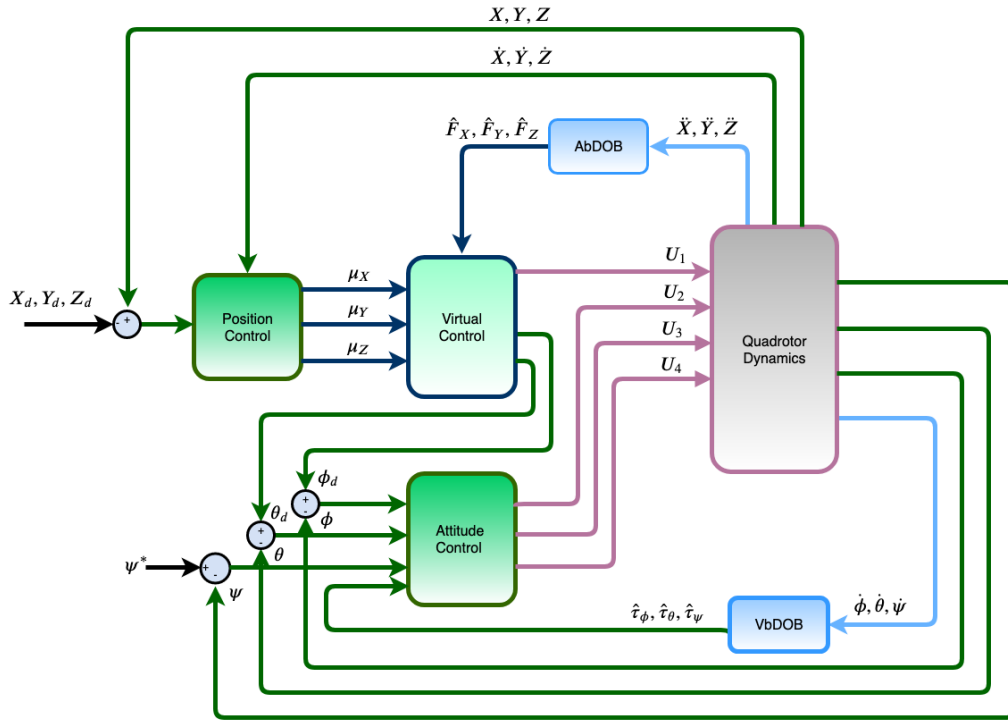


FIGURE 7.1: Closed loop control system

where  $U_1$  is the control input.  $D_X, D_Y$  and  $D_Z$  are the disturbances. Errors are defined as

$$e_X = X_d - X, \quad e_Y = Y_d - Y, \quad e_Z = Z_d - Z \quad (7.3)$$

Error dynamics can be formulated as

$$\dot{e}_X = \dot{X}_d - \dot{X} \Rightarrow \ddot{e}_X = \ddot{X}_d - \ddot{X} \quad (7.4)$$

$$\dot{e}_Y = \dot{Y}_d - \dot{Y} \Rightarrow \ddot{e}_Y = \ddot{Y}_d - \ddot{Y} \quad (7.5)$$

$$\dot{e}_Z = \dot{Z}_d - \dot{Z} \Rightarrow \ddot{e}_Z = \ddot{Z}_d - \ddot{Z} \quad (7.6)$$

From the positional dynamics,  $\ddot{X}$  can be defined as

$$\ddot{X} = \mu_X + D_X \quad (7.7)$$

Therefore, error dynamics in (7.4) becomes

$$\ddot{e}_X = \ddot{X}_d - \mu_X - D_X \quad (7.8)$$

where  $\mu_X$  can be designed using both feedforward and feedback terms as

$$\mu_X = \ddot{X}_d + K_{p,X}e_X + K_{d,X}\dot{e}_X + K_{i,X} \int e_X dt - \hat{D}_X \quad (7.9)$$

$\hat{D}_X$  is the estimated disturbance, which is used as feedforward term along with the  $\ddot{X}_d$ . PID is used as the feedback controller. Closed-loop error dynamics in (7.8) becomes

$$\ddot{e}_X + K_{p,X}e_X + K_{d,X}\dot{e}_X + K_{i,X} \int e_X dt = \tilde{D}_X \quad (7.10)$$

By selecting positive controller gains for PID, the second order error dynamics will imply a stable system with zero steady-state error for constant disturbances. Similarly, the following virtual controllers can be designed for  $Y$  and  $Z$  positional axes.

$$\begin{aligned} \mu_Y &= \ddot{Y}_d + K_{p,Y}e_Y + K_{d,Y}\dot{e}_Y + K_{i,Y} \int e_Y dt - \hat{D}_Y \\ \mu_Z &= \ddot{Z}_d + K_{p,Z}e_Z + K_{d,Z}\dot{e}_Z + K_{i,Z} \int e_Z dt - \hat{D}_Z \end{aligned} \quad (7.11)$$

Once the virtual controllers are synthesized as above,  $U_1$  can be calculated from  $\mu_x, \mu_y$  and  $\mu_z$  in eq (6.12) and desired roll and pitch angle can be obtained through eq (6.13) and eq (6.14), respectively.

## 7.2 Attitude Control Utilizing Velocity Based Disturbance Observer

Translational motion of the aerial vehicle depends on the behavior of the roll, pitch and yaw angles; therefore, attitude control is an important part for the motion control of the quadrotor. In order to get more robustness with minimum control efforts, integral non-singular and nonlinear sliding surface is designed. Note that attitude dynamics is fully actuated. With three inputs ( $U_2, U_3, U_4$ ) to control three degrees of freedom motion, separate controllers can be designed for each angular motion.

Since it is difficult to obtain reliable angular acceleration, a velocity based disturbance observer (VbDOB) is utilized to estimate the disturbances acting on the attitude dynamics. The following nominal plant is used in the proposed DOB structure.

$$G_n(s) = \begin{bmatrix} \frac{1}{I_{xx,n}s} & 0 & 0 \\ 0 & \frac{1}{I_{yy,n}s} & 0 \\ 0 & 0 & \frac{1}{I_{zz,n}s} \end{bmatrix} \quad (7.12)$$

where  $I_{xx,n}$ ,  $I_{yy,n}$  and  $I_{zz,n}$  are the nominal inertias. Errors are defined as

$$e_\phi = \phi_d - \phi, \quad e_\theta = \theta_d - \theta, \quad e_\psi = \psi_d - \psi \quad (7.13)$$

Similarly, error dynamics are obtained as

$$\dot{e}_\phi = \dot{\phi}_d - \dot{\phi} \Rightarrow \ddot{e}_\phi = \ddot{\phi}_d - \ddot{\phi} \quad (7.14)$$

$$\dot{e}_\theta = \dot{\theta}_d - \dot{\theta} \Rightarrow \ddot{e}_\theta = \ddot{\theta}_d - \ddot{\theta} \quad (7.15)$$

$$\dot{e}_\psi = \dot{\psi}_d - \dot{\psi} \Rightarrow \ddot{e}_\psi = \ddot{\psi}_d - \ddot{\psi} \quad (7.16)$$

In order to develop controllers for attitude control, we first recall the attitude dynamics of the quadrotor.

$$\ddot{\phi} = \frac{I_{yy} - I_{zz}}{I_{xx}} \dot{\theta} \dot{\psi} - \frac{J_{prop}}{I_{xx}} \dot{\theta} \omega_p + \frac{U_2}{I_{xx}} + D_\phi \quad (7.17)$$

$$\ddot{\theta} = \frac{I_{zz} - I_{xx}}{I_{yy}} \dot{\phi} \dot{\psi} + \frac{J_{prop}}{I_{yy}} \dot{\phi} \omega_p + \frac{U_3}{I_{yy}} + D_\theta \quad (7.18)$$

$$\ddot{\psi} = \frac{I_{xx} - I_{yy}}{I_{zz}} \dot{\phi} \dot{\theta} + \frac{U_4}{I_{zz}} + D_\psi \quad (7.19)$$

where  $D_\phi$ ,  $D_\theta$  and  $D_\psi$  are the external disturbances. Eq (7.17-7.19) can be rewritten as

$$\ddot{\phi} = \Gamma_\phi + \frac{U_2}{I_{xx}} + D_\phi \quad (7.20)$$

$$\ddot{\theta} = \Gamma_{\theta} + \frac{U_3}{I_{yy}} + D_{\theta} \quad (7.21)$$

$$\ddot{\psi} = \Gamma_{\psi} + \frac{U_4}{I_{zz}} + D_{\psi} \quad (7.22)$$

where  $\Gamma_{\phi} = \frac{I_{yy} - I_{zz}}{I_{xx}} \dot{\theta} \dot{\psi}$ ,  $\Gamma_{\theta} = \frac{I_{zz} - I_{xx}}{I_{yy}} \dot{\phi} \dot{\psi}$  and  $\Gamma_{\psi} = \frac{I_{xx} - I_{yy}}{I_{zz}} \dot{\phi} \dot{\theta}$ .

The following integral non-singular and nonlinear sliding surface has been chosen.

$$s = \dot{e} + \alpha \int e dt + \Upsilon e^{\eta} \quad (7.23)$$

where  $\alpha$  and  $\Upsilon$  are positive constants and  $1 < \eta < 2$ .

**Theorem 1** *Considering the system in (7.20)-(7.22) and the sliding surface in (7.23), the following control laws have been designed.*

$$U_2 = I_{xx}(\ddot{\phi}_d - \Gamma_{\phi} + \alpha_{\phi} e_{\phi} + \eta \Upsilon_{\phi} e_{\phi}^{\eta-1} \dot{e}_{\phi} + K_D s_{\phi} + K \operatorname{sgn}(s_{\phi}) - \hat{D}_{\phi}) \quad (7.24)$$

$$U_3 = I_{yy}(\ddot{\theta}_d - \Gamma_{\theta} + \alpha_{\theta} e_{\theta} + \eta \Upsilon_{\theta} e_{\theta}^{\eta-1} \dot{e}_{\theta} + K_D s_{\theta} + K \operatorname{sgn}(s_{\theta}) - \hat{D}_{\theta}) \quad (7.25)$$

$$U_4 = I_{zz}(\ddot{\psi}_d - \Gamma_{\psi} + \alpha_{\psi} e_{\psi} + \eta \Upsilon_{\psi} e_{\psi}^{\eta-1} \dot{e}_{\psi} + K_D s_{\psi} + K \operatorname{sgn}(s_{\psi}) - \hat{D}_{\psi}) \quad (7.26)$$

where  $\hat{D}_{\phi}$ ,  $\hat{D}_{\theta}$  and  $\hat{D}_{\psi}$  are the estimates from the disturbance observer.  $K$  and  $K_D$  are positive constants and selected to satisfy the following condition.

$$K > \tilde{D}_{max} \quad (7.27)$$

where  $|\tilde{D}_{(\cdot)}| \leq \tilde{D}_{max}$  and  $\operatorname{sgn}(s_{(\cdot)})$  is defined as

$$\operatorname{sgn}(s_{(\cdot)}) = \begin{cases} 1 & \text{if } s_{(\cdot)} \geq 0 \\ -1 & \text{if } s_{(\cdot)} < 0 \end{cases} \quad (7.28)$$

The state  $e$  reaches sliding surface  $s_{(\cdot)} = 0$  in a finite time and then converges to zero asymptotically along  $s_{(\cdot)} = 0$ .

**Proof.** Since the control laws have the same form for  $U_2, U_3$  and  $U_4$ , proof will be given only for  $U_2$ . Selecting the Lyapunov function as

$$V = \frac{1}{2}s_\phi^2 \quad (7.29)$$

Time derivative of the Lyapunov function implies

$$\begin{aligned} \dot{V} &= s_\phi \dot{s}_\phi \\ &= s_\phi(\ddot{e}_\phi + \alpha_\phi e_\phi + \eta \Upsilon_\phi e_\phi^{\eta-1} \dot{e}_\phi) \\ &= s_\phi(\ddot{\phi}_d - \ddot{\phi} + \alpha_\phi e_\phi + \eta \Upsilon_\phi e_\phi^{\eta-1} \dot{e}_\phi) \\ &= s_\phi(\ddot{\phi}_d - \Gamma_\phi - \frac{U_2}{I_{xx}} - D_\phi + \alpha_\phi e_\phi + \eta \Upsilon_\phi e_\phi^{\eta-1} \dot{e}_\phi) \end{aligned} \quad (7.30)$$

Substituting the control law from (7.24) into (7.30) yields

$$\dot{V} = s_\phi \dot{s}_\phi = s_\phi(-K \operatorname{sgn}(s_\phi) - K_D s_\phi - (D_\phi - \hat{D}_\phi)) \quad (7.31)$$

$$\dot{V} = s_\phi(-K \operatorname{sgn}(s_\phi) - K_D s_\phi - \tilde{D}_\phi) \quad (7.32)$$

$$\dot{V} = -K|s_\phi| - K_D s_\phi^2 - s_\phi \tilde{D}_\phi \quad (7.33)$$

Eq (7.33) can be rewritten as

$$\dot{V} \leq -K|s_\phi| - K_D s_\phi^2 + |s_\phi| \tilde{D}_{max} \quad (7.34)$$

where  $|\tilde{D}_\phi| \leq \tilde{D}_{max}$  and it follows that

$$\dot{V} \leq -(K - \tilde{D}_{max})|s_\phi| - K_D s_\phi^2 \quad (7.35)$$

In light of (7.27), one can define  $\bar{K} \triangleq K - \tilde{D}_{max} > 0$ , and it then follows that

$$\begin{aligned} \dot{V} &\leq -\bar{K}|s_\phi| - K_D s_\phi^2 \\ &\leq -\sqrt{2\bar{K}}(V)^{\frac{1}{2}} - 2K_D V \end{aligned} \quad (7.36)$$

Therefore, according to the Lyapunov stability criterion, the sliding manifold in (7.23) converges to zero in finite time and the convergence time ( $t_c$ ) is given as

$$t_c \leq \frac{1}{K_D} \ln \left[ 1 + \frac{K_D}{\bar{K}} (2V(0))^{1/2} \right] \quad (7.37)$$

where  $V(0) = V(s_\phi(0))$ . If  $s_\phi$  is reached as shown in Theorem 1, then

$$e_\phi \rightarrow 0 \Rightarrow \phi \rightarrow \phi_d \quad (7.38)$$

This concludes the proof.

**Signal Chasing.** When (7.27) is satisfied, it follows that  $V(t) \in \mathcal{L}_\infty$  based on (7.29) and (7.36). Since the signals in  $V(t)$  remain bounded, it can be concluded that  $s_\phi \in \mathcal{L}_\infty$ . If  $s_\phi \in \mathcal{L}_\infty$ , it follows from (7.23) that  $e_\phi(t), \dot{e}_\phi(t) \in \mathcal{L}_\infty$ . Finally it can be observed that  $s_\phi, e(t), \dot{e}(t) \in \mathcal{L}_\infty$  implies that  $U_2 \in \mathcal{L}_\infty$  using (7.24). If  $U_2$  remains bounded then it can be concluded that  $\ddot{\phi} \in \mathcal{L}_\infty$  and  $\ddot{e}_\phi \in \mathcal{L}_\infty$  from (7.20) and (7.14) respectively. Therefore, all signals remain bounded.

# Chapter 8

## Simulation Results and Discussions

Simulation results for the proposed algorithms developed in Chapter 6 and 7 are presented in this chapter. The performances of the proposed methods are evaluated on a high fidelity model of the quadrotor where nonlinear dynamics, external disturbances, and parametric uncertainty are taken into account along with the sensor noise and biases. Acceleration feedback based control, which is given in Fig 6.1 is utilized to get robust trajectory tracking of the quadrotor in the presence of wind disturbances generated through the Dryden wind model [89].

Results for the controllers based on the novel disturbance observer shown in Fig 4.4 and Fig 7.1 have been presented to evaluate the performance of the proposed method for both hovering and trajectory tracking. Both periodic and aperiodic disturbances are taken into account along with the parametric uncertainties and sensor noise and biases. Aperiodic disturbances are generated through Dryden wind model, and periodic disturbances are generated through the series of sine functions. The sensitivity of the increased number and bandwidth of the band-pass filters (BPFs) of the proposed DOB is also studied for the proposed DOB

and results are compared with controllers based on classical DOB structure. During simulations, in terms of BPFs, the following two scenarios are considered to evaluate the hovering and trajectory tracking performance.

- During the first scenario, the bandwidth of the BPFs of the proposed DOB is taken to be fixed and effect of increasing the number of band-pass filters on the translational and angular motion of the quadrotor is evaluated.
- In the second scenario, the effect of the increased bandwidth of the BPFs of the proposed DOB on the stabilization and tracking performance of the quadrotor is investigated where the number of BPFs is taken to be fixed.

## 8.1 Results for Trajectory Tracking Control Using Acceleration Feedback

In this section, simulation results are presented to show the efficiency of the acceleration feedback (AF) based control in the presence of external disturbances and measurement noise. Simulations are performed on a high fidelity model where sensor biases, noise and mass uncertainty of 15% are also taken into account. Circular helix type 3-D trajectory is considered for simulations. Results for the proposed method are compared with the similar acceleration feedback based control where the analytical method for reference attitude angles calculation is considered and the yaw angle ( $\psi$ ) is taken to be some fixed value ( $\psi^*$ ) i.e.,  $\psi^* = 3.5^\circ$ . Also, the importance of the acceleration feedback in the inner loop is investigated by providing the comparison results for the proposed method with and without acceleration feedback when the similar numerical method is used for generating reference attitude angles. Model parameters are presented in Table 8.1.

External disturbances acting on the positional and attitude dynamics of the quadrotor are generated through the Dryden wind model [89] which are presented in Fig 8.1 and Fig 8.2 respectively.

TABLE 8.1: Model Parameters

| <i>Symbols</i> | <i>Description</i>             | <i>Magnitude</i>  |
|----------------|--------------------------------|-------------------|
| $m$            | Mass of the quadrotor          | 1.15 kg           |
| $I_{xx}$       | Moment of inertia about x axis | $1.1 e^{-1}kgm^2$ |
| $I_{yy}$       | Moment of inertia about y axis | $1.1 e^{-1}kgm^2$ |
| $I_{zz}$       | Moment of inertia about z axis | $15 e^{-2}kgm^2$  |
| $g$            | Acceleration due to gravity    | $9.8 m/sec^2$     |
| $l$            | Length of the rotor arm        | 0.25 m            |

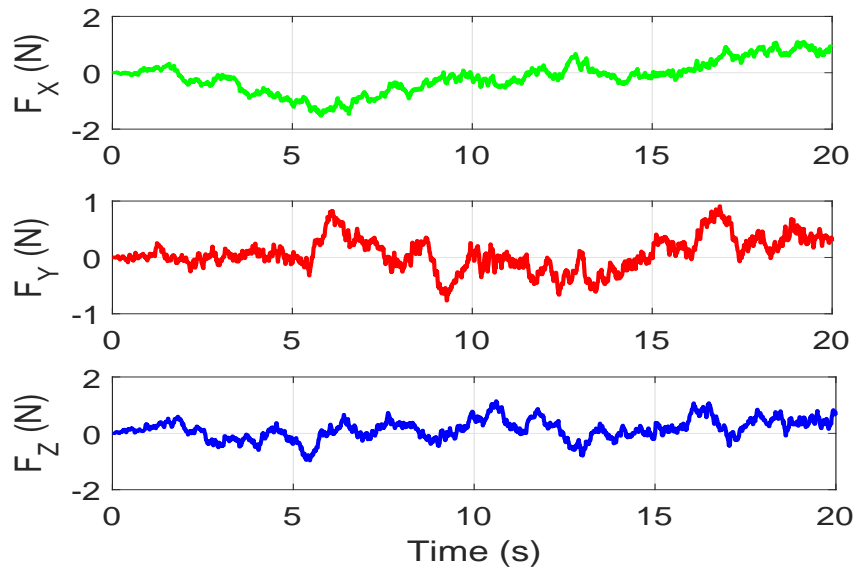


FIGURE 8.1: Disturbances acting on the positional dynamics

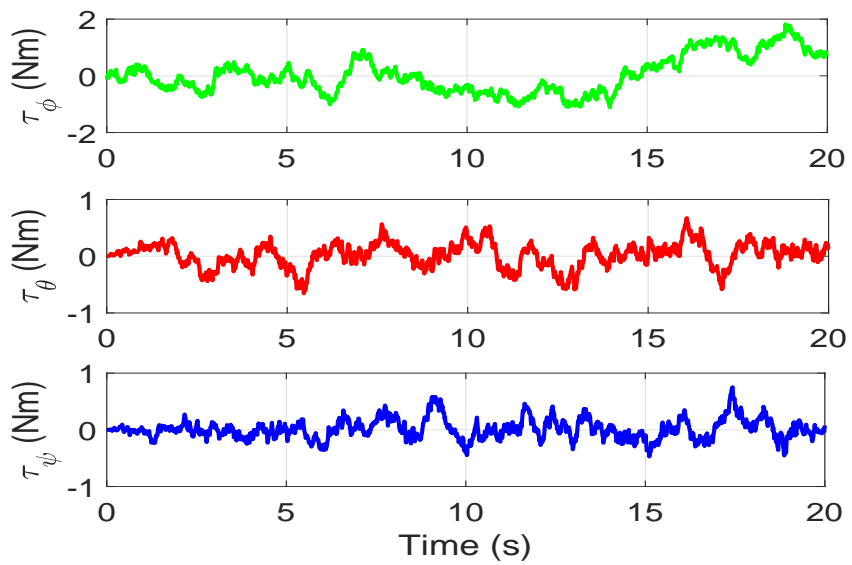


FIGURE 8.2: Disturbances acting on the attitude dynamics

Cartesian position tracking of the vehicle is depicted in Fig 8.3, Fig 8.4 and Fig 8.5 where it can be observed that the proposed control technique provided very accurate trajectory tracking with very small errors despite the external disturbances and parametric uncertainties, e.g., mass. From X Cartesian position plot, it can be inferred that both methods showed similar performance, but during the change of the roll angle, the proposed method showed better performance due to the smooth transition of the roll angle which will be elaborated further in the Euler angle plots. In Y Cartesian plot, it can be observed that the proposed method maintained its position in the close vicinity of the desired values again because of the smooth transitions in the desired pitch angle. Both methods showed similar performance in the Z Cartesian position plot. In order to show a broader picture of the efficiency of the proposed method, the position error plots are presented in Fig 8.6. 3-D trajectory tracking results are shown in Fig 8.7. Position tracking performance of the quadrotor is quantified as RMS and maximum errors in Table 8.2 which shows that with the proposed method, the quadrotor trajectory remains in close vicinity of the desired trajectory despite the disturbance forces.

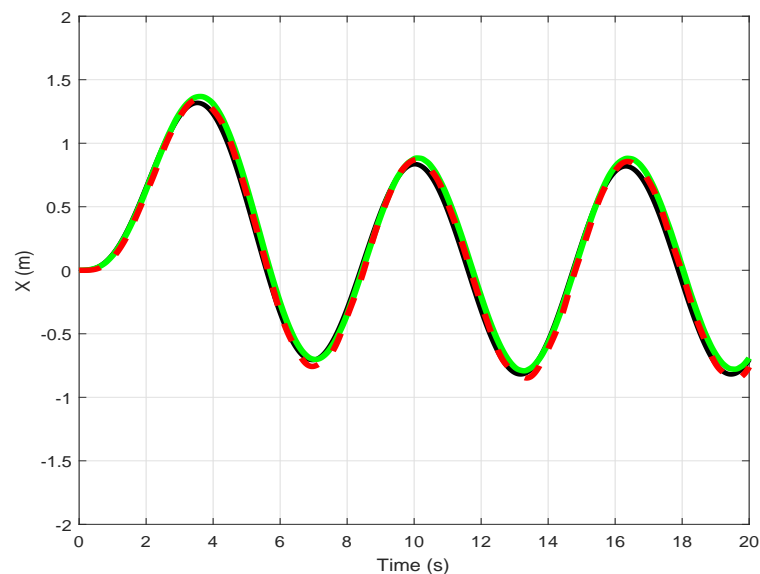


FIGURE 8.3: X Cartesian position of the quadrotor vs Time (desired in black, proposed in red, analytical in green)

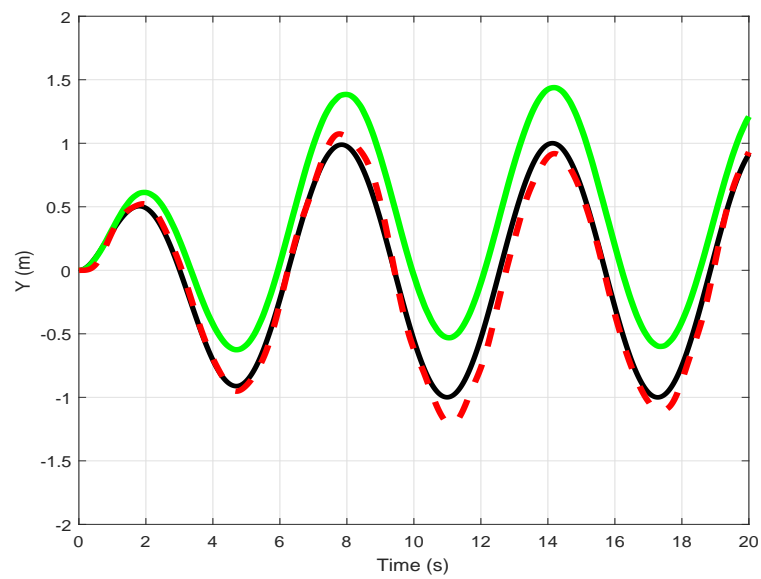


FIGURE 8.4: Y Cartesian position of the quadrotor vs Time (desired in black, proposed in red, analytical in green)

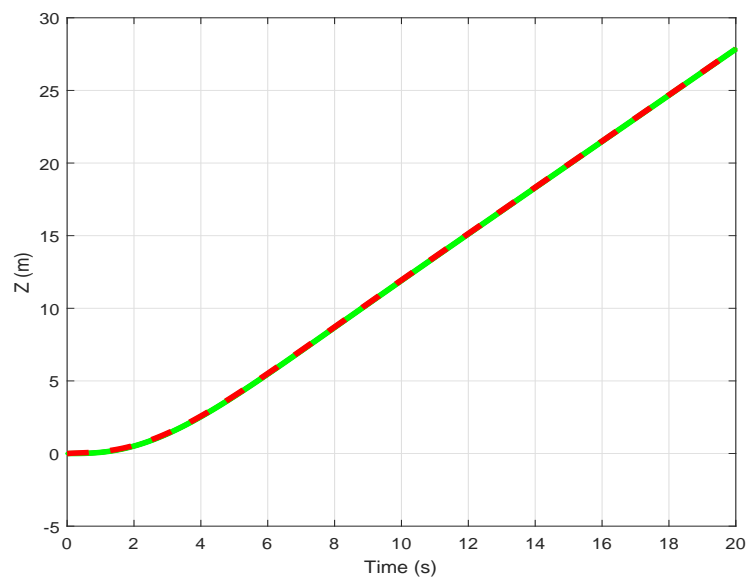


FIGURE 8.5: Z Cartesian position of the quadrotor vs Time (desired in black, proposed in red, analytical in green)

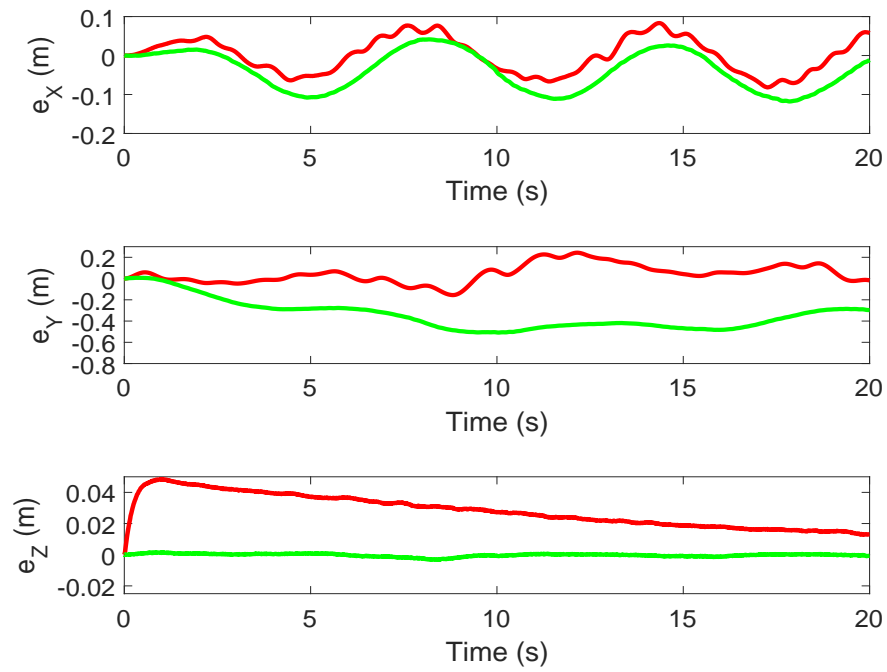


FIGURE 8.6: Position errors (proposed in red, analytical in green)

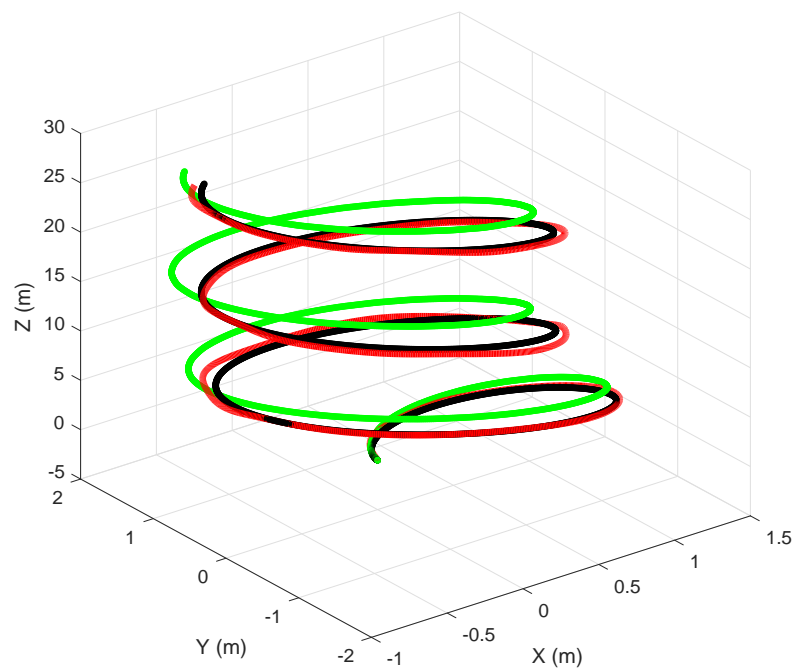


FIGURE 8.7: 3-D Trajectory (desired in black, proposed in red, analytical in green)

Attitude tracking performance can be assessed from the roll, pitch, and yaw angle plots, which are presented Fig 8.8, Fig 8.9 and Fig 8.10. From the Euler angle plots it can be seen that with the help of the optimization technique, the proposed method provides attitude angles within the desired bounds due to the magnitude constrained considered in the sequential quadratic programming (SQP). Furthermore, it can be noticed that the proposed method also provides much smoother results, which are the consequences of the rate constrained utilized in the implementation of SQP. As the translational motion of the quadrotor relies on the attitude angles, the consequences of acquiring the desired bounded and smooth attitude angles are reflected in Cartesian position plots where it can be clearly noticed that the proposed method retained its position in the close vicinity of the desired trajectory. However, results for the analytical method show fluctuated outputs, which in turn produced more Cartesian position errors. Quantitative comparison of the tracking performance for both methods is tabulated in Table 8.2.

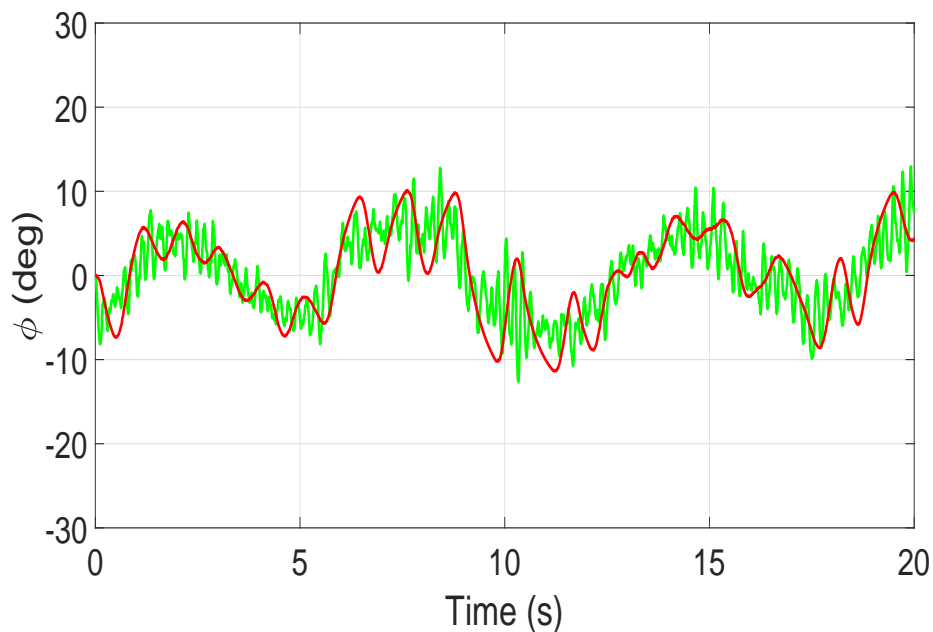


FIGURE 8.8: Roll angle (proposed in red, analytical in green)

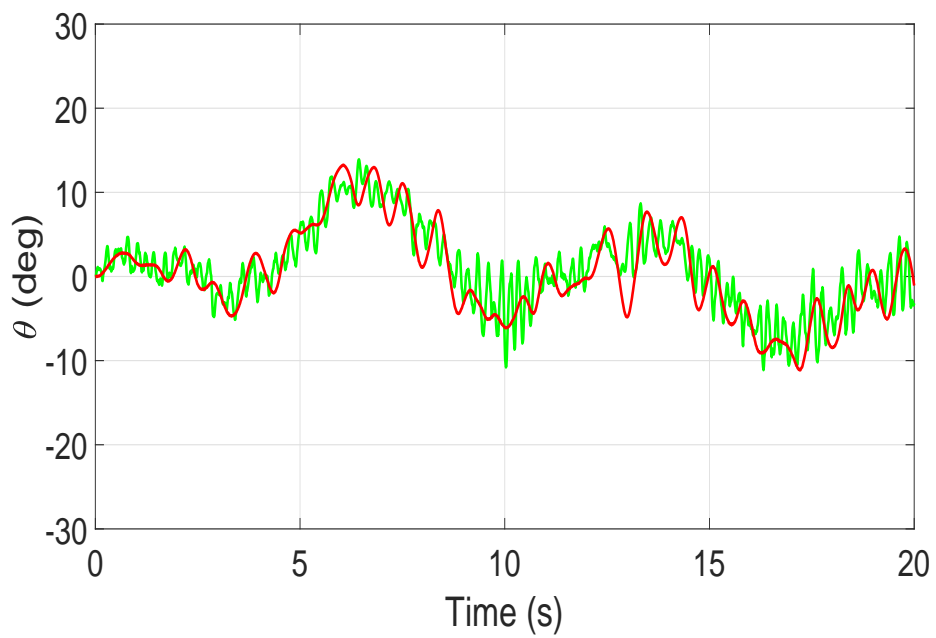


FIGURE 8.9: Pitch angle (proposed in red, analytical in green)

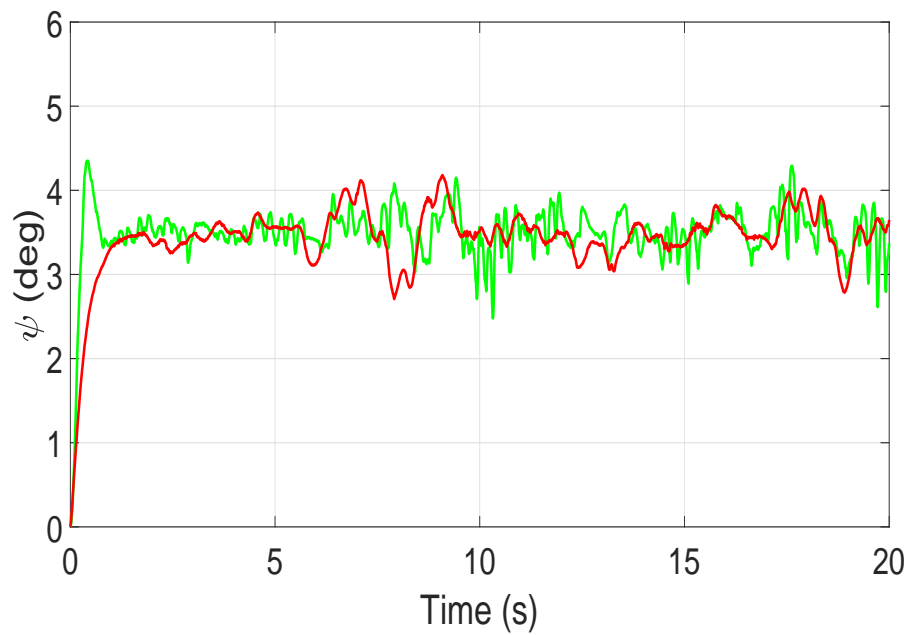


FIGURE 8.10: Yaw angle (proposed in red, analytical in green)

TABLE 8.2: Trajectory Tracking Performance

| <i>Criteria</i>       | <i>Proposed Method</i> | <i>Analytical Method</i> |
|-----------------------|------------------------|--------------------------|
| $RMS(e_X)$ m          | 0.04                   | 0.06                     |
| $Max( e_X )$ m        | 0.09                   | 0.12                     |
| $RMS(e_Y)$ m          | 0.1                    | 0.37                     |
| $Max( e_Y )$ m        | 0.243                  | 0.51                     |
| $RMS(e_Z)$ m          | 0.048                  | 0.003                    |
| $Max( e_Z )$ m        | 0.03                   | 0.009                    |
| $RMS(e_\phi)$ deg     | 4.6                    | 5.22                     |
| $Max( e_\phi )$ deg   | 11.04                  | 12.93                    |
| $RMS(e_\theta)$ deg   | 4.94                   | 5.14                     |
| $Max( e_\theta )$ deg | 12.3                   | 13.9                     |
| $RMS(e_\psi)$ deg     | 0.07                   | 0.1                      |
| $Max( e_\psi )$ deg   | 0.7                    | 0.84                     |

Estimated disturbance response has been shown in Fig 8.11, Fig 8.12 and Fig 8.13. From the estimation plot, it can be noticed that the proposed method showed better estimations than the analytical method.

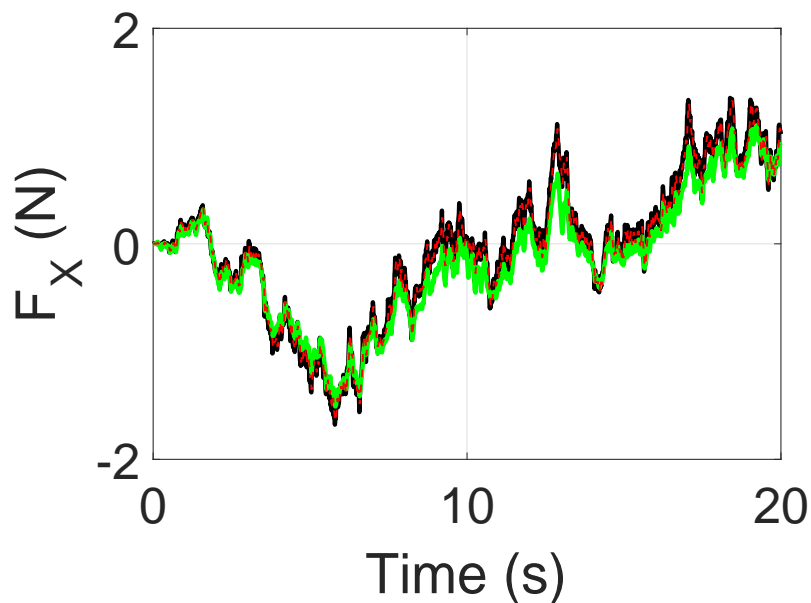


FIGURE 8.11: X axis disturbance estimation (desired in black, proposed in red, analytical in green)

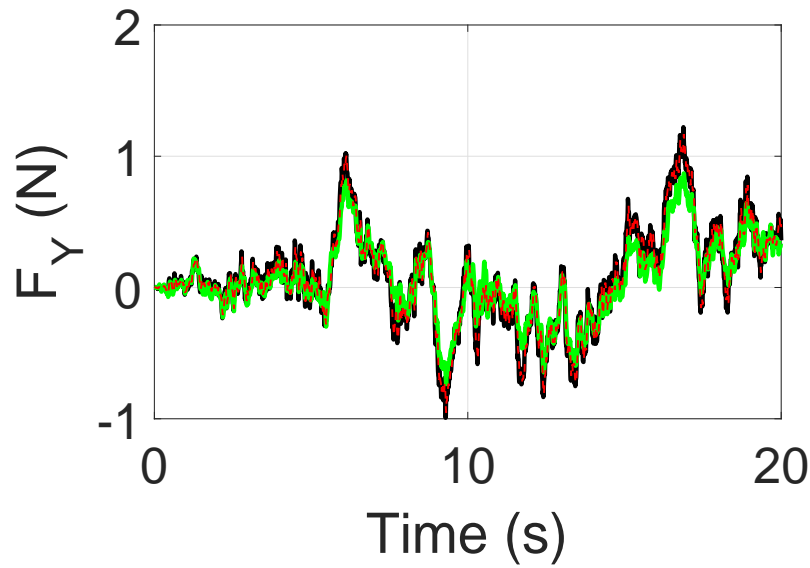


FIGURE 8.12: Y axis disturbance estimation (desired in black, proposed in red, analytical in green)

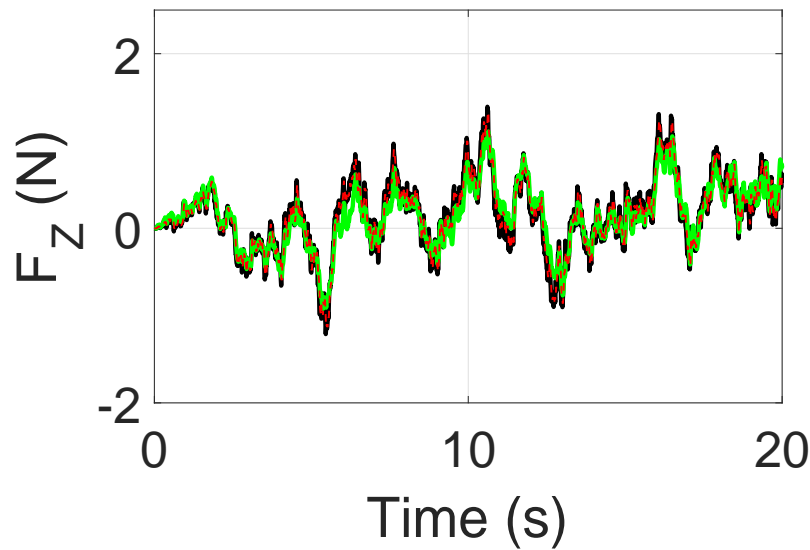


FIGURE 8.13: Z axis disturbance estimation (desired in black, proposed in red, analytical in green)

Control efforts required to get the desired trajectory tracking results are depicted in Fig 8.14. From the plot, it can be observed that utilization of the acceleration feedback in both position and attitude dynamics does not create large control efforts. In particular, the total thrust ( $U_1$ ) is approximately equal to the weight

of the vehicle ( $\sim 10.3N$ ) ; the rolling and pitching moments ( $U_2, U_3$ ) are being around  $\pm 8Nm$  and  $\pm 5Nm$ , respectively; and finally the yawing moment ( $U_4$ ) is around  $\pm 2Nm$ . Consequently, the control efforts are within reasonable limits and they provide desired maneuvers despite wind disturbances.

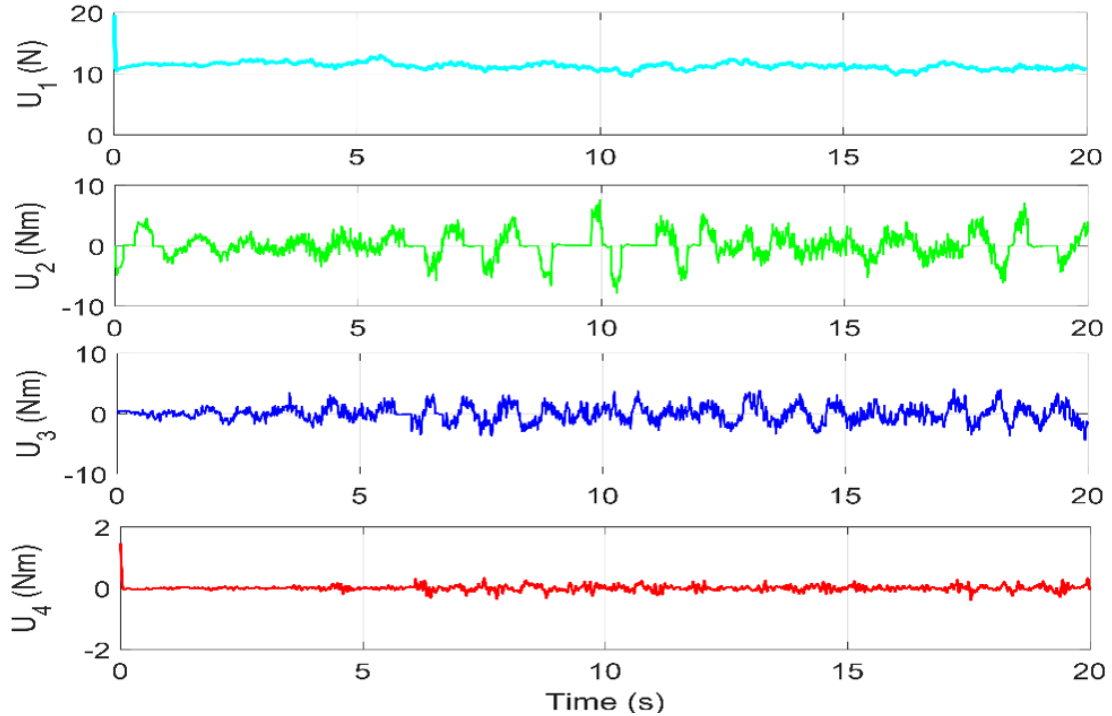


FIGURE 8.14: Control efforts

Also, in this section, the proposed method is investigated without acceleration feedback (AF) in the inner nested loop to illustrate its importance. Cartesian position plots are depicted in Fig 8.15, Fig 8.16 and Fig 8.17. From these plots, it can be observed that acceleration feedback provided more stiffness against the external disturbances, especially in the maneuvering parts of the trajectory. Position error plots are presented in Fig 8.18 where it can be noticed that the proposed method with AF provided better trajectory tracking performance with less errors despite the external disturbances and parametric uncertainties. The summary of the position errors is tabulated in Table 8.3 in terms of RMS and maximum errors.

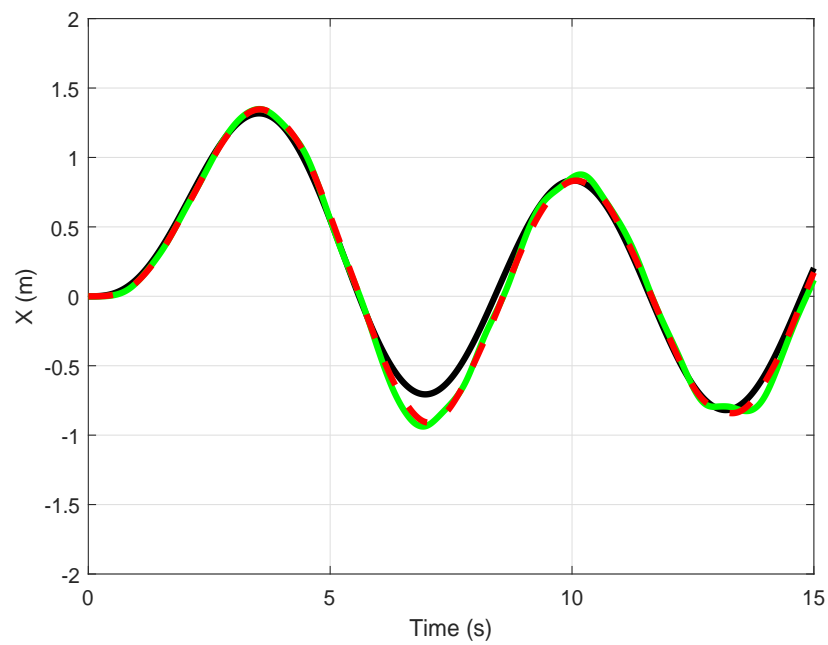


FIGURE 8.15: X Cartesian position of the quadrotor vs Time (desired in black, with AF in red, without AF in green)

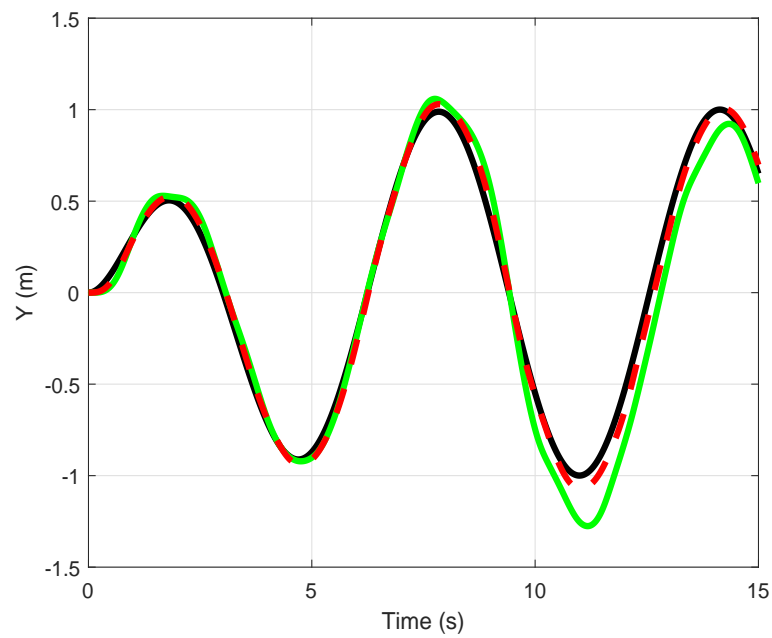


FIGURE 8.16: Y Cartesian position of the quadrotor vs Time (desired in black, with AF in red, without AF in green)

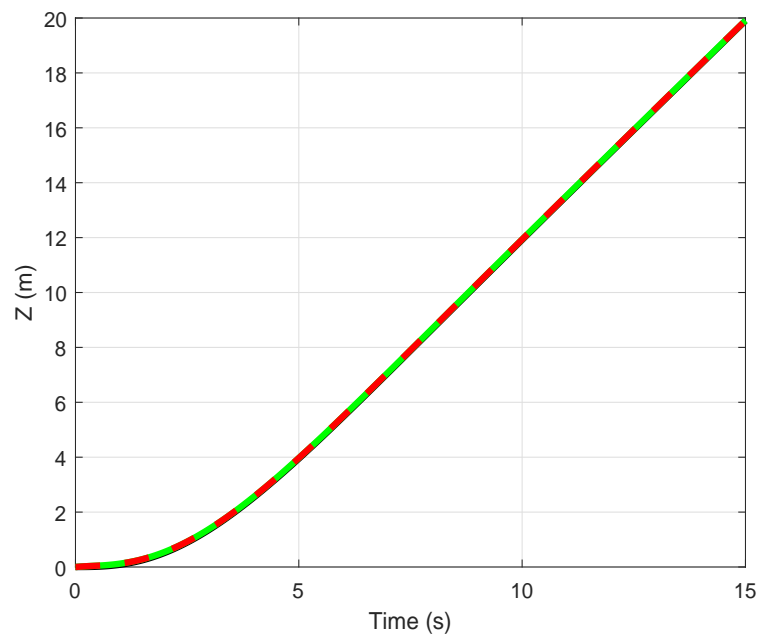


FIGURE 8.17: Z Cartesian position of the quadrotor vs Time (desired in black, with AF in red, without AF in green)

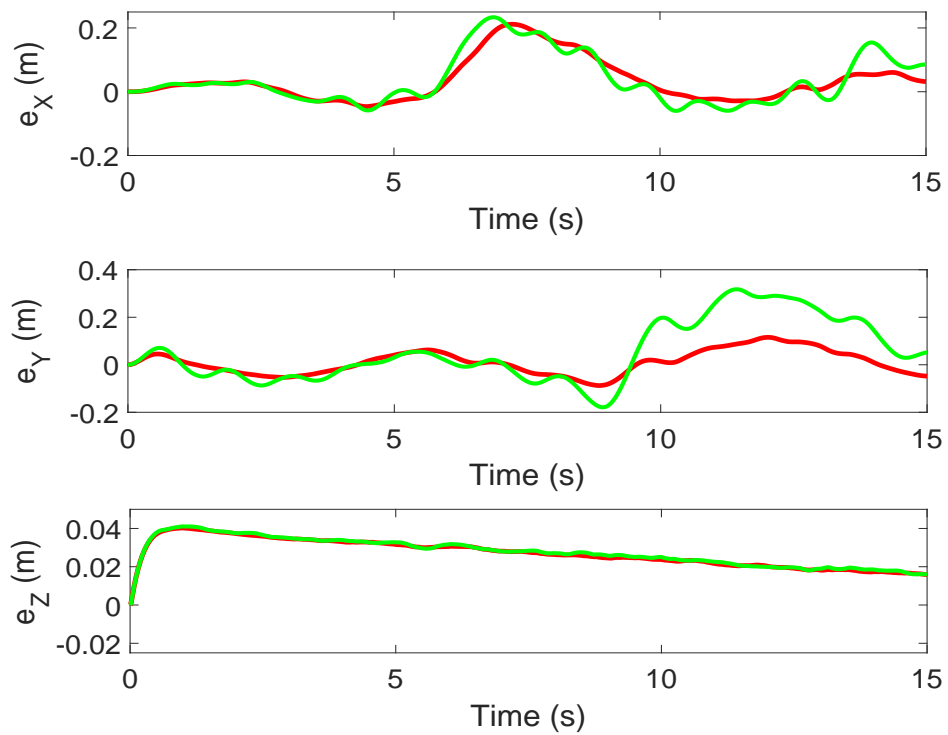


FIGURE 8.18: Position errors (with AF in red, without AF in green)

Attitude tracking performance is presented through corresponding Euler angle plots in Fig 8.19, Fig 8.20 and Fig 8.21. From the plots, it can be seen that more oscillations occurred when the proposed method was used without acceleration feedback. Therefore, utilization of the acceleration feedback in the nested feedback loops showed a significant impact on the attitude control of the quadrotor.

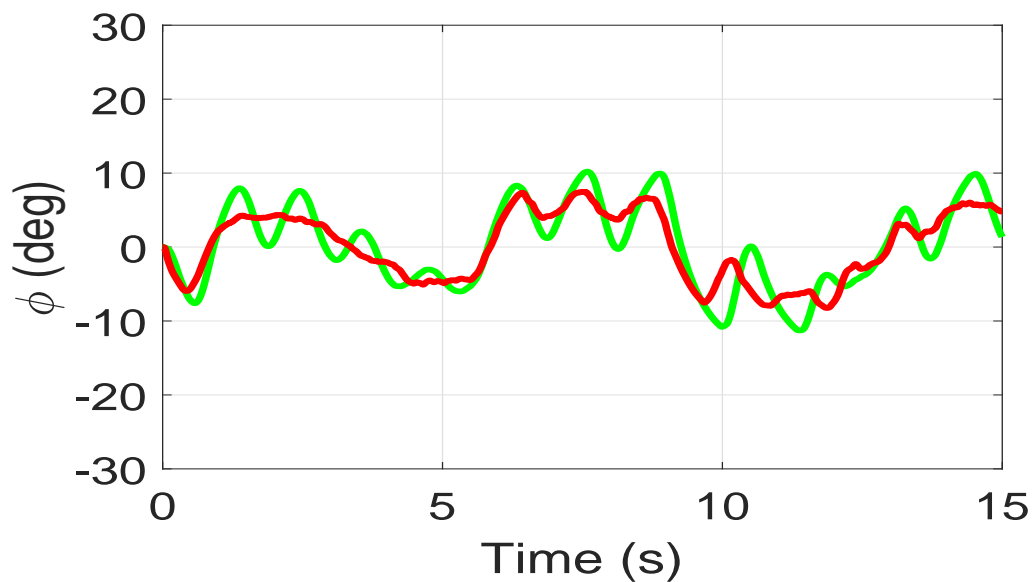


FIGURE 8.19: Roll angle (with AF in red, without AF in green)

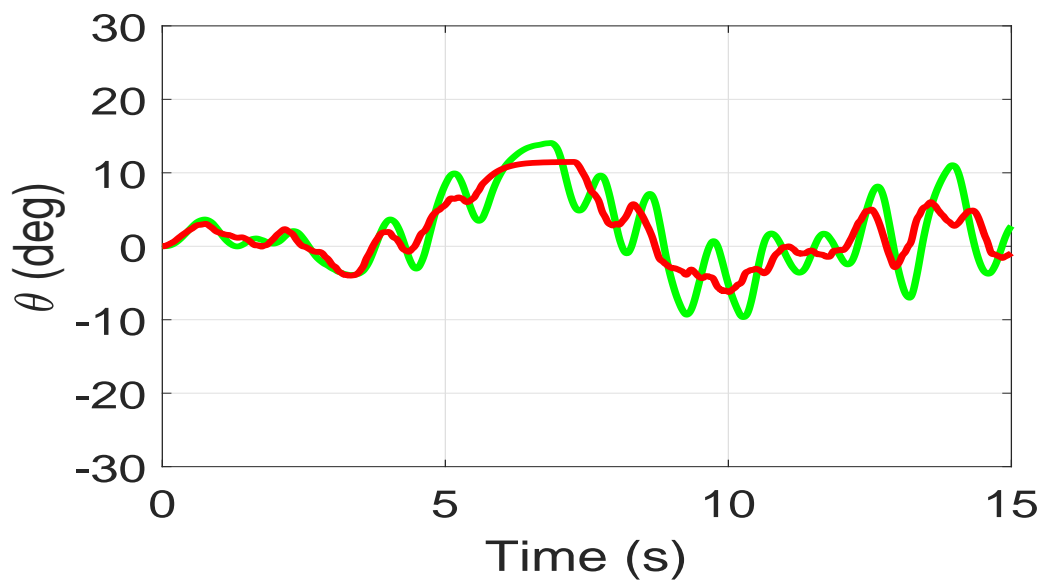


FIGURE 8.20: Pitch angle (with AF in red, without AF in green)

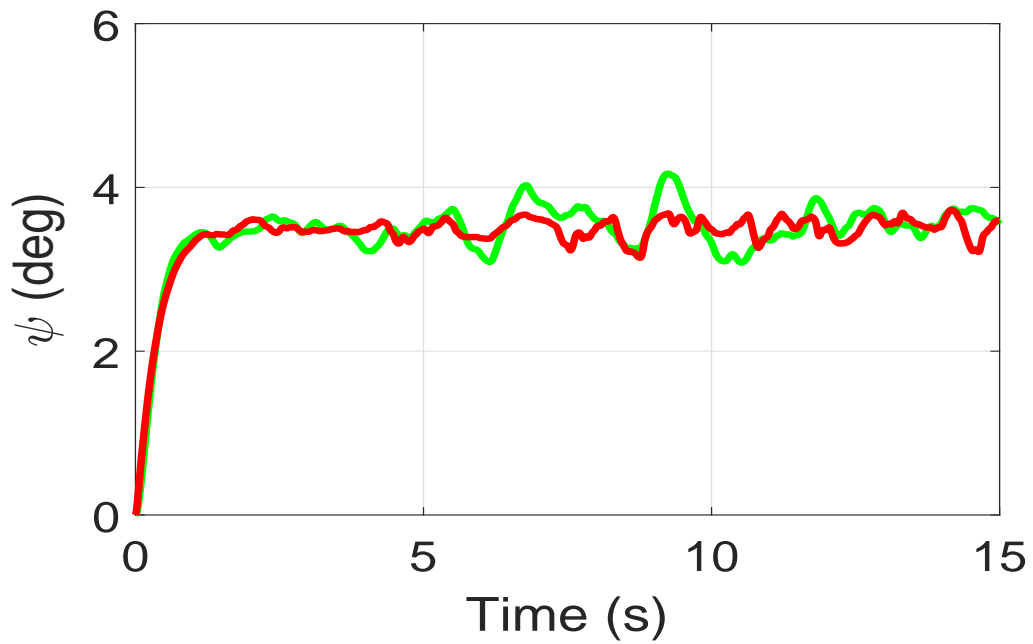


FIGURE 8.21: Yaw angle (with AF in red, without AF in green)

Trajectory tracking performance is quantified in Table 8.3 to provide a better picture of the efficiency of the proposed method with AF in terms of RMS and maximum errors.

TABLE 8.3: Trajectory Tracking Performance

| <i>Criteria</i>       | <i>with AF</i> | <i>without AF</i> |
|-----------------------|----------------|-------------------|
| $RMS(e_X)$ m          | 0.075          | 0.086             |
| $Max( e_X )$ m        | 0.21           | 0.235             |
| $RMS(e_Y)$ m          | 0.05           | 0.14              |
| $Max( e_Y )$ m        | 0.12           | 0.32              |
| $RMS(e_Z)$ m          | 0.028          | 0.029             |
| $Max( e_Z )$ m        | 0.04           | 0.041             |
| $RMS(e_\phi)$ deg     | 4.64           | 5.58              |
| $Max( e_\phi )$ deg   | 8.25           | 11.27             |
| $RMS(e_\theta)$ deg   | 4.93           | 5.75              |
| $Max( e_\theta )$ deg | 11.48          | 14.06             |
| $RMS(e_\psi)$ deg     | 3.43           | 3.48              |
| $Max( e_\psi )$ deg   | 3.73           | 4.17              |

## 8.2 Results for Hovering and Trajectory Tracking Control Using a Novel Disturbance Observer

This section evaluates the performance of the novel disturbance observer based controllers developed in chapter 7. The performance of the designed controllers is investigated in the presence of both periodic and aperiodic disturbances. Furthermore, parametric uncertainties and measurement noise are also taken into account to check the robustness of the proposed control method. Aperiodic disturbances are generated through the Dryden wind model, and the following periodic components are added to them.

$$D_{X,Y,Z} = \sum_{j=1}^{10} \sin(j15t) \quad (8.1)$$

$$D_{\phi,\theta,\psi} = \sum_{j=1}^5 2\sin(2\pi j15t) \quad (8.2)$$

For numerical simulations, two cases are considered, which include hovering at a certain altitude and three dimensional (3D) Cartesian reference trajectory tracking. Model parameters are given in Table 8.1. During the trajectory tracking, yaw angle  $\psi$  is fixed to a constant value ( $\psi^*$ ) i.e.,  $3.5^\circ$  for the calculation of desired attitude angles.

### 8.2.1 Hovering Case

The quadrotor is forced to hover at a certain altitude and the stabilizing performance is evaluated in the presence of external disturbances, parametric uncertainties and measurement noise. Disturbances acting on the positional and attitude dynamics during hovering period are given in Fig 8.22 and Fig 8.23 respectively. Additionally, this case is further divided into two scenarios where the sensitivity

of the band-pass filters used in the novel DOB is explored through the number and bandwidth of the band-pass filters.

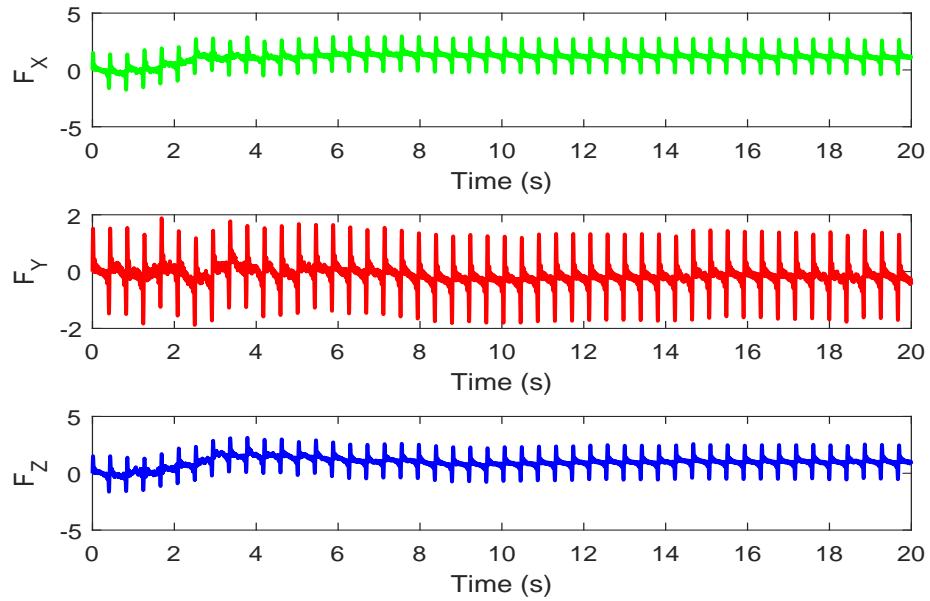


FIGURE 8.22: Disturbances acting on the positional dynamics

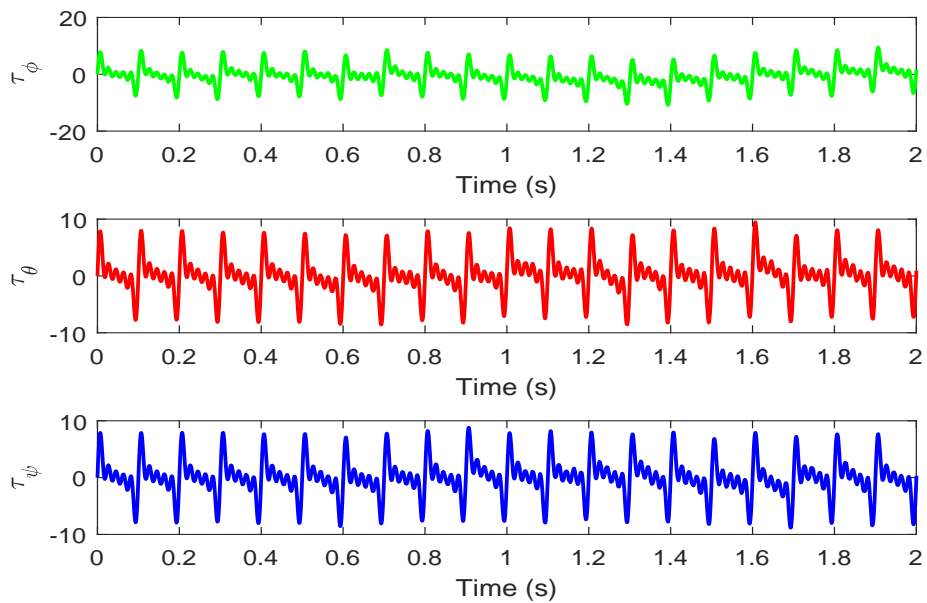


FIGURE 8.23: Disturbances acting on the attitude dynamics

### 8.2.1.1 Number of the Bandpass filters

During this hovering scenario, simulations are performed to observe the efficiency of the proposed DOB and also the effect of the increased number of band-pass filters with fixed bandwidth is investigated. In order to show the translational motion of the quadrotor, Cartesian position plots are presented in Fig 8.24, Fig 8.25 and Fig 8.26. From the position plots, it can be inferred that the proposed DOB showed better stiffness against the disturbances by retaining the position in the close vicinity of the desired values whereas classical DOB showed more deviation due to the periodic disturbances. From the X and Y position plots, it can be observed that the proposed method remains in the area of approximately  $0.055 \text{ m}^2$  in the X-Y plane whereas the classical DOB achieved hovering in the area of approximately  $0.12 \text{ m}^2$  when subjected to similar disturbances. Also, from the Z position plot, the proposed DOB hovering is closer to the desired altitude as compared to classical DOB. Furthermore, the sensitivity to the increasing number

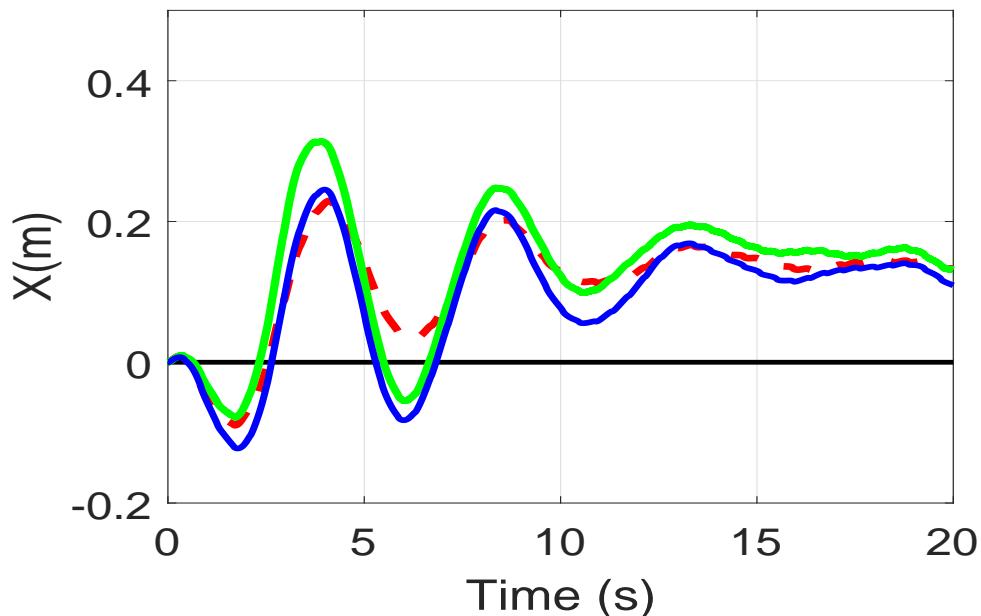


FIGURE 8.24: X Cartesian position (proposed DOB (5 BPFs in red, 3 BPFs in blue), DOB in green)

of the BPFs can be observed where increasing the number of BPFs improves the hovering performance of the quadrotor and forces the motion of the quadrotor to

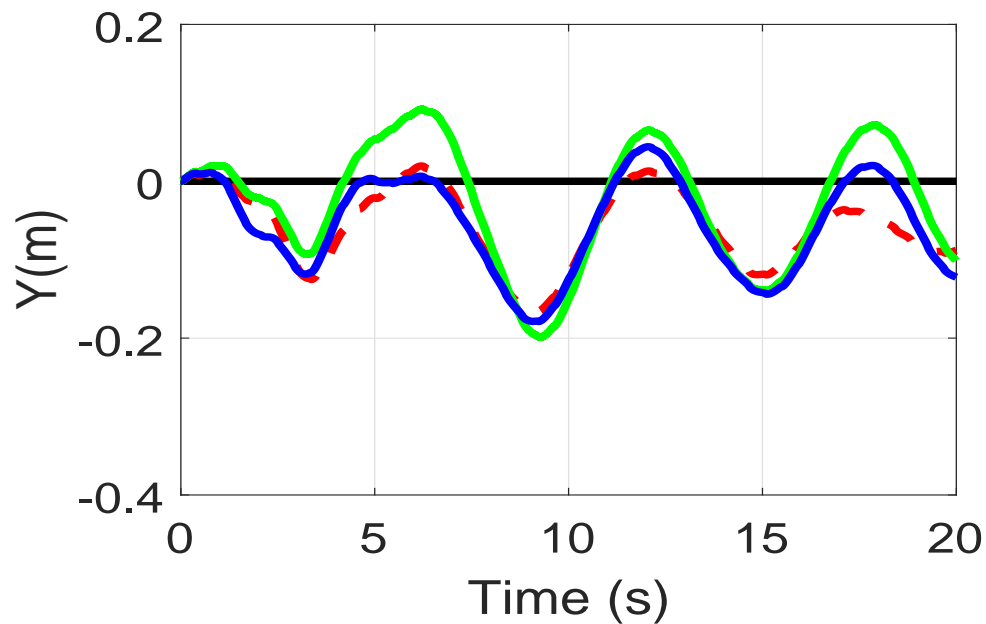


FIGURE 8.25: Y Cartesian position (proposed DOB (5 BPFs in red, 3 BPFs in blue), DOB in green)

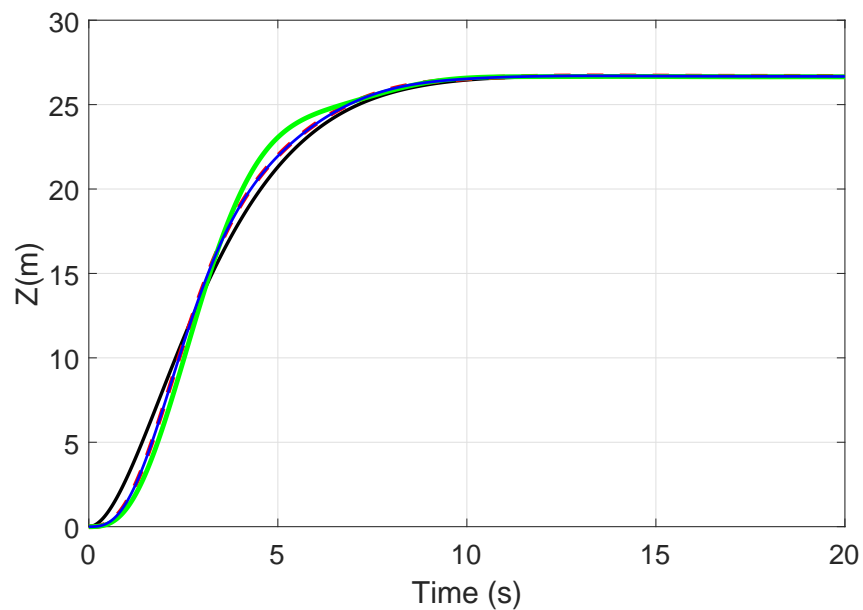


FIGURE 8.26: Z Cartesian position (proposed DOB (5 BPFs in red, 3 BPFs in blue), DOB in green)

be in the close vicinity of the desired altitude. Fig 8.27 presents the Cartesian position errors plot where it can be seen that the proposed disturbance observer structure provides better results than the classical structure and also the position errors decrease with the increasing number of band-pass filters.

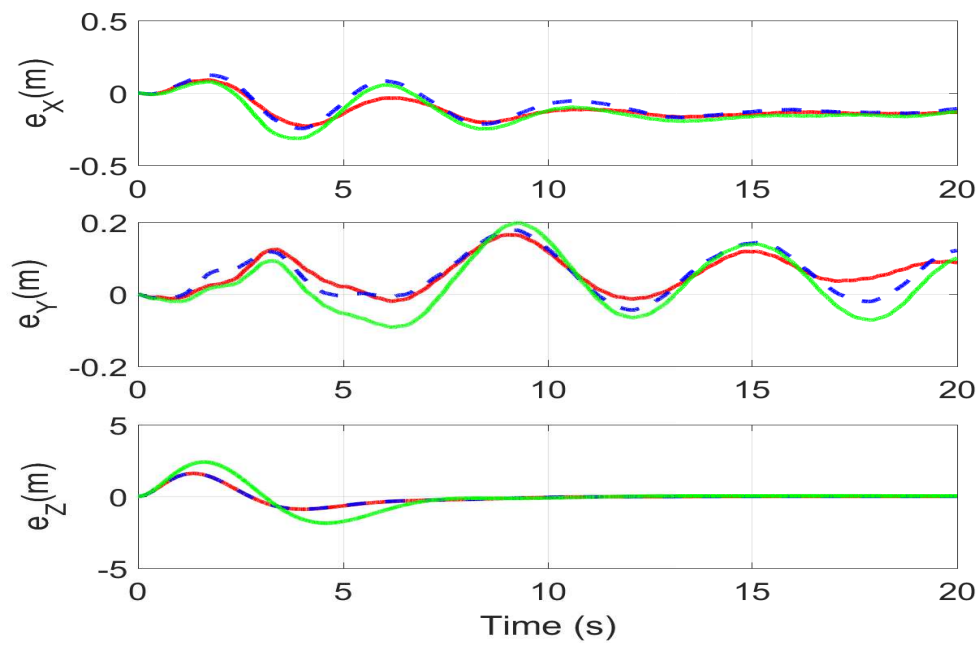


FIGURE 8.27: Position errors (proposed DOB (5 BPFs in red, 3 BPFs in blue), DOB in green)

In order to show the attitude performance of the quadrotor, Euler angle plots are presented in Fig 8.28, Fig 8.29 and Fig 8.30. These results illustrate that the proposed DOB shows less peaks and smoother results as compare to the classical DOB which explains the limitation of the classical DOB to tackle the periodic disturbances which in turn affect the translational motion of the quadrotor against the external disturbances.

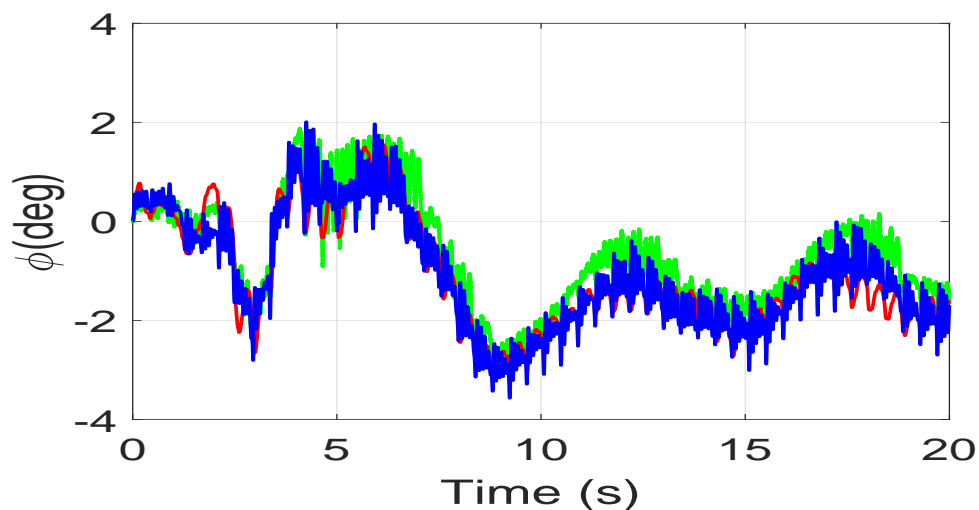


FIGURE 8.28: Roll angle (proposed DOB (5 BPFs in red, 3 BPFs in blue), DOB in green)

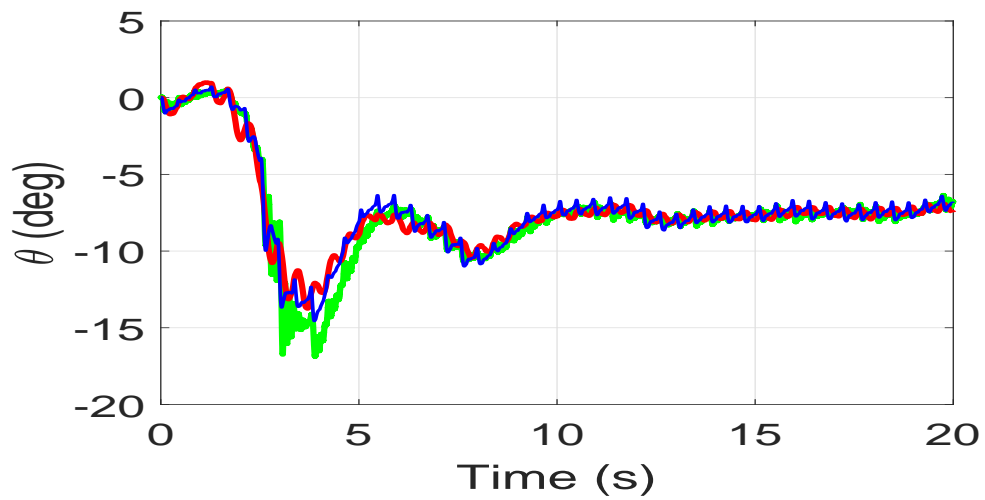


FIGURE 8.29: Pitch angle (proposed DOB (5 BPFs in red, 3 BPFs in blue), DOB in green)

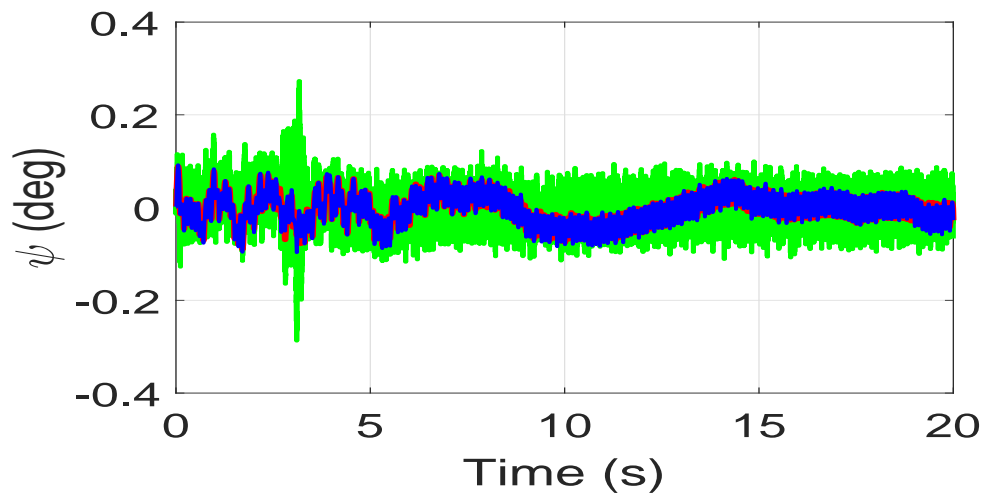


FIGURE 8.30: Yaw angle (proposed DOB (5 BPFs in red, 3 BPFs in blue), DOB in green)

From the attitude plots, the proposed structure with larger number of band-pass filters provides less peaks and fluctuations. Table 8.4 presents a quantitative analysis of the hovering performance of the quadrotor in terms of root mean square (RMS) errors and maximum errors.

TABLE 8.4: Hovering Performance with Different Number of the BPFs

| <i>Criteria</i>       | <i>DOB</i> | <i>Proposed DOB with 5 BPFs</i> | <i>Proposed DOB with 3 BPFs</i> |
|-----------------------|------------|---------------------------------|---------------------------------|
| $RMS(e_X)$ m          | 0.24       | 0.1                             | 0.13                            |
| $Max( e_X )$ m        | 0.33       | 0.12                            | 0.24                            |
| $RMS(e_Y)$ m          | 0.1        | 0.07                            | 0.08                            |
| $Max( e_Y )$ m        | 0.2        | 0.15                            | 0.17                            |
| $RMS(e_Z)$ m          | 0.9        | 0.47                            | 0.5                             |
| $Max( e_Z )$ m        | 2.4        | 1.5                             | 1.6                             |
| $RMS(e_\phi)$ deg     | 1.3        | 1.5                             | 1.53                            |
| $Max( e_\phi )$ deg   | 3.14       | 3.2                             | 3.4                             |
| $RMS(e_\theta)$ deg   | 8.6        | 7.7                             | 7.8                             |
| $Max( e_\theta )$ deg | 17.1       | 13.7                            | 14.5                            |
| $RMS(e_\psi)$ deg     | 0.05       | 0.03                            | 0.033                           |
| $Max( e_\psi )$ deg   | 0.28       | 0.08                            | 0.18                            |

### 8.2.1.2 Bandwidth of the Bandpass filters

This scenario presents results for the hovering control of the quadrotor to show the effect of the increased bandwidth of the BPFs of the DOB, and results are then compared with classical DOB structure. Translational motion of the quadrotor is represented through Cartesian position plots in Fig 8.31, Fig 8.32 and Fig 8.33.

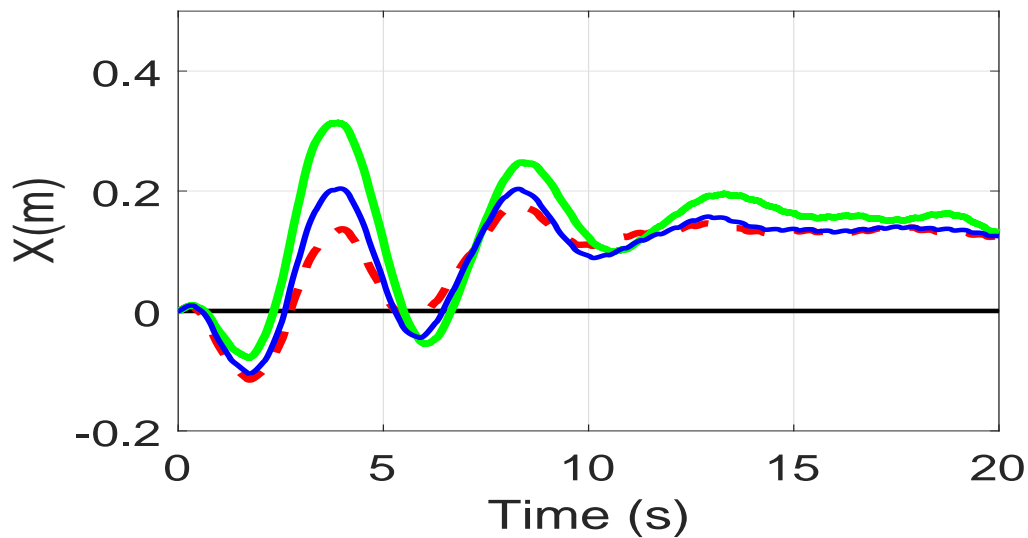


FIGURE 8.31: X Cartesian position (proposed DOB (30 rad/sec in red, 20 rad/sec in blue), DOB in green)

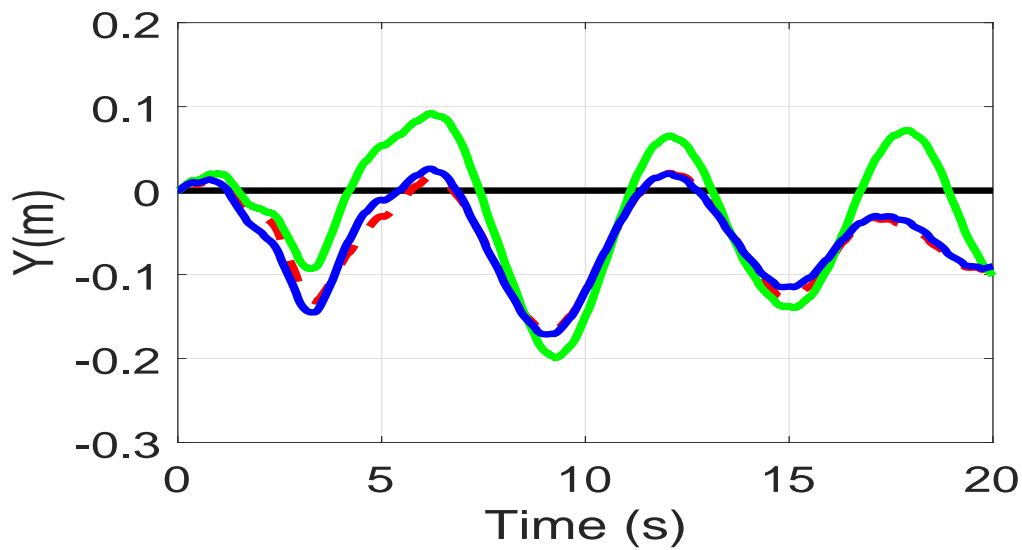


FIGURE 8.32: Y Cartesian position (proposed DOB (30 rad/sec in red, 20 rad/sec in blue), DOB in green)

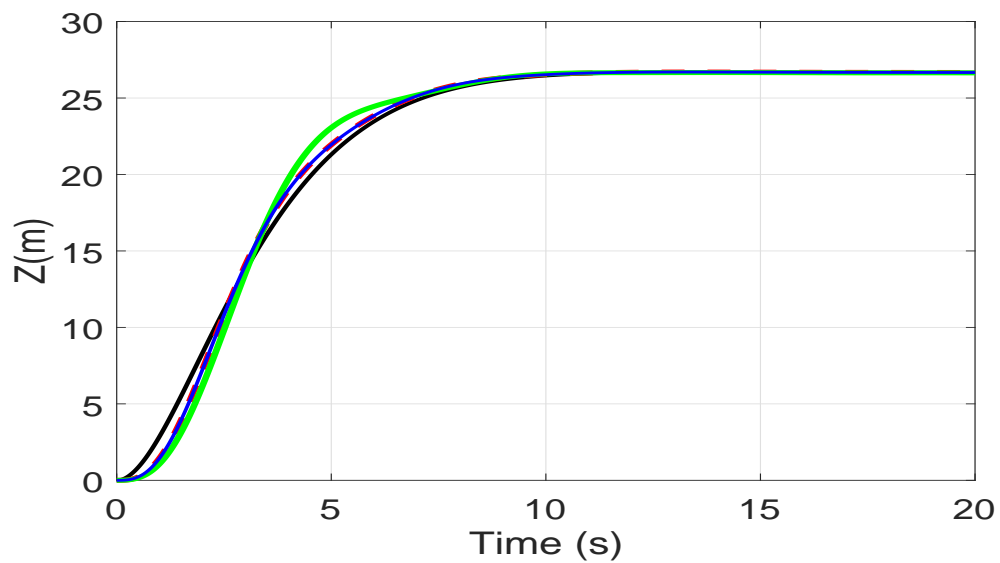


FIGURE 8.33: Z Cartesian position (proposed DOB (30 rad/sec in red, 20 rad/sec in blue), DOB in green)

X and Y position plots showed that increasing the bandwidth of the band-pass filters forced the quadrotor to remain in an area of approximately  $0.045 \text{ m}^2$  whereas the classical DOB achieved hovering in an area of approximately  $0.12 \text{ m}^2$  which implies that hovering performance of the proposed DOB is improved with more bandwidth. Also, the proposed DOB shows better stiffness against the external disturbances than the classical DOB to stabilize the quadrotor at a certain altitude,

which is depicted in the Z-position plot. The effect of the increased bandwidth can be further investigated through position errors plot in Fig 8.34 where it can be noticed that the errors decrease with the increased bandwidth.

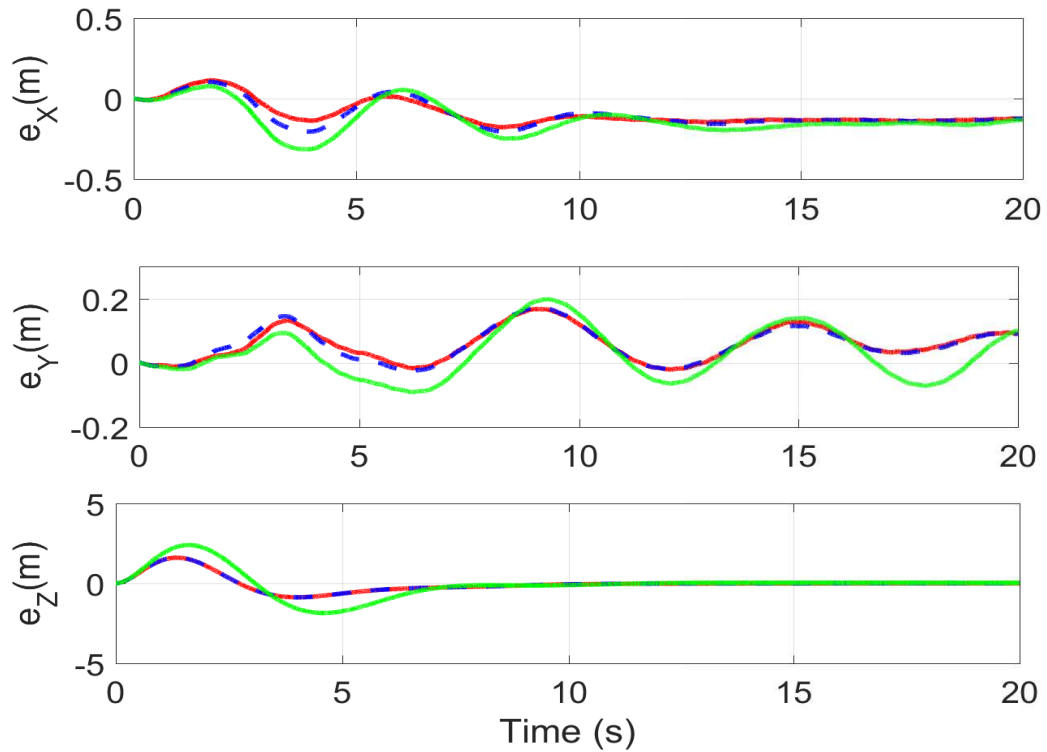


FIGURE 8.34: Position errors (proposed DOB with bandwidth (30 rad/sec in red, 20 rad/sec in blue), DOB in green)

Attitude performance of the proposed controller is presented through the corresponding Euler angles plots in Fig 8.35, Fig 8.36 and Fig 8.37. Through the plots, it can be observed that the proposed method shows improved results where much smoother results are obtained by increasing the bandwidth of the BPFs. Also, the proposed DOB causes a reduction in the peak amplitude, which shows that by increasing the bandwidth of the proposed DOB, periodic disturbances can be handled more efficiently. Quantification of the hovering performance for this scenario in terms of the maximum and root mean square errors is provided in Table 8.5.

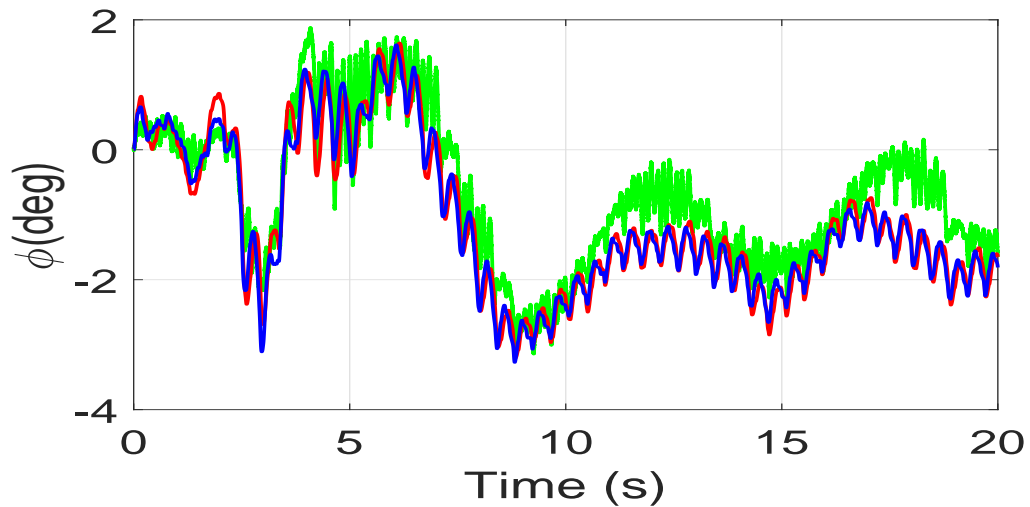


FIGURE 8.35: Roll angle (proposed DOB with bandwidth (30 rad/sec in red, 20 rad/sec in blue), DOB in green)

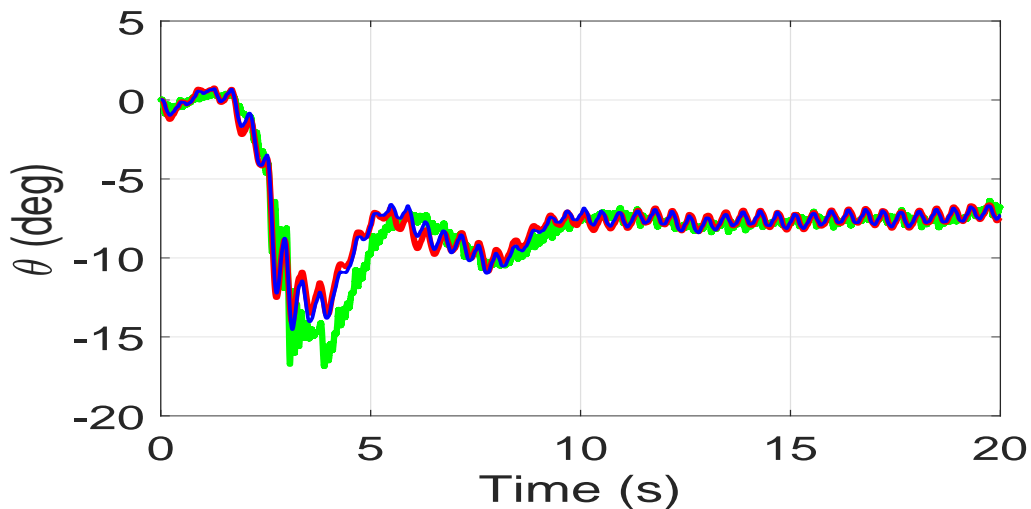


FIGURE 8.36: Pitch angle (proposed DOB with bandwidth (30 rad/sec in red, 20 rad/sec in blue), DOB in green)

## 8.2.2 Trajectory Tracking Case

This section investigates the trajectory tracking performance of the proposed controller with novel disturbance observer. In this case, 3D Circular helix type trajectory is used to study the more challenging task than the hovering where quadrotor is required to do more maneuvers in the presence of external disturbances, parametric uncertainties, and noise. Like hovering case in section 8.2.1, two similar scenarios are considered where the effects of the bandwidth and the number of

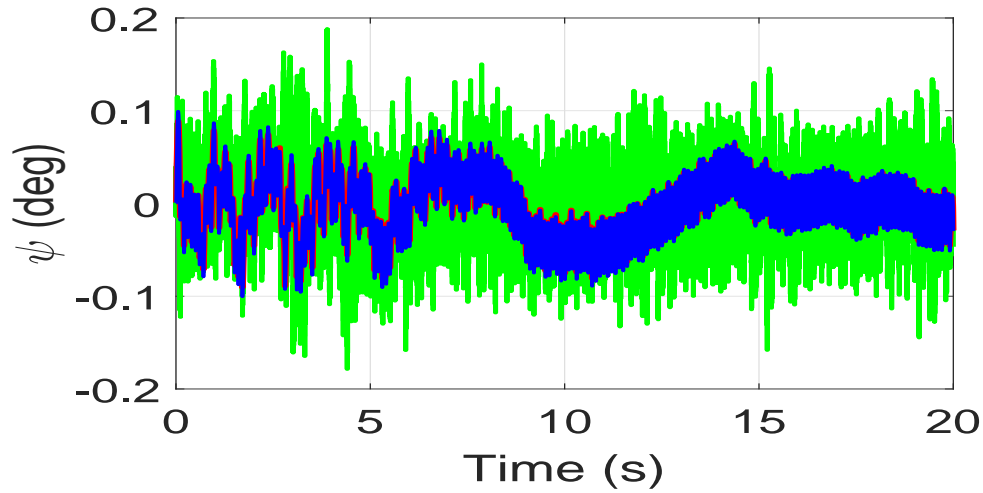


FIGURE 8.37: Yaw angle (proposed DOB with bandwidth (30 rad/sec in red, 20 rad/sec in blue), DOB in green)

TABLE 8.5: Hovering Performance with Different Bandwidths of the BPFs

| <i>Criteria</i>       | <i>DOB</i> | <i>Proposed DOB with <math>2\sigma=30</math> rad/sec</i> | <i>Proposed DOB with <math>2\sigma=20</math> rad/sec</i> |
|-----------------------|------------|--|--|
| $RMS(e_X)$ m          | 0.24       | 0.11   | 0.13   |
| $Max( e_X )$ m        | 0.33       | 0.12   | 0.24   |
| $RMS(e_Y)$ m          | 0.1        | 0.07   | 0.078  |
| $Max( e_Y )$ m        | 0.2        | 0.15   | 0.17   |
| $RMS(e_Z)$ m          | 0.9        | 0.48   | 0.485  |
| $Max( e_Z )$ m        | 2.4        | 1.5  | 1.6  |
| $RMS(e_\phi)$ deg     | 1.3        | 1.5  | 1.55   |
| $Max( e_\phi )$ deg   | 3.14       | 3.2  | 3.27   |
| $RMS(e_\theta)$ deg   | 8.6        | 7.8  | 7.8  |
| $Max( e_\theta )$ deg | 17.1       | 13.9   | 14.6   |
| $RMS(e_\psi)$ deg     | 0.05       | 0.03   | 0.036  |
| $Max( e_\psi )$ deg   | 0.28       | 0.08   | 0.12   |

band-pass filters used in the novel DOB are investigated on the position and attitude performance of the quadrotor. Results in both scenarios are compared with the controller based on classical DOB to show the trajectory tracking performance of the proposed controller. External disturbances are generated through the Dryden wind model and series of sine functions. Fig 8.38 and Fig 8.39 show the disturbances acting on the positional and attitude dynamics respectively.

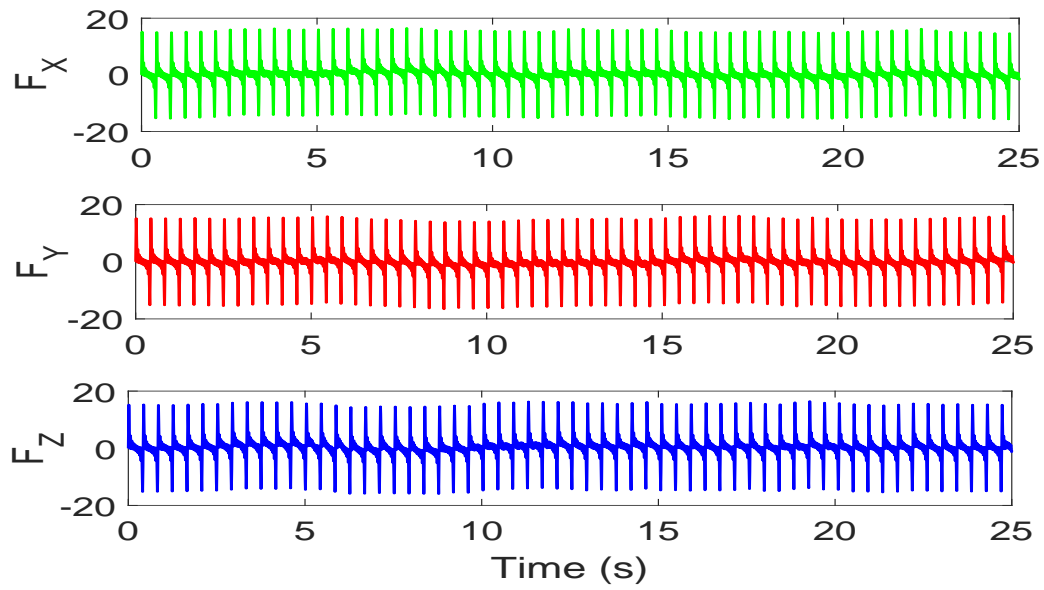


FIGURE 8.38: Disturbances acting on positional dynamics

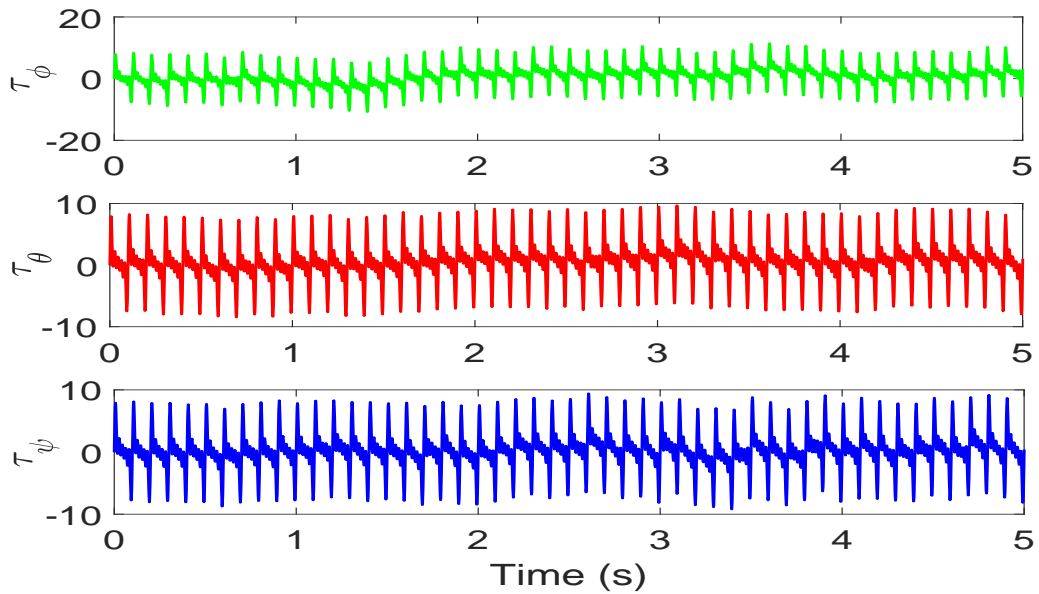


FIGURE 8.39: Disturbances acting on attitude dynamics

### 8.2.2.1 Number of the Bandpass filters

In this scenario, trajectory tracking performance of the quadrotor is evaluated for the proposed DOB, and the effect of more band-pass filters on the translational and angular motion is studied when the quadrotor is subject to external disturbance along with the noise and parametric uncertainties. Cartesian position tracking

of the vehicle is depicted in Fig 8.40, Fig 8.41 and Fig 8.42. From the plots, it can be observed that the proposed DOB provides better performance, especially during the maneuvers where the quadrotor remains in the close vicinity of the desired values. Results for the classical DOB show deviations from the desired trajectory at the maneuver sections. Furthermore, it is also observed that the proposed method shows more stiffness against the disturbance when the number of BPFs is increased.

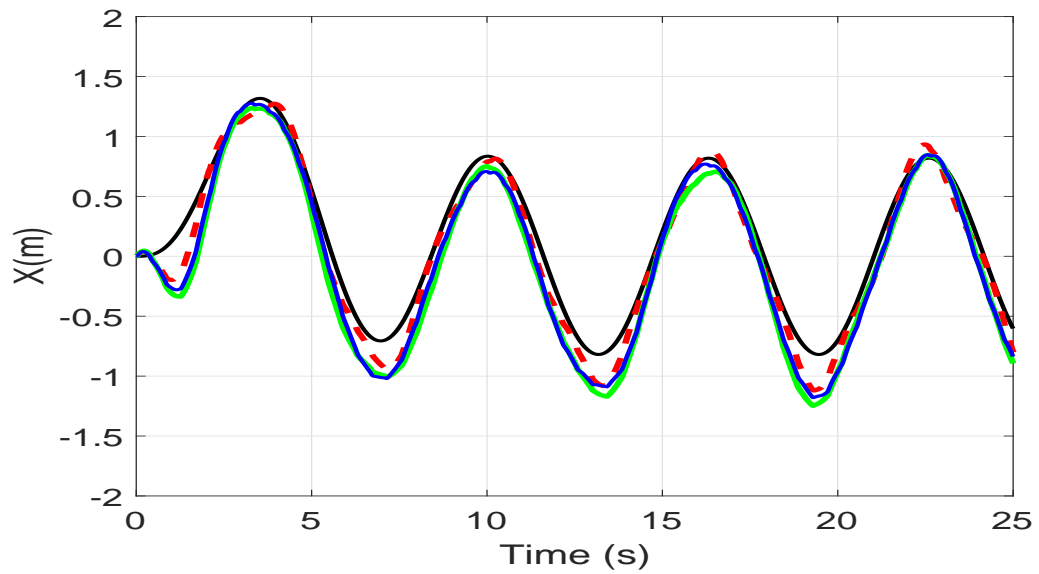


FIGURE 8.40: X Cartesian position (proposed DOB (5 BPFs in red, 3 BPFs in blue), DOB in green)

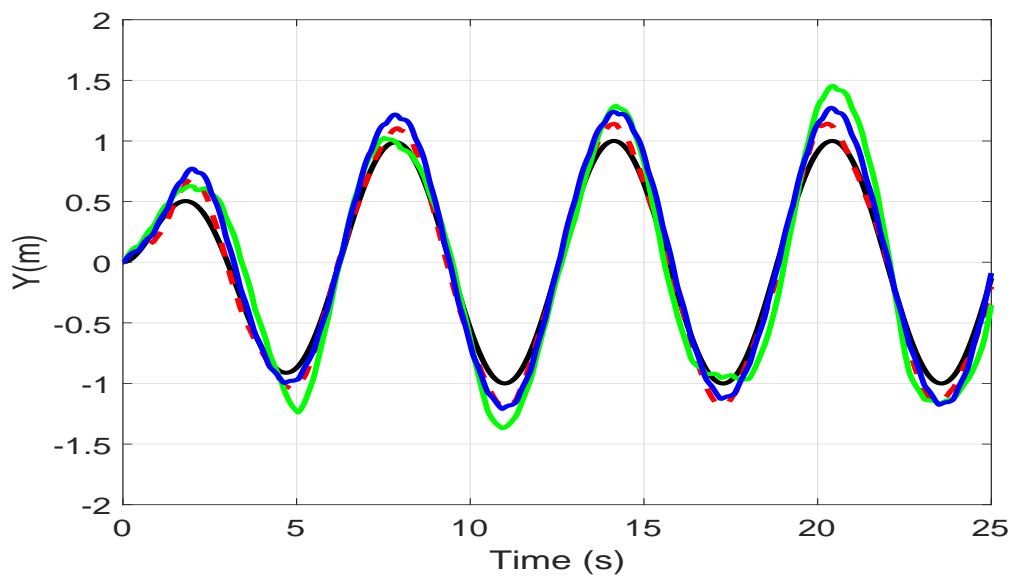


FIGURE 8.41: Y Cartesian position (proposed DOB (5 BPFs in red, 3 BPFs in blue), DOB in green)

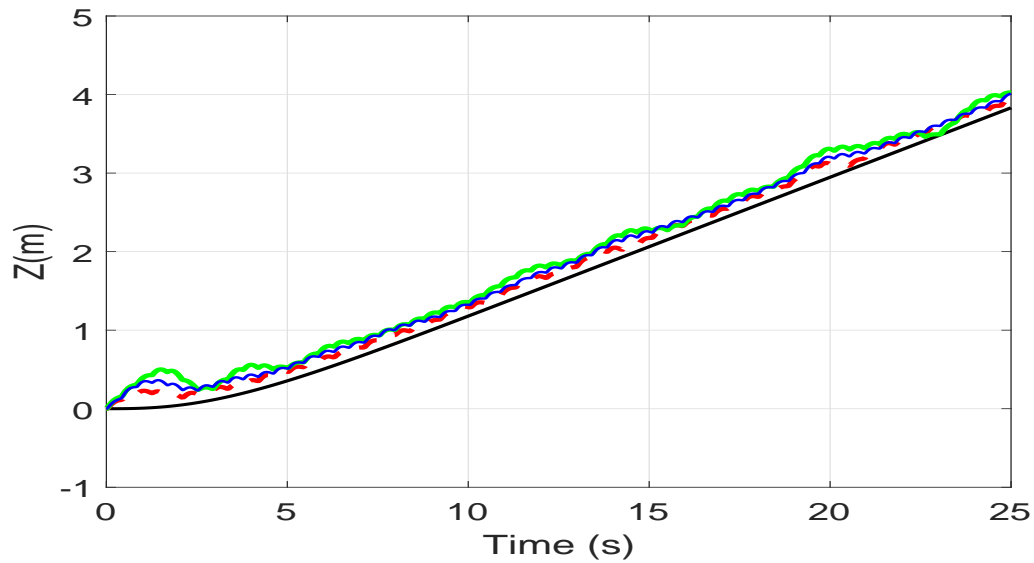


FIGURE 8.42: Z Cartesian position (proposed DOB (5 BPFs in red, 3 BPFs in blue), DOB in green)

To show the better picture of the robustness provided by the proposed method and to study the sensitivity to the number of BPFs, Cartesian position errors plot is provided in Fig 8.43 where it can be seen that errors for the proposed method decrease with the increasing number of band-pass filters.

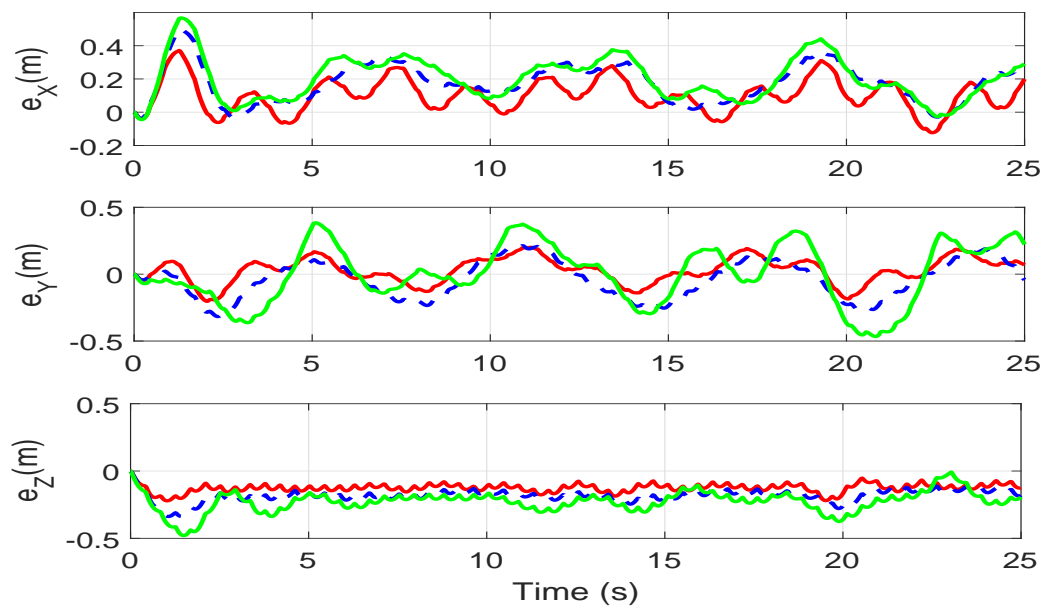


FIGURE 8.43: Position errors (proposed DOB (5 BPFs in red, 3 BPFs in blue), DOB in green)

Attitude performance of the quadrotor in this scenario is depicted through Corresponding Euler angles plots in Fig 8.44, Fig 8.45 and Fig 8.46. Euler angle plots depict that the proposed method provides better performance with less peaks than the classical DOB, which indicates the efficiency of the novel DOB to reject the disturbances. Also, the increased number of band-pass filters affects the attitude response, which in turn manifest itself in the translational motion of the quadrotor. It should be noticed from the plots that response gets closer to the classical DOB when the number of BPFs is decreased.

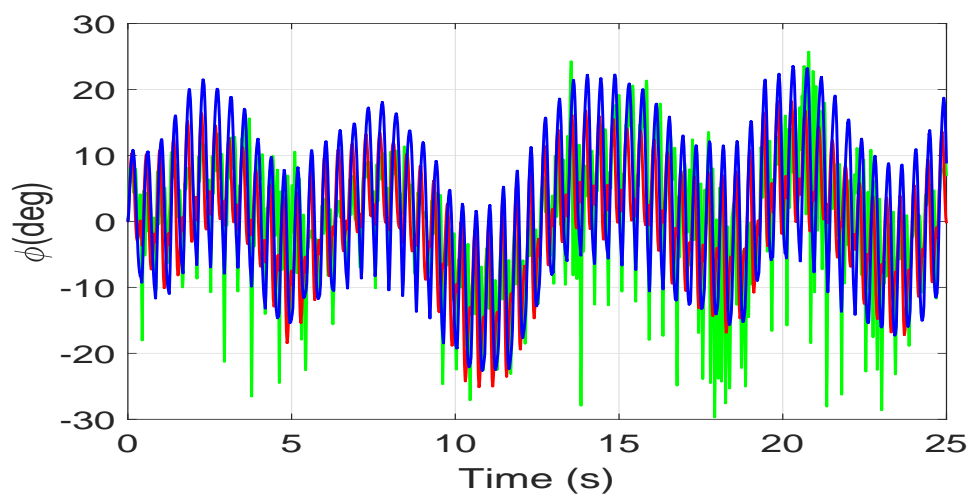


FIGURE 8.44: Roll angle (proposed DOB (5 BPFs in red, 3 BPFs in blue), DOB in green)

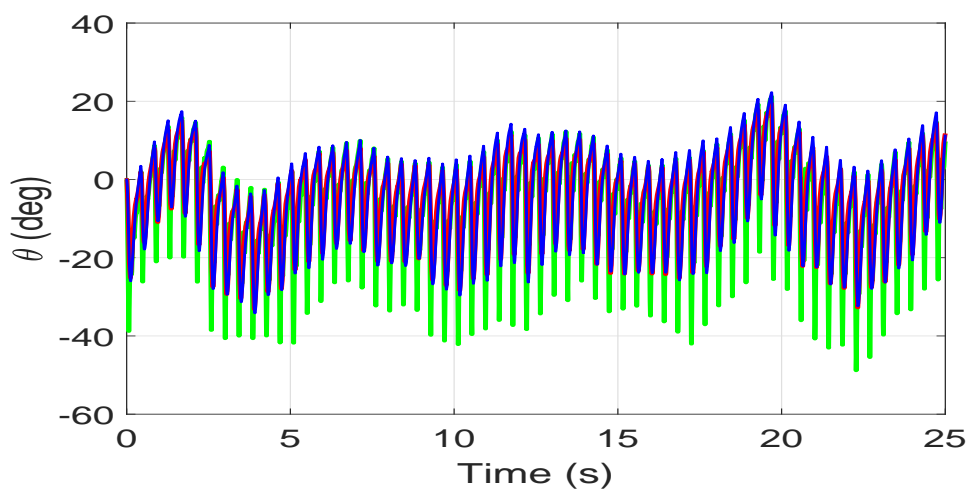


FIGURE 8.45: Pitch angle (proposed DOB (5 BPFs in red, 3 BPFs in blue), DOB in green)

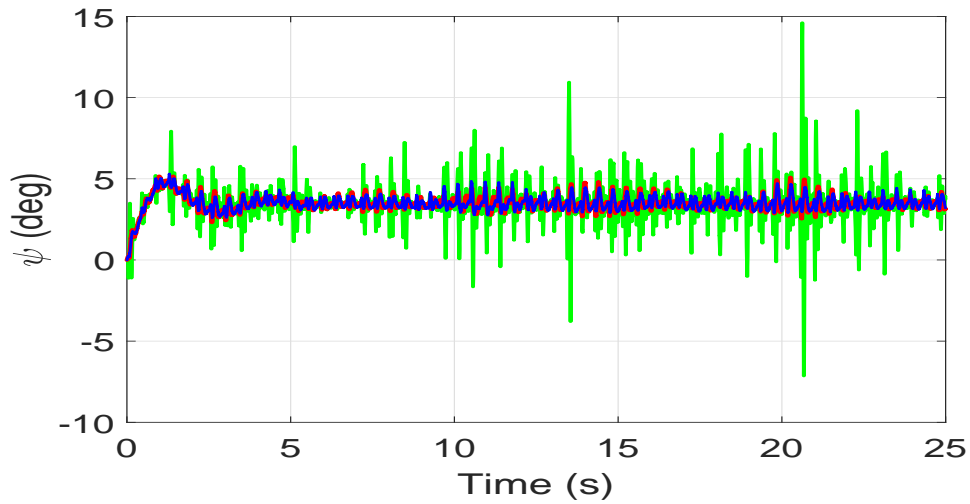


FIGURE 8.46: Yaw angle (proposed DOB (5 BPFs in red, 3 BPFs in blue), DOB in green)

Trajectory tracking performance for this scenario is summarized in terms of RMS and maximum values for errors in Table 8.6.

TABLE 8.6: Trajectory Tracking Performance with Different Number of the BPFs

| <i>Criteria</i>       | <i>DOB</i> | <i>Proposed DOB<br/>with 5 BPFs</i> | <i>Proposed DOB<br/>with 3 BPFs</i> |
|-----------------------|------------|-------------------------------------|-------------------------------------|
| $RMS(e_X)$ m          | 0.24       | 0.13                                | 0.18                                |
| $Max( e_X )$ m        | 0.56       | 0.37                                | 0.45                                |
| $RMS(e_Y)$ m          | 0.217      | 0.098                               | 0.14                                |
| $Max( e_Y )$ m        | 0.48       | 0.2                                 | 0.31                                |
| $RMS(e_Z)$ m          | 0.24       | 0.13                                | 0.19                                |
| $Max( e_Z )$ m        | 0.49       | 0.22                                | 0.33                                |
| $RMS(e_\phi)$ deg     | 9.5        | 8.1                                 | 9.3                                 |
| $Max( e_\phi )$ deg   | 29.8       | 22.3                                | 23.6                                |
| $RMS(e_\theta)$ deg   | 13.1       | 10.1                                | 11.5                                |
| $Max( e_\theta )$ deg | 49.2       | 32.2                                | 32.8                                |
| $RMS(e_\psi)$ deg     | 3.78       | 3.55                                | 3.58                                |
| $Max( e_\psi )$ deg   | 14.6       | 5.05                                | 5.07                                |

### 8.2.2.2 Bandwidth of the Bandpass Filters

This scenario deals with trajectory tracking of the quadrotor when the bandwidth of the BPFs is increased and results are provided to study the effect of the bandwidth change on the tracking performance. Cartesian position tracking of the vehicle is presented in Fig 8.47, Fig 8.48 and Fig 8.49 where improved tracking performance is obtained when the bandwidth of the BPFs is increased.

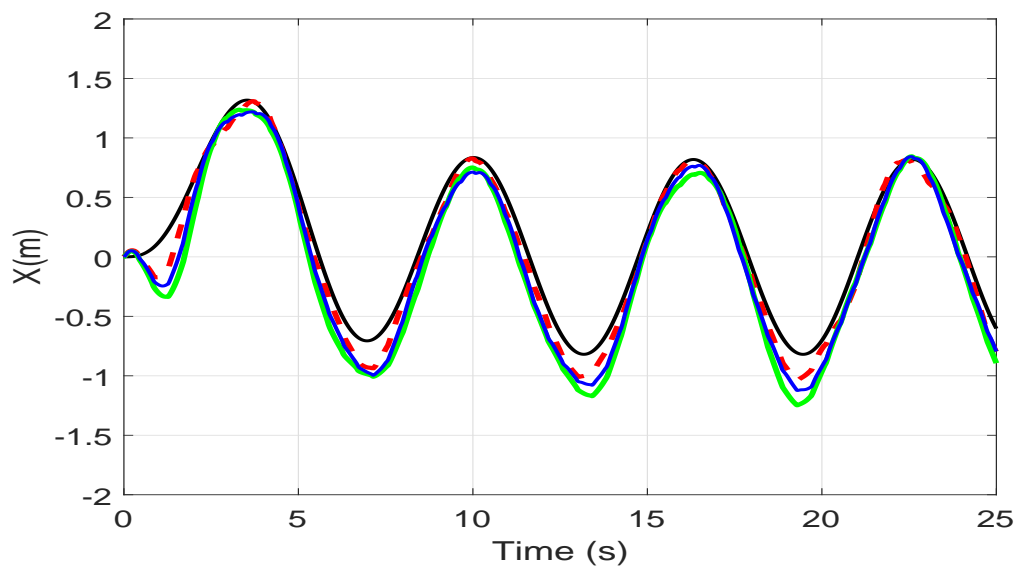


FIGURE 8.47: X Cartesian position (proposed DOB (30 rad/sec in red, 20 rad/sec in blue), DOB in green)

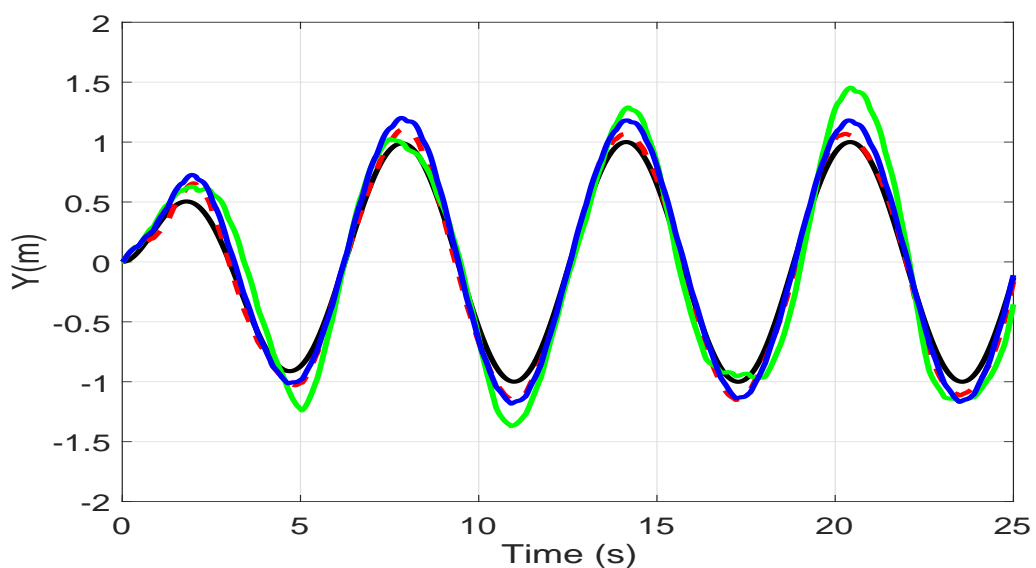


FIGURE 8.48: Y Cartesian position (proposed DOB (30 rad/sec in red, 20 rad/sec in blue), DOB in green)

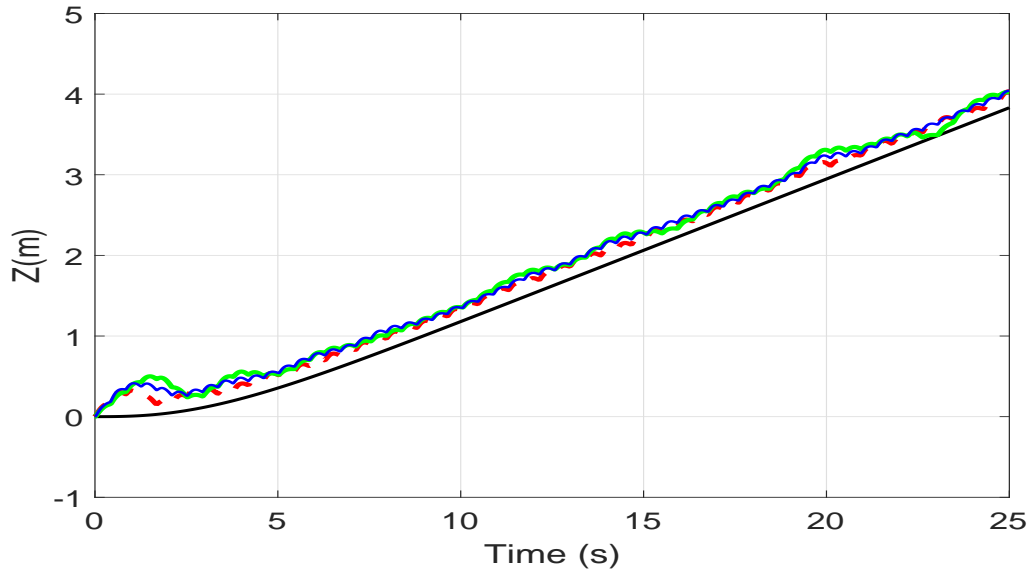


FIGURE 8.49: Z Cartesian position (proposed DOB (30 rad/sec in red, 20 rad/sec in blue), DOB in green)

During the maneuvers on the trajectory, the proposed DOB provides more robustness and flexibility to tackle the disturbances than the controllers with classical DOB structure by maintaining its position in the close vicinity of the desired values. Consequently, the position errors plot in Fig 8.50 illustrates that the proposed DOB structure with more bandwidth shows less errors than the classical DOB.

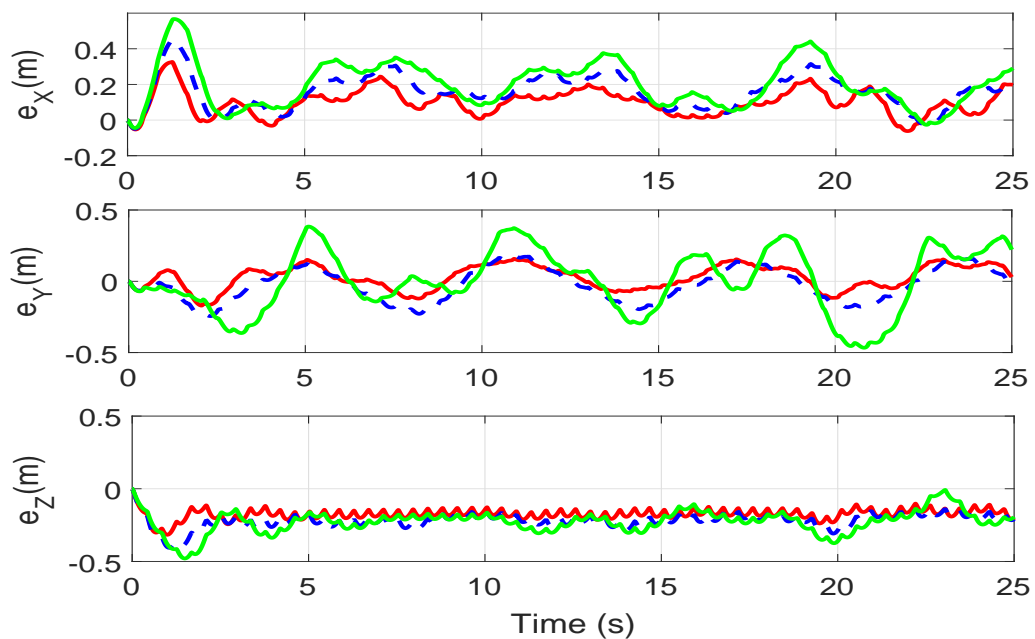


FIGURE 8.50: Position errors (proposed DOB with bandwidth (30 rad/sec in red, 20 rad/sec in blue), DOB in green)

The increased bandwidth of the BPFs in the novel DOB also affects the attitude performance of the vehicle, which is depicted through Euler angle plots in Fig 8.51, Fig 8.52 and Fig 8.53. From the plots, it can be noticed that during rolling, pitching and yawing motion, proposed DOB method provides less peak amplitudes for the attitude angles. Consequently, the quadrotor has better trajectory tracking performance than the classical DOB during the maneuvers due to the improved robustness introduced by the increasing bandwidth of the BPFs.

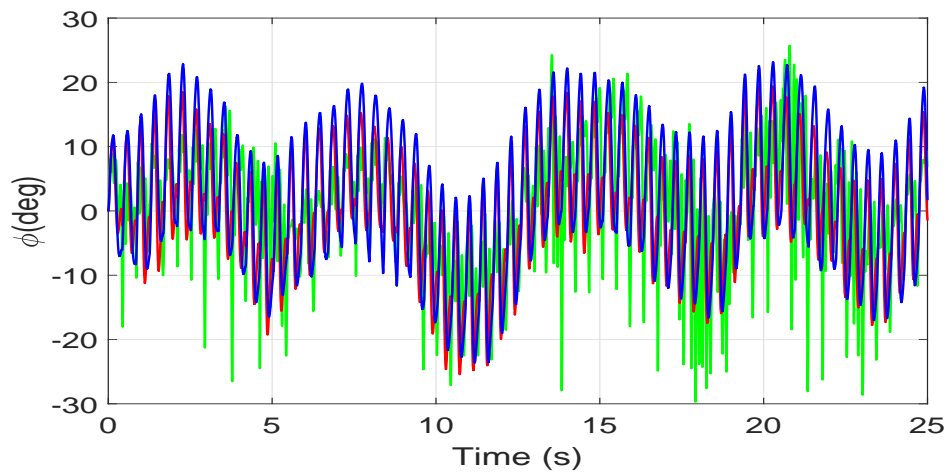


FIGURE 8.51: Roll angle (proposed DOB with bandwidth (30 rad/sec in red, 20 rad/sec in blue), DOB in green)

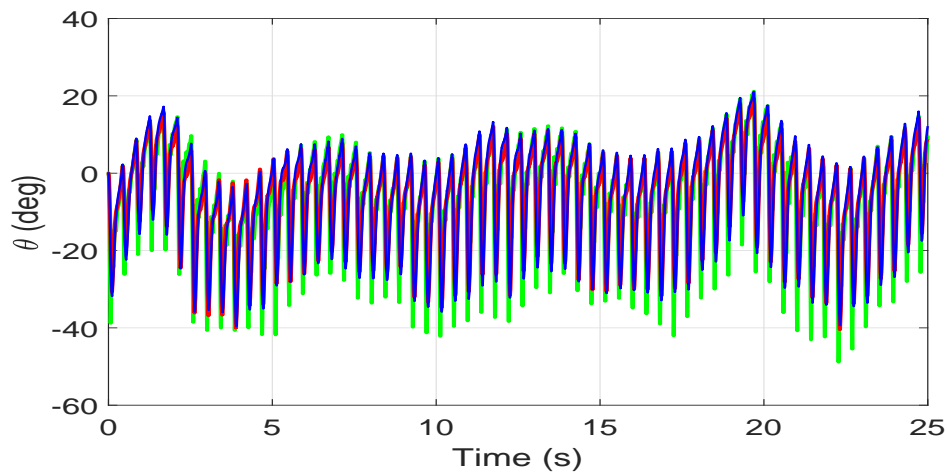


FIGURE 8.52: Pitch angle (proposed DOB with bandwidth (30 rad/sec in red, 20 rad/sec in blue), DOB in green)

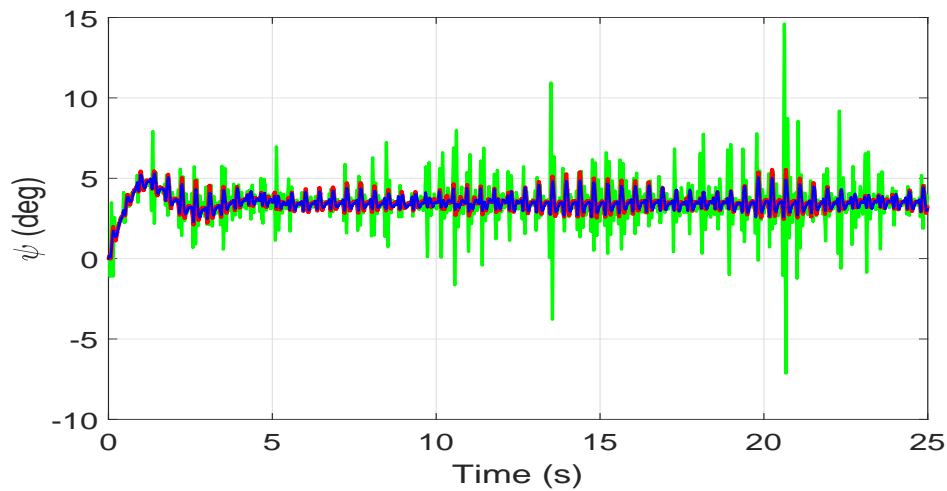


FIGURE 8.53: Yaw angle (proposed DOB with bandwidth (30 rad/sec in red, 20 rad/sec in blue), DOB in green)

The sensitivity to the bandwidth increase on the trajectory tracking performance and quantitative comparison with the classical DOB are provided in Table 8.7.

TABLE 8.7: Trajectory Tracking Performance with Different Bandwidths of the BPFs

| <i>Criteria</i>       | <i>DOB</i> | <i>Proposed DOB<br/>with <math>2\sigma=30</math> rad/sec</i> | <i>Proposed DOB<br/>with <math>2\sigma=20</math> rad/sec</i> |
|-----------------------|------------|--|--|
| $RMS(e_X)$ m          | 0.24       | 0.13   | 0.18   |
| $Max( e_X )$ m        | 0.56       | 0.37   | 0.45   |
| $RMS(e_Y)$ m          | 0.217      | 0.098  | 0.14   |
| $Max( e_Y )$ m        | 0.48       | 0.17   | 0.24   |
| $RMS(e_Z)$ m          | 0.24       | 0.14   | 0.23   |
| $Max( e_Z )$ m        | 0.49       | 0.28   | 0.39   |
| $RMS(e_\phi)$ deg     | 9.5        | 8.1  | 9.3  |
| $Max( e_\phi )$ deg   | 29.8       | 22.3   | 23.6   |
| $RMS(e_\theta)$ deg   | 13.1       | 10.1   | 11.5   |
| $Max( e_\theta )$ deg | 49.2       | 32.2   | 32.8   |
| $RMS(e_\psi)$ deg     | 3.78       | 3.55   | 3.58   |
| $Max( e_\psi )$ deg   | 14.6       | 5.05   | 5.07   |

# Chapter 9

## Conclusions

In this work, robust trajectory tracking control of a quadrotor subject to external disturbances is developed using angular acceleration feedback. The hierarchical control structure is used as a control framework. Acceleration based disturbance observer integrated with PID controllers is designed for the positional dynamics of the quadrotor where linear acceleration signals provide better stiffness against the disturbance forces. For attitude control, a nested angular position, velocity and acceleration control structure is employed where PID and PI controllers are used. In order to get reliable angular position, velocity and acceleration signals, an estimation algorithm based on the cascaded structure of extended and classical Kalman filters is utilized. Furthermore, in this work, a nonlinear optimization technique is used to obtain the reference attitude angles from command signals generated from the high-level control of the hierarchical control structure. Unlike analytical method for calculating the reference attitude angles where nonsmooth and large Euler angles might be obtained, the constrained nonlinear optimization technique provides smooth and desired bounded values. Also in the analytical approach, the desired yaw angle ( $\psi$ ) needs to be fixed to some value ( $\psi^*$ ), but in case of the proposed method, yaw angle need not be constant. The efficiency of the proposed control method is tested on a high fidelity model of the quadrotor where sensor bias and noise in measurements are also taken into account when 3-D circular helix type trajectory is considered. Results are compared with a

similar control scheme where reference angles are calculated through analytical formulas. From the simulation results, it is shown that by using the acceleration signals, positional tracking performance of the quadrotor is improved significantly. Results are compared with a similar control scheme where reference angles are calculated through analytical formulas. From the attitude tracking, it is deduced that nonlinear optimization provides smooth attitude angles response as compared to the analytical method, which results in better position tracking performance.

In this thesis, we have developed a new disturbance observer based control system for the robust control of a quadrotor performing hovering and/or trajectory tracking tasks subject to both aperiodic and periodic disturbances. Proposed observer structure consists of a bank of band-pass filters centered at the integer multiples of the fundamental frequency of the disturbance signal in addition to a low-pass filter which is responsible for low-frequency aperiodic disturbances. PID control and nonlinear control are used for position and attitude control in a hierarchical control structure. Acceleration based disturbance observer is designed in the positional dynamics by utilizing the new DOB structure. In order to increase the robustness in the attitude dynamics, nonsingular and nonlinear sliding surface is designed based on Lyapunov stability analysis. Furthermore, an integral term is also injected into the sliding surface to reduce steady-state errors. PID is used as a high-level controller along with acceleration based disturbance observer to derive virtual controls. Reference attitude angles are calculated analytically from these virtual controls for the desired trajectory tracking. Nonlinear controller is used as a low-level controller along with the velocity based disturbance observer for more stiffness against the disturbances in the attitude control. Closed-loop stability of the attitude subsystem is proved using a Lyapunov analysis. Utilizing a high fidelity simulation model which takes nonlinearities in the dynamics, external disturbances acting on the system and sensor measurement noise into account, the performance of the proposed control system is tested in both hovering at a certain altitude and 3D Cartesian trajectory tracking. The sensitivity of the control system with respect to the number and bandwidth of the band-pass filters is also investigated. During the trajectory tracking task, yaw angle ( $\psi$ ) is taken to be

fixed at  $3.5^\circ$ . Conventional disturbance observer is also implemented for comparison. Aperiodic disturbances are generated according to the Dryden wind model with added periodic disturbances to evaluate the effectiveness of the proposed control system. From simulation results, it can be inferred that the proposed method with increased number and bandwidth of the band-pass filters showed better hovering and trajectory tracking performance than conventional disturbance observer by suppressing the disturbances more effectively with less errors.

As future work, frequency estimation algorithms will be used to estimate the frequency of the periodic disturbance and the proposed disturbance observer structure will be made adaptive by adjusting the central frequency of the band-pass filters accordingly. Also, the estimation of the attitude angles through optimization method will be made real-time by using algorithms with fast convergence. The proposed control algorithms will also be tested on a physical system to evaluate the performance in a real environment.

# Bibliography

- [1] U. Commercial, “Market analysis by product (fixed wing, rotary blade, nano, hybrid), by application (agriculture, energy, government, media & entertainment) and segment forecasts to 2022.”
- [2] A. A. Pereira, J. P. Espada, R. G. Crespo, and S. R. Aguilar, “Platform for controlling and getting data from network connected drones in indoor environments,” *Future Generation Computer Systems*, vol. 92, pp. 656–662, 2019.
- [3] A. Kampker, K. Kreiskoether, J. Wagner, and S. Fluchs, “Mobile assembly of electric vehicles: Decentralized, low-invest and flexible,” *International Journal of Mechanical, Aerospace, Industrial, Mechatronic and Manufacturing Engineering*, vol. 10, no. 12, pp. 1920–1926, 2016.
- [4] J. Eggers and M. H. Draper, “Multi-uav control for tactical reconnaissance and close air support missions: operator perspectives and design challenges,” in *Proc. NATO RTO Human Factors and Medicine Symp. HFM-135. NATO TRO, Neuilly-sur-Siene, CEDEX, Biarritz, France*, pp. 2011–06, 2006.
- [5] T. Tomic, K. Schmid, P. Lutz, A. Domel, M. Kassecker, E. Mair, I. L. Grixia, F. Ruess, M. Suppa, and D. Burschka, “Toward a fully autonomous uav: Research platform for indoor and outdoor urban search and rescue,” *IEEE robotics & automation magazine*, vol. 19, no. 3, pp. 46–56, 2012.
- [6] M. Elloumi, R. Dhaou, B. Escrig, H. Idoudi, and L. A. Saidane, “Monitoring road traffic with a uav-based system,” in *2018 IEEE Wireless Communications and Networking Conference (WCNC)*, pp. 1–6, IEEE, 2018.

- 
- [7] D. W. Murphy and J. Cycon, “Applications for mini vtol uav for law enforcement,” in *Sensors, C3I, Information, and Training Technologies for Law Enforcement*, vol. 3577, pp. 35–43, International Society for Optics and Photonics, 1999.
- [8] Z. Li, Y. Liu, R. Hayward, J. Zhang, and J. Cai, “Knowledge-based power line detection for uav surveillance and inspection systems,” in *2008 23rd International Conference Image and Vision Computing New Zealand*, pp. 1–6, IEEE, 2008.
- [9] J. C. Hodgson, S. M. Baylis, R. Mott, A. Herrod, and R. H. Clarke, “Precision wildlife monitoring using unmanned aerial vehicles,” *Scientific reports*, vol. 6, p. 22574, 2016.
- [10] D. Hausamann, W. Zirinig, G. Schreier, and P. Strobl, “Monitoring of gas pipelines—a civil uav application,” *Aircraft Engineering and Aerospace Technology*, vol. 77, no. 5, pp. 352–360, 2005.
- [11] L. Merino, F. Caballero, J. R. M. de Dios, I. Maza, and A. Ollero, “Automatic forest fire monitoring and measurement using unmanned aerial vehicles,” in *Proceedings of the 6th International Congress on Forest Fire Research*, Cite-seer, 2010.
- [12] B. Chan, H. Guan, J. Jo, and M. Blumenstein, “Towards uav-based bridge inspection systems: A review and an application perspective,” *Structural Monitoring and Maintenance*, vol. 2, no. 3, pp. 283–300, 2015.
- [13] N. G. Smith, L. Passone, S. Al-Said, M. Al-Farhan, and T. E. Levy, “Drones in archaeology: integrated data capture, processing, and dissemination in the al-ula valley, saudi arabia,” *Near Eastern Archaeology*, vol. 77, no. 3, pp. 176–181, 2014.
- [14] C. Sabo and K. Cohen, “Smart heuristic for pickup and delivery problem (pdp) with cooperative uavs,” in *Infotech@ Aerospace 2011*, p. 1464, 2011.

- [15] G. Ristorto, F. Mazzetto, G. Guglieri, and F. Quagliotti, "Monitoring performances and cost estimation of multicopter unmanned aerial systems in precision farming," in *2015 International Conference on Unmanned Aircraft Systems (ICUAS)*, pp. 502–509, IEEE, 2015.
- [16] A. Abdullah, E. A. Bakar, and M. Z. M. Pauzi, "Monitoring of traffic using unmanned aerial vehicle in malaysia landscape perspective," *Jurnal Teknologi*, vol. 76, no. 1, 2015.
- [17] S. Gupte, P. I. T. Mohandas, and J. M. Conrad, "A survey of quadrotor unmanned aerial vehicles," in *2012 Proceedings of IEEE Southeastcon*, pp. 1–6, IEEE, 2012.
- [18] P. B. Schmidt and R. D. Lorenz, "Design principles and implementation of acceleration feedback to improve performance of dc drives," *IEEE Transactions on Industry Applications*, vol. 28, no. 3, pp. 594–599, 1992.
- [19] D. Simon, *Optimal state estimation: Kalman, H infinity, and nonlinear approaches*. John Wiley & Sons, 2006.
- [20] F. Nishi and S. Katsura, "Nanoscale motion control using composite filter for disturbance observer," *IEEJ Journal of Industry Applications*, vol. 4, no. 2, pp. 98–104, 2015.
- [21] J. Su, W.-H. Chen, and B. Li, "High order disturbance observer design for linear and nonlinear systems," in *2015 IEEE International Conference on Information and Automation*, pp. 1893–1898, IEEE, 2015.
- [22] S. Bouabdallah, A. Noth, and R. Siegwart, "Pid vs lq control techniques applied to an indoor micro quadrotor," in *2004 IEEE/RSJ International Conference on Intelligent Robots and Systems (IROS)(IEEE Cat. No. 04CH37566)*, vol. 3, pp. 2451–2456, IEEE, 2004.
- [23] G. Hoffmann, H. Huang, S. Waslander, and C. Tomlin, "Quadrotor helicopter flight dynamics and control: Theory and experiment," in *AIAA guidance, navigation and control conference and exhibit*, p. 6461, 2007.

- [24] H. Bouadi, M. Bouchoucha, and M. Tadjine, "Sliding mode control based on backstepping approach for an uav type-quadrotor," *World Academy of Science, Engineering and Technology*, vol. 26, no. 5, pp. 22–27, 2007.
- [25] T. Madani and A. Benallegue, "Adaptive control via backstepping technique and neural networks of a quadrotor helicopter," *IFAC Proceedings Volumes*, vol. 41, no. 2, pp. 6513–6518, 2008.
- [26] S. Bouabdallah and R. Siegwart, "Backstepping and sliding-mode techniques applied to an indoor micro quadrotor," in *Proceedings of the 2005 IEEE international conference on robotics and automation*, pp. 2247–2252, IEEE, 2005.
- [27] E.-H. Zheng, J.-J. Xiong, and J.-L. Luo, "Second order sliding mode control for a quadrotor uav," *ISA transactions*, vol. 53, no. 4, pp. 1350–1356, 2014.
- [28] F. Yacef, O. Bouhali, and M. Hamerlain, "Adaptive fuzzy backstepping control for trajectory tracking of unmanned aerial quadrotor," in *2014 International Conference on Unmanned Aircraft Systems (ICUAS)*, pp. 920–927, IEEE, 2014.
- [29] F. Yacef, O. Bouhali, M. Hamerlain, and N. Rizoug, "Observer-based adaptive fuzzy backstepping tracking control of quadrotor unmanned aerial vehicle powered by li-ion battery," *Journal of Intelligent & Robotic Systems*, vol. 84, no. 1-4, pp. 179–197, 2016.
- [30] E. Kayacan and R. Maslim, "Type-2 fuzzy logic trajectory tracking control of quadrotor vtol aircraft with elliptic membership functions," *IEEE/ASME Transactions on Mechatronics*, vol. 22, no. 1, pp. 339–348, 2016.
- [31] K. Alexis, G. Nikolakopoulos, and A. Tzes, "Model predictive quadrotor control: attitude, altitude and position experimental studies," *IET Control Theory & Applications*, vol. 6, no. 12, pp. 1812–1827, 2012.

- [32] K. Alexis, G. Nikolakopoulos, and A. Tzes, "On trajectory tracking model predictive control of an unmanned quadrotor helicopter subject to aerodynamic disturbances," *Asian Journal of Control*, vol. 16, no. 1, pp. 209–224, 2014.
- [33] A. Abdessameud and A. Tayebi, "Global trajectory tracking control of vtol-uavs without linear velocity measurements," *Automatica*, vol. 46, no. 6, pp. 1053–1059, 2010.
- [34] G. V. Raffo, M. G. Ortega, and F. R. Rubio, "Nonlinear h infinity controller for the quad-rotor helicopter with input coupling," *IFAC Proceedings Volumes*, vol. 44, no. 1, pp. 13834–13839, 2011.
- [35] K. Ohnishi, M. Shibata, and T. Murakami, "Motion control for advanced mechatronics," *IEEE/ASME transactions on mechatronics*, vol. 1, no. 1, pp. 56–67, 1996.
- [36] E. Sariyildiz and K. Ohnishi, "Stability and robustness of disturbance-observer-based motion control systems," *IEEE Transactions on Industrial Electronics*, vol. 62, no. 1, pp. 414–422, 2014.
- [37] K. Ohishi, M. Nakao, K. Ohnishi, and K. Miyachi, "Microprocessor-controlled dc motor for load-insensitive position servo system," *IEEE transactions on industrial electronics*, no. 1, pp. 44–49, 1987.
- [38] K. Ohishi, "Torque-speed regulation of dc motor based on load torque estimation," in *IEEJ International Power Electronics Conference, IPEC-TOKYO, 1983-3*, vol. 2, pp. 1209–1216, 1983.
- [39] S. Li, J. Yang, W.-H. Chen, and X. Chen, *Disturbance observer-based control: methods and applications*. CRC press, 2016.
- [40] M. S. Katsura *et al.*, "Periodic disturbance suppression based on infinite-order disturbance observer," 2016.

- 
- [41] K. Yamada, S. Komada, M. Ishida, and T. Hori, "Characteristics of servo system using high order disturbance observer," in *Proceedings of 35th IEEE Conference on Decision and Control*, vol. 3, pp. 3252–3257, IEEE, 1996.
- [42] H. Muramatsu and S. Katsura, "Design of an infinite-order disturbance observer enhancing disturbance suppression performance," *IEEJ Journal of Industry Applications*, vol. 6, no. 3, pp. 192–198, 2017.
- [43] J. Han, "From pid to active disturbance rejection control," *IEEE transactions on Industrial Electronics*, vol. 56, no. 3, pp. 900–906, 2009.
- [44] Z. Gao, Y. Huang, and J. Han, "An alternative paradigm for control system design," in *Proceedings of the 40th IEEE conference on decision and control (Cat. No. 01CH37228)*, vol. 5, pp. 4578–4585, IEEE, 2001.
- [45] Y. Xia, P. Shi, G. Liu, D. Rees, and J. Han, "Active disturbance rejection control for uncertain multivariable systems with time-delay," *IET Control Theory & Applications*, vol. 1, no. 1, pp. 75–81, 2007.
- [46] Y. Huang and W. Xue, "Active disturbance rejection control: methodology and theoretical analysis," *ISA transactions*, vol. 53, no. 4, pp. 963–976, 2014.
- [47] C. Johnson, "Optimal control of the linear regulator with constant disturbances," *IEEE Transactions on Automatic Control*, vol. 13, no. 4, pp. 416–421, 1968.
- [48] C. Johnson, "Further study of the linear regulator with disturbances—the case of vector disturbances satisfying a linear differential equation," *IEEE Transactions on Automatic Control*, vol. 15, no. 2, pp. 222–228, 1970.
- [49] C. Johnson, "A new approach to adaptive control," in *Control and Dynamic Systems V27: Advances in Theory and Applications*, vol. 27, pp. 1–69, Academic, 1988.
- [50] Z.-J. Yang, H. Tsubakihara, S. Kanae, K. Wada, and C.-Y. Su, "A novel robust nonlinear motion controller with disturbance observer," in *2006 IEEE*

- Conference on Computer Aided Control System Design, 2006 IEEE International Conference on Control Applications, 2006 IEEE International Symposium on Intelligent Control*, pp. 320–325, IEEE, 2006.
- [51] Z.-J. Yang, H. Tsubakihara, S. Kanae, K. Wada, and C.-Y. Su, “A novel robust nonlinear motion controller with disturbance observer,” *IEEE Transactions on Control Systems Technology*, vol. 16, no. 1, pp. 137–147, 2007.
- [52] W.-H. Chen, D. J. Ballance, P. J. Gawthrop, and J. O’Reilly, “A nonlinear disturbance observer for robotic manipulators,” *IEEE Transactions on industrial Electronics*, vol. 47, no. 4, pp. 932–938, 2000.
- [53] W.-H. Chen, “Nonlinear disturbance observer-enhanced dynamic inversion control of missiles,” *Journal of Guidance, Control, and Dynamics*, vol. 26, no. 1, pp. 161–166, 2003.
- [54] W.-H. Chen, “Disturbance observer based control for nonlinear systems,” *IEEE/ASME transactions on mechatronics*, vol. 9, no. 4, pp. 706–710, 2004.
- [55] W.-H. Chen, “Harmonic disturbance observer for nonlinear systems,” *Journal of dynamic systems, measurement, and control*, vol. 125, no. 1, pp. 114–117, 2003.
- [56] K.-S. Kim, K.-H. Rew, and S. Kim, “Disturbance observer for estimating higher order disturbances in time series expansion,” *IEEE Transactions on automatic control*, vol. 55, no. 8, pp. 1905–1911, 2010.
- [57] E. Kim, “A fuzzy disturbance observer and its application to control,” *IEEE Transactions on fuzzy systems*, vol. 10, no. 1, pp. 77–84, 2002.
- [58] J.-S. Ko and B.-M. Han, “Precision position control of pmsm using neural network disturbance observer and parameter compensator,” in *2005 IEEE 36th Power Electronics Specialists Conference*, pp. 1313–1319, IEEE, 2005.

- [59] P. B. Schmidt and R. D. Lorenz, "Design principles and implementation of acceleration feedback to improve performance of dc drives," in *Conference Record of the 1990 IEEE Industry Applications Society Annual Meeting*, pp. 422–427, IEEE, 1990.
- [60] J. Han, Y. He, and W. Xu, "Angular acceleration estimation and feedback control: An experimental investigation," *Mechatronics*, vol. 17, no. 9, pp. 524–532, 2007.
- [61] T. Insperger, J. Milton, and G. Stépán, "Acceleration feedback improves balancing against reflex delay," *Journal of the Royal Society Interface*, vol. 10, no. 79, p. 20120763, 2013.
- [62] Y. Hori, "Disturbance suppression on an acceleration control type dc servo system," in *PESC'88 Record., 19th Annual IEEE Power Electronics Specialists Conference*, pp. 222–229, IEEE, 1988.
- [63] H. Kobayashi, S. Katsura, and K. Ohnishi, "An analysis of parameter variations of disturbance observer for haptic motion control," in *31st Annual Conference of IEEE Industrial Electronics Society, 2005. IECON 2005.*, pp. 6–pp, IEEE, 2005.
- [64] H. Kobayashi, S. Katsura, and K. Ohnishi, "An analysis of parameter variations of disturbance observer for motion control," *IEEE Transactions on Industrial Electronics*, vol. 54, no. 6, pp. 3413–3421, 2007.
- [65] S. H. Jeong, S. Jung, and M. Tomizuka, "Attitude control of a quad-rotor system using an acceleration-based disturbance observer: An empirical approach," in *2012 IEEE/ASME International Conference on Advanced Intelligent Mechatronics (AIM)*, pp. 916–921, IEEE, 2012.
- [66] T. Tomić, "Evaluation of acceleration-based disturbance observation for multicopter control," in *2014 European Control Conference (ECC)*, pp. 2937–2944, IEEE, 2014.

- [67] S. Katsura, K. Irie, and K. Ohishi, "Wideband force control by position-acceleration integrated disturbance observer," *IEEE Transactions on Industrial Electronics*, vol. 55, no. 4, pp. 1699–1706, 2008.
- [68] M. Mizuochi, T. Tsuji, and K. Ohnishi, "Multirate sampling method for acceleration control system," *IEEE Transactions on Industrial Electronics*, vol. 54, no. 3, pp. 1462–1471, 2007.
- [69] W. Shang and S. Cong, "Motion control of parallel manipulators using acceleration feedback," *IEEE Transactions on Control Systems Technology*, vol. 22, no. 1, pp. 314–321, 2013.
- [70] A. Rubaai, A. R. Ofoli, and D. Cobbinah, "Dsp-based real-time implementation of a hybrid infinity adaptive fuzzy tracking controller for servo-motor drives," *IEEE Transactions on Industry Applications*, vol. 43, no. 2, pp. 476–484, 2007.
- [71] E. Çetinsoy, S. Dikyar, C. Hancı, K. Oner, E. Sirimoglu, M. Unel, and M. Aksit, "Design and construction of a novel quad tilt-wing uav," *Mechatronics*, vol. 22, no. 6, pp. 723–745, 2012.
- [72] C. Hancı, K. T. Oner, E. Sirimoglu, E. Cetinsoy, and M. Unel, "Robust position control of a tilt-wing quadrotor," in *49th IEEE Conference on Decision and Control (CDC)*, pp. 4908–4913, IEEE, 2010.
- [73] Y. Yildiz, M. Unel, and A. E. Demirel, "Adaptive nonlinear hierarchical control of a quad tilt-wing uav," in *2015 European Control Conference (ECC)*, pp. 3623–3628, IEEE, 2015.
- [74] Y. Yildiz, M. Unel, and A. E. Demirel, "Nonlinear hierarchical control of a quad tilt-wing uav: An adaptive control approach," *International Journal of Adaptive Control and Signal Processing*, vol. 31, no. 9, pp. 1245–1264, 2017.
- [75] A. Drouot, E. Richard, and M. Boutayeb, "Hierarchical backstepping-based control of a gun launched mav in crosswinds: Theory and experiment," *Control Engineering Practice*, vol. 25, pp. 16–25, 2014.

- [76] S. Formentin and M. Lovera, "Flatness-based control of a quadrotor helicopter via feedforward linearization," in *2011 50th IEEE Conference on Decision and Control and European Control Conference*, pp. 6171–6176, IEEE, 2011.
- [77] A. Aboudonia, R. Rashad, and A. El-Badawy, "Composite hierarchical anti-disturbance control of a quadrotor uav in the presence of matched and mismatched disturbances," *Journal of Intelligent & Robotic Systems*, vol. 90, no. 1-2, pp. 201–216, 2018.
- [78] M. R. Mokhtari, B. Cherki, and A. C. Braham, "Disturbance observer based hierarchical control of coaxial-rotor uav," *ISA transactions*, vol. 67, pp. 466–475, 2017.
- [79] T. Bresciani, "Modelling, identification and control of a quadrotor helicopter," *MSc Theses*, 2008.
- [80] K. T. Öner, E. Çetinsoy, E. SIRIMOĞLU, C. Hançer, M. Ünel, M. F. Akşit, K. Gülez, and I. Kandemir, "Mathematical modeling and vertical flight control of a tilt-wing uav," *Turkish Journal of Electrical Engineering & Computer Sciences*, vol. 20, no. 1, pp. 149–157, 2012.
- [81] F. Sabatino, "Quadrotor control: modeling, nonlinear control design, and simulation," 2015.
- [82] X. Chen, J. Yang, S. Li, and Q. Li, "Disturbance observer based multi-variable control of ball mill grinding circuits," *Journal of Process Control*, vol. 19, no. 7, pp. 1205–1213, 2009.
- [83] T. A. Johansen and T. I. Fossen, "Control allocation—a survey," *Automatica*, vol. 49, no. 5, pp. 1087–1103, 2013.
- [84] T. A. Johansen, T. I. Fossen, and S. P. Berge, "Constrained nonlinear control allocation with singularity avoidance using sequential quadratic programming," *IEEE Transactions on Control Systems Technology*, vol. 12, no. 1, pp. 211–216, 2004.

- 
- [85] J. Nocedal and S. Wright, *Numerical optimization*. Springer Science & Business Media, 2006.
- [86] T. Coleman, M. A. Branch, and A. Grace, “Optimization toolbox,” *For Use with MATLAB. User’s Guide for MATLAB 5, Version 2, Release II*, 1999.
- [87] S. Evren, F. Yavuz, and M. Unel, “High precision stabilization of pan-tilt systems using reliable angular acceleration feedback from a master-slave kalman filter,” *Journal of Intelligent & Robotic Systems*, vol. 88, no. 1, pp. 97–127, 2017.
- [88] H. K. Khalil, *Nonlinear control*. Pearson Higher Ed, 2014.
- [89] S. Allison, H. Bai, and B. Jayaraman, “Modeling trajectory performance of quadrotors under wind disturbances,” in *2018 AIAA Information Systems-AIAA Infotech@ Aerospace*, p. 1237, 2018.